



U.S. Department
of Transportation

**Federal Highway
Administration**

PB90208273


Publication No. FHWA-RD-89-077
March 1989

Calibration of Road Roughness Measuring Equipment,

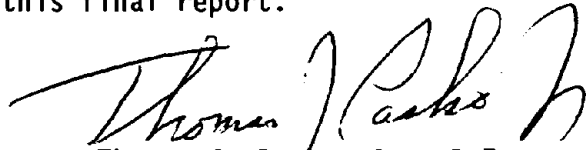
Volume I: Experimental Investigation

Research, Development, and Technology
Turner-Fairbank Highway Research Center
6300 Georgetown Pike
McLean, Virginia 22101-2296

REPRODUCED BY
U.S. DEPARTMENT OF COMMERCE
NATIONAL TECHNICAL INFORMATION SERVICE
SPRINGFIELD, VA. 22161

FOREWORD

Road roughness data are among the primary inputs to pavement management systems. Reliable equipment as well as test and calibration procedures are essential for providing high quality road roughness data. Two distinct methods of measuring road roughness are in use. One method profiles the road surface in one or both wheel tracks. While this is the preferred method, it is currently not widely used because of cost and complexity. A widely used, simple and inexpensive method measures the response of an automobile or trailer to road roughness. Obviously, the response depends on vehicle characteristics and on the speed of testing. The operating principles of both measuring methods have been analyzed in the research reported in Volume I. Limitations and error sources were identified from the analysis and from field test results. The findings provided the basis for recommended calibration and field verification procedures for both test methods and equipment. These procedures are given in Volume II of this final report.



Thomas J. Pasko, Jr., P.E.
Director, Office of Engineering
and Highway Operations
Research and Development

NOTICE

This document is disseminated under the sponsorship of the Department of Transportation in the interest of information exchange. The United States Government assumes no liability for its contents or use thereof. The contents of this report reflect the views of the contractor, who is responsible for the accuracy of the data presented herein. The contents do not necessarily reflect the official policy of the Department of Transportation. This report does not constitute a standard, specification, or regulation.

The United States Government does not endorse products or manufacturers. Trade or manufacturers names appear herein only because they are considered essential to the object of this document.

1. Report No. FHWA-RD-89-077		2. Government Accession No. PB 90 208273/AS		3. Recipient's Catalog No.	
4. Title and Subtitle CALIBRATION OF ROAD ROUGHNESS MEASURING EQUIPMENT Volume I: Experimental Investigation				5. Report Date March 1989	
				6. Performing Organization Code	
7. Author(s) T. F. Vorburger, D. C. Robinson, S. E. Fick, and D. R. Flynn				8. Performing Organization Report No.	
9. Performing Organization Name and Address National Institute of Standards and Technology U. S. Department of Commerce Gaithersburg, MD 20899				10. Work Unit No. (TRAIS) 3C3A 1162	
				11. Contract or Grant No. DTFH61-85-Y-10004	
12. Sponsoring Agency Name and Address Office of Engineering and Highway Operations R&D Federal Highway Administration 6300 Georgetown Pike McLean, Virginia 22101-2296				13. Type of Report and Period Covered Final September 85 - November 88	
				14. Sponsoring Agency Code	
15. Supplementary Notes Contract Officer's Technical Representative: Dr. R. R. Hegmon (HNR-20)					
16. Abstract An extensive series of measurements was made of the performance of a particular model of an inertial road profiling system (IRPS), including evaluation of the noncontact height sensors, the accelerometers used to establish the inertial reference frame, the distance encoder, the associated instrumentation, and the software used to convert the raw data into road elevation profiles. A field program was carried out which included rod-and-level surveys of several roads which were also profiled using the IRPS. The IRPS was also equipped with a commercial response-type road roughness measurement (RTRRM) system, with accelerometers to measure the vertical vibration of both the axle and the body of the vehicle, and with a linear potentiometer to measure the relative displacement between the axle and the body of the vehicle. Separate laboratory measurements were made to characterize the performance of the commercial RTRRM. Data collected with the RTRRM and with the auxiliary accelerometers and the linear potentiometer were compared with single-number ratings of road roughness as computed from the profiles measured using the IRPS. This report documents the measurements and analyses that were carried out in order to enable rational development of the calibration and testing procedures that are given in the companion report, FHWA-RD-89-078, Calibration of Road Roughness Measuring Equipment, Volume II: Calibration Procedures.					
17. Key Words Pavement management; pavement performance; profilometer; ride quality; road meter; road roughness; roughness; serviceability			18. Distribution Statement No restrictions. This document is available to the public through the National Technical Information Service, Springfield, VA 22161		
19. Security Classif. (of this report) Unclassified		20. Security Classif. (of this page) Unclassified		21. No. of Pages 92	22. Price

Table of Contents

	<u>Page</u>
1. INTRODUCTION	1
Background	1
Vehicle Description	2
2. ROAD PROFILOMETER TEST RESULTS	3
Description of Road Profilometer Operation	3
Accelerometers	4
Orientation Errors	4
Transducer Errors	5
Field Test	7
Noncontact Sensors	9
Repeatability	10
Linearity	12
Contribution to Profiling Uncertainty	14
Signal Sensitivity to Pavement Reflectivity	14
Wheel Encoder	14
Expected Profiling Accuracy	15
Error Estimates For Accelerometer System	15
Error Estimates For Noncontact Sensor	15
Error Estimates For Wheel Encoder	15
Combining Sources of Error	16
Software	17
Rocking Tests	18
Profiling Consistency	19
Profiling Accuracy Tests	24
Rod-and-Level Testing	24
Flat Plate Tests	33
Single-Number Roughness Ratings	38
3. RESPONSE-TYPE ROAD ROUGHNESS MEASUREMENT SYSTEM TEST RESULTS	52
Mays Ride Meter Testing	52

Table of Contents (continued)

	<u>Page</u>
Static Tests of Rotary Encoder	52
Installation of RTRRM in Road Profilometer Van	56
Field Tests	57
Comparison with Road Profilometer	59
 Accelerometer Testing	 61
Description of Sensors and Instrumentation	61
Spectral Analysis	62
Comparison with Road Profilometer	74
 4. CONCLUSIONS	 76
 APPENDIX A ROD-AND-LEVEL ANALYSIS PROGRAM	 78
 REFERENCES	 83

List of Figures

Figure

1	Pitch, roll, and yaw motions of the road profiling van with respect to the road coordinate system.	6
2	Sensitivity versus frequency for accelerometer S/N 236	8
3	Sensitivity versus frequency for accelerometer S/N 237	9
4	Optical setup of the noncontact sensor showing a measurement of the calibration block	10
5	Variation in the measurement of the 1-in calibration block with the noncontact sensor between 4/22/87 and 12/11/87	12
6	Measured t_p of a 1-in block versus surface height	13
7	Typical recorded profiles for the road profilometer (a) while sitting completely still and (b) with a yaw excitation	19
8	Typical recorded profiles for the road profilometer under (a) pitch and (b) roll excitations	20
9	Example of the repeatability of the road profilometer during three measurements on South Drive	21
10	Example of the repeatability of the road profilometer during eight measurements on the Blue Grass Parkway in Eastern Kentucky	22

List of Figures (continued)

<u>Figure</u>		<u>Page</u>
11	Example of the repeatability of the road profilometer during four measurements on Route 60 in Eastern Kentucky	23
12	Unfiltered rod and level profiles of four roadways	27
13	Road profilometer results for South Drive compared with filtered rod-and-level data taken along the right wheeltrack	28
14	Road profilometer results for the Blue Grass Parkway compared with rod-and-level data taken along the right wheeltrack	29
15	Road profilometer results for Kentucky Rt. 151, Northbound, with filtered rod-and-level data for both wheeltracks	30
16	Road profilometer results for Kentucky Rt. 151, Northbound, with filtered rod-and-level data for the left wheeltrack measured over 1582.5 ft	30
17	Road profiling results obtained by the UMTRI system compared with rod-and-level data filtered by a moving average, high-pass digital filter	34
18	Design sketch of a road plate for testing the short-wavelength response of road profiling vehicles	35
19	Road profiles obtained when two test plates are positioned along the left wheeltrack of the road profilometer	36
20	Detail of a profile for a single plate	36
21	Mathematical simulation of road profilometer response to a square pulse input with height of 5/8 in and width of 2 ft	37
22	Quarter-car model of vibrational response to road excitations	38
23	Magnitude of the transfer function, equation 17, between the body-to-axle motion and the input motion due to the road profile	41
24	Normalized power spectral densities for the velocity of the body relative to the axle. The vehicle is assumed to be moving at 50 mph over "average" roads	42
25	Frequency weighting to simulate human sensitivity to vertical acceleration	43

List of Figures (continued)

<u>Figure</u>		<u>Page</u>
26	Normalized power spectral densities, weighted for human sensitivity, for vertical acceleration of the vehicle body. The vehicle is assumed to be moving at 50 mph over "average" roads	44
27	Comparison of the Mays indices computed from profilometer data with those computed from rod-and-level data	46
28	Comparison of root-mean-square accelerations computed from profilometer data with those computed from rod-and-level data	46
29	Schematic of laboratory test arrangement for determination of Mays Ride Meter quantization and hysteresis	53
30	Rotary transmitter output voltage for the light bulb in two positions relative to the transmitter optical slit	55
31	Schematic of the installation of the Mays Ride Meter and the continuous displacement transducer in the road profilometer	57
32	Example of Mays Ride Meter calibration by regression with calculated Mays indices from road profilometer	61
33	Measured 1/3-octave-band acceleration of the road profilometer <u>axle</u> for a 50-mph run at Test Site 101 (PCC)	63
34	Measured 1/3-octave-band acceleration of the road profilometer <u>body</u> for a 50-mph run at Test Site 101 (PCC)	63
35	Measured 1/3-octave-band acceleration of the road profilometer <u>axle</u> for a 50-mph run at Test Site 104 (PCC)	64
36	Measured 1/3-octave-band acceleration of the road profilometer <u>body</u> for a 50-mph run at Test Site 104 (PCC)	64
37	Measured 1/3-octave-band acceleration of the road profilometer <u>axle</u> for a 50-mph run at Test Site 107 (PCC)	65
38	Measured 1/3-octave-band acceleration of the road profilometer <u>body</u> for a 50-mph run at Test Site 107 (PCC)	65
39	Measured 1/3-octave-band acceleration of the road profilometer <u>axle</u> for a 50-mph run at Test Site 201 (BC)	66
40	Measured 1/3-octave-band acceleration of the road profilometer <u>body</u> for a 50-mph run at Test Site 201 (BC)	66

List of Figures (continued)

<u>Figure</u>	<u>Page</u>
41 Measured 1/3-octave-band acceleration, for the 2-Hz band, of the vehicle body plotted versus A_{rms} computed from road profilometer profiles	67
42 Measured 1/3-octave-band acceleration, for the 4-Hz band, of the vehicle body plotted versus A_{rms} computed from road profilometer profiles	67
43 Axle-to-body transfer function for the quarter-car model (solid curve) and for the road profilometer (solid circles) traveling at 50 mph over Road 0107	69
44 Root-mean-square vertical displacement of the body of the road profilometer while traveling at 50 mph over Road 0101	69
45 Root-mean-square vertical displacement of the body of the road profilometer while traveling at 50 mph over Road 0104	70
46 Root-mean-square vertical displacement of the body of the road profilometer while traveling at 50 mph over Road 0107	70
47 Root-mean-square vertical displacement of the body of the road profilometer while traveling at 50 mph over Road 0201	71
48 Spectra of the root-mean-square vertical displacement for Road 0101 as functions of frequency for 50 mph travel	72
49 Spectra of the root-mean-square vertical displacement for Road 0104 as functions of frequency for 50 mph travel	72
50 Spectra of the root-mean-square vertical displacement for Road 0107 as functions of frequency for 50 mph travel	73
51 Spectra of the root-mean-square vertical displacement for Road 0201 as functions of frequency for 50 mph travel	73
52 Root-mean-square acceleration, A_{rms} , computed by applying human-response weighting to data from body accelerometer, versus A_{rms} computed from road profilometer profiles	74
53 Root-mean-square acceleration, A_{rms} , computed by applying human-response weighting to data from body accelerometer, versus Mays index computed from road profilometer profiles	75
54 Main menu of NBSROAD.BAS program	79
55 Flow chart of main elements in the 3-pole Butterworth filter subroutine used in the K. J. Law Model 690DNC road profilometer.	80

List of Figures (continued)

<u>Figure</u>		<u>Page</u>
56	Flow chart of main elements in the UMTRI moving-average filter subroutine	81
57	Flow chart of subroutine to calculate Mays index and rms acceleration from profile data	82

List of Tables

<u>Table</u>		
1	Noncontact sensor calibration data	11
2	Mays index (MI) and rms acceleration (A_{rms}) calculated from profiles generated with both rod and level and road profilometer . . .	45
3	Comparison of analytical and computer results for MI and A_{rms} for three sinusoidal road profiles with varying wavelength (λ)	49
4	Quantization levels of Mays Rotary Encoder	55
5	Inertial profilometer measurements	60



1. INTRODUCTION

Background

Road roughness is a very old engineering problem. On the one hand, rough roads produce wear and tear on the vehicles, people, and materials transported over them. On the other hand, rough roads themselves wear out faster than smooth roads. Thus, the quantification of road roughness is an important civil engineering endeavor because it enables engineers to set criteria for when to resurface roads and how to evaluate the irregularities of newly finished roads.

Pavement irregularities, generally random in nature, are divided into three scales: roughness, macrotexture, and microtexture. The dividing lines between these regions are based upon functional considerations such as traffic safety and ride quality. Roughness is the largest scale, with characteristic wave lengths of 0.3 to 300 ft and amplitudes of 0.04 to 4 in - it is of interest with regard to ride comfort. Macro- and microtexture describe smaller scale pavement irregularities, generally related to tire-pavement traction characteristics.

Road roughness is measured by: (1) inertial road profiling systems (IRPS), which measure actual pavement profiles, and (2) response-type road roughness measurement (RTRRM) systems which measure vehicle response to roughness. Ideally, road profiling systems yield accurate, scaled reproductions of the pavement profile along the path of vehicle travel. In practice, the range and resolution of any IRPS are limited, but within the wavelength and amplitude limitations of the system, a profile measurement may be called "absolute," in the sense that it does not require comparison to any other system, except for the calibration of its several sensors and the associated electronics. A response-type method records some measure of the dynamic response of a particular mechanical system as it travels over the pavement. It is, therefore, a relative method whose result depends on the characteristics of the mechanical system and the speed of travel.

The advantages of a profiling system are evident. It provides pavement-profile information that can be evaluated according to specific needs. The first high-speed road-profiling system, using an inertial reference concept, was developed in the early 1960's.⁽¹⁾ It used two spring-loaded, road-following wheels, instrumented with a linear potentiometer to measure relative displacements between the vehicle frame and the road surface. The vertical displacement of the vehicle frame was obtained by double integration of the signals from accelerometers mounted on the frame over each of the follower wheels. The road profile was obtained from the algebraic sum of the vehicle displacement and the relative frame-to-road displacement. In a modern IRPS, noncontact sensors (usually optical, but sometimes acoustical) are used for measuring the frame-to-road displacement.

Although, as stated above, an IRPS is an "absolute" method, it is necessary to ascertain that the sensors (accelerometers, height sensors, distance encoder) and electronics are calibrated and that the computer and software are functioning properly. The present study, and the IRPS calibration procedures given in

volume II of this report, are intended to assist users of an IRPS to make a field assessment of the proper functionality of their equipment.

RTRRM systems typically accumulate a measure of the vertical movements of the rear axle of an automobile or trailer relative to the vehicle frame. This method of measurement is simpler and cheaper than profiling equipment. However, since the results obtained depend upon the dynamic characteristics of the vehicle or trailer and upon the mechanical behavior of the device itself, the data from RTRRM systems are critically dependent upon suitable test procedures. A field calibration guide for RTRRM systems is included in volume II of this report.

Vehicle Description

The IRPS used in the present study was a Model 690DNC Road Profilometer, manufactured by K. J. Law Engineers, Inc., in Farmington Hills, Michigan. This IRPS, hereafter simply called the road profilometer except where further clarification is needed, consists of a Ford Econoline Van equipped with special sensors, instrumentation, and a computer.

Two noncontact height sensors, one installed in front of each rear wheel, each project a light pattern, nominally 4-in wide by 1/4-in in the direction of vehicle travel, onto the road. A scanning mirror assembly in each height sensor reflects the light pattern from the road onto a photodetector. The signal from the photodetector is processed to obtain an analog signal that is related to the angle from the scanner to the light pattern on the road surface.

Each height sensor is provided with an accelerometer which produces an analog signal proportional to vertical acceleration.

One front wheel of the vehicle is provided with an encoder that generates a train of pulses whose frequency is proportional to vehicle speed.

The analog signals from the two noncontact height sensors and from the two system accelerometers are digitized and, along with the pulse train from the distance encoder, sent to a minicomputer which processes the data to obtain the elevation profile for each wheel track. The operation of the profilometer is described in more detail in section 2.

The road profilometer was temporarily modified for this project by the addition of a commercial RTRRM (a Mays Ride Meter, manufactured by the Rainhart Co., in Austin, Texas), a linear potentiometer to indicate the displacement between the vehicle body and the rear axle (specifically, the differential housing), and two accelerometers, one to measure the vertical acceleration of the rear axle and the other to measure the acceleration of the vehicle body directly above the rear axle. Care was taken to ensure that these modifications did not interfere with the normal operation of the road profilometer. An FM tape recorder, with appropriate signal conditioning, was used to record the signals from the linear potentiometer and auxiliary accelerometers. Additional details regarding the auxiliary sensors and instrumentation are given in section 3.

2. ROAD PROFILOMETER TEST RESULTS

Description of Road Profilometer Operation

An inertial road profiling system (IRPS) requires four basic subsystems:

- Accelerometer(s) for determination of the height of the vehicle relative to an inertial reference frame (i.e., a reference frame that does not depend on riding height or position of the vehicle along the road).
- Height sensor(s) for measurement of the instantaneous riding height of the vehicle relative to a location on the road below the sensor.
- Distance or speed sensor for measurement of the position of the vehicle along the length of the road (i.e., an odometer which indicates fractions of a foot rather than fractions of a mile).
- Computer hardware and software for computation of road profiles from the above sensor inputs.

The FHWA's road profilometer determines the road roughness profile along each wheel track of the path followed by the vehicle. A proprietary noncontact height sensor mounted directly in front of each rear wheel of the vehicle projects a light pattern straight down onto the road. A rotary scanning mirror is used to image the light pattern onto a photodetector, with electronic circuitry which produces an analog signal related to the angle between the scanner and the road, and hence to the distance between the vehicle and the road.

Each sensor channel is also provided with an accelerometer to measure vertical acceleration. The two accelerometers that serve as inertial references for the road profilometer are Sunstrand Model QA-1400 servo accelerometers. Each accelerometer consists of an analog torque-balance sensor incorporating a fused quartz flexure with support structure and permanent magnet torquer, a capacitive displacement sensor, and self-contained restoring electronics. The output signal is a current equal to the analog restoring current and proportional to acceleration, the nominal sensitivity being 1.3 mA/g. The manufacturer's specifications indicate a linear output range of ± 30 g, a resolution of 1 micro-g, a flat frequency response (0.05 percent nominal from 0 to 10 Hz and 2 percent nominal from 0 to 100 Hz), and a damping ratio of 0.3 to 0.8. The electronics for the road profilometer can accommodate an acceleration range of approximately ± 2 g.

An encoder, on the left front wheel, emits a series of electrical pulses as the wheel rotates, thus providing a measure of the distance traveled.

The road profilometer is equipped with appropriate signal-conditioning electronics and analog-to-digital converters for the signals from the two noncontact height sensors and the two accelerometers. These digitized signals, along with the pulse train from the wheel encoder, are input to a minicomputer. Proprietary software is used to compute the algebraic sum of the signal from each noncontact height sensor and the double-integrated signal from the correspond-

ing accelerometer, combine the result with the signal from the distance encoder, and compute the road profile for each wheel track. These profiles are high-pass filtered to take out the effect of long-wavelength elevation changes (e.g., wavelengths longer than 300 ft) and are smoothed to reduce short-wavelength (high-frequency) noise. The profile is stored for 0.5-ft intervals along the road. The signals from the individual sensors are not saved.

The resulting surface profile may be expressed as⁽²⁾

$$W_f(i) = Z_s(i) + (S/V)^2 \sum_{j=1}^i \sum_{k=1}^j a(k) - \left[s^3 T_3 \sum_{j=1}^{i-1} \sum_{k=1}^j \sum_{m=1}^k W_f(m) + s^2 T_2 \sum_{j=1}^{i-1} \sum_{k=1}^j W_f(k) - s T_1 \sum_{j=1}^{i-1} W_f(j) \right], \quad (1)$$

where $W_f(i)$ is the calculated road profile as a function of digital position i along the road, $Z_s(i)$ is the height measurement obtained from the noncontact sensor, $a(k)$ are accelerometer readings that are doubly integrated to calculate the inertial position of the van, S is the sampling interval, V is the velocity of the van, and the terms inside the brackets describe the action of the high-pass digital filter. The three time constants (T_1 , T_2 , T_3) are appropriate to the profilometer's three-pole Butterworth filter, having a selectable cutoff normally chosen to be 300 ft.

The road profilometer is also provided with software to compute, from the stored profiles, several single-number descriptors of the roughness of a pavement segment. In the present study, the Mays index and the weighted root-mean-square acceleration were computed.

In the following three subsections the major components of the profiling system are discussed, along with the associated sources of error. The next subsection is a discussion of an uncertainty budget for the system, followed by a subsection on the road profilometer software and four subsections containing test results for the entire system.

Accelerometers

Errors in measurement of the vertical acceleration of the van will directly affect the accuracy of the surface profile. The two sources of error are misorientation of the accelerometer and inaccuracies associated with the transducer and its associated electronics. A brief discussion of each error source follows.

Orientation Errors

Because the response of a servo accelerometer extends downward in frequency to dc, the sensitive axis of the sensor can always be made truly vertical by simply adjusting its position so as to maximize the output signal. For convenience, the type of servo accelerometer that is used in the FHWA road profilometer comes equipped with a mounting flange that serves as a reference

plane. The angular error between the sensitive axis of the accelerometer and the perpendicular to the reference plane is specified by the manufacturer not to exceed ± 2 milliradian between -40 and $+185$ °F; this uncertainty is far exceeded by those uncertainties associated with mounting the accelerometer in the van. The possible use of an adjustable accelerometer mount is made unnecessary by the much larger uncertainties inherent in defining a plane parallel to a conventional, nonplanar roadway, and in establishing the angular position of a moving vehicle relative to the roadway. In view of these difficulties, and because each accelerometer was mounted in the road profilometer with its sensitive axis nominally perpendicular to the floor pan of the van, no attempt was made to determine the actual angular orientation of either accelerometer relative to the vehicle or to any specific reference plane.

The accelerometer is intended to measure acceleration perpendicular to the plane of the road. Considering the nature of hills and curves and the high pass cutoff of the profiling instrument, the plane of the road is hard to define rigorously. However, the vehicle motions of roll and pitch (see figure 1) contribute to small errors in the accelerometer signal. These may be described as follows:⁽³⁾

$$\epsilon_a = -g(1 - \cos \phi) - a_z (1 - \cos \theta_z) + a_x \cos \theta_x + a_y \cos \theta_y . \quad (2)$$

where ϵ_a is the error in the accelerometer reading, g is the acceleration of gravity in the vertical direction, $\cos \theta_x$, $\cos \theta_y$, and $\cos \theta_z$ are the direction cosines of the accelerometer axis with respect to an ideal Cartesian coordinate system squared up to the road, a_x , a_y , and a_z are induced accelerations in the vehicle along the Cartesian axes, and ϕ is the angle between the sensitive axis of the accelerometer and the true vertical direction. The acceleration to be measured is a_z . The angles of the accelerometer axis, when it is properly aligned, are $\theta_x = 90^\circ$, $\theta_y = 90^\circ$, and $\theta_z = 0$.

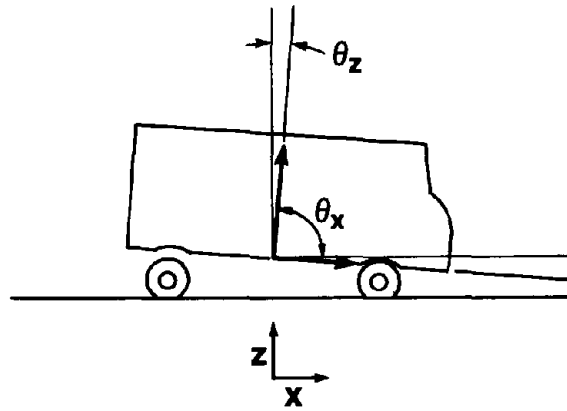
Since the road profile is filtered to exclude the dc component, a fixed value for ϕ does not introduce an error associated with the g term in equation 1. However, if the angle ϕ changes with time, such an error may occur. In addition, if the sensitive axis of the accelerometer is not oriented perpendicularly to the road surface, there will be a cosine error of the form $a_z(1 - \cos \theta_z)$ in the measured component a_z .

The size of the accelerometer orientation error depends in a complex fashion on road roughness and vehicle stiffness. However, Watugala has calculated that the fractional orientation error is $\sim 10^{-5}$ of the measured acceleration and smaller for road profilometer speeds greater than 10 mph.⁽³⁾ This source of error is therefore considered to be negligible.

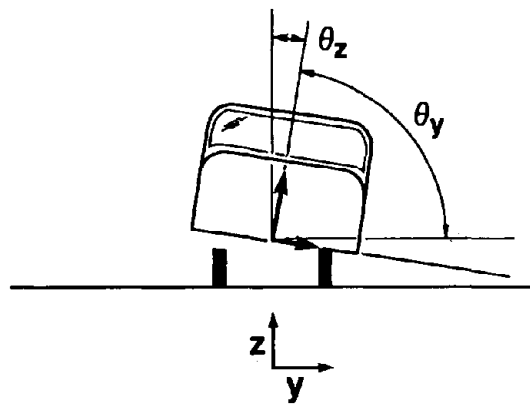
Transducer Errors

In addition to errors in the sensitivity of an accelerometer and its signal conditioning electronics as a function of frequency, transducer errors include linearity, hysteresis, zero offset, alignment, and noise. For the QA-1400 transducers used in the road profilometer, the manufacturer's specifications for these five components are as follows:

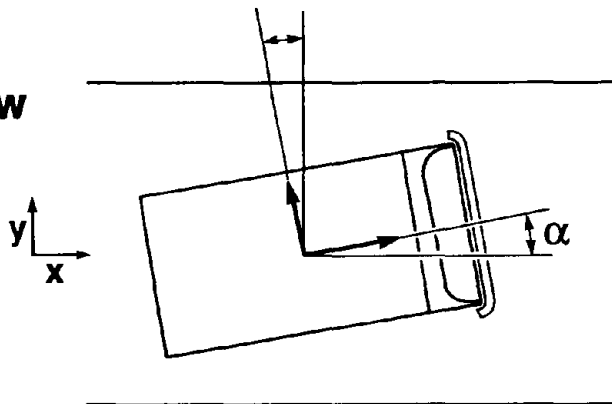
Pitch



Roll



Yaw



Accelerometer Axis Orientation: $\theta_x, \theta_y, \theta_z$

Yaw Angle: α

Road Coordinates: x, y, z

Figure 1. Pitch, roll, and yaw motions of the road profiling van with respect to the road coordinate system.

Range	± 30 g
Linearity	0.01 % @ ± 2 g
Hysteresis	0.001 % of full scale
Zero Offset	0.01 % of full scale
Alignment Error	0.06° @ 2 g
Output Noise	< 100 nA rms

The zero offset should not affect the accuracy of the accelerometer measurements because it is a dc component. The other errors are sufficiently small that they may be neglected in comparison to uncertainties in the overall sensitivity of the accelerometers with their associated electronics.

Accelerometers of the type used on the road profilometer are capable of high accuracy over a frequency range wider than that necessary for road profiling, and are characterized by long-term stability (specified by the manufacturer as 0.1 percent/yr) sufficient to negate any concern over drift. The uncertainties intrinsic to the operation of servo accelerometers are all of the sort whose effects can be effectively removed at the time of manufacture of the road profilometer. Variations in the accelerometer's sensitivity (electrical current output per unit acceleration input) with acceleration amplitude and frequency, ambient temperature, power supply voltage, and the passage of time are all insignificant under operating conditions likely to exist in normal use. The calibration factor, which is what the sensitivity of an accelerometer is called when that sensitivity is essentially independent of frequency (i.e., a flat frequency response), is specified loosely, to ± 10 percent, by the manufacturer but should be determined very accurately during fit-out of the associated electronics of the road profilometer. Although no independent testing of these electronics was done, it is reasonable to assume that the initial use of good electronic design by the manufacturer of the road profilometer should result in short- and long-term uncertainties in the processed accelerometer signals not significantly greater than the ± 0.1 percent/yr drift claimed for the accelerometers themselves.

The two servo accelerometers were temporarily removed from the van and calibrated, at a nominal acceleration of 1 g, over the frequency range from 2 to 50 Hz in order to ascertain that their frequency response was essentially flat. The results of these calibrations, shown in figures 2 and 3, confirm that the sensitivity of each of these accelerometers was flat to within the ± 2 -percent tolerances of the calibration.

Since ac accelerometer calibrations are inherently less accurate than the dc calibrations that are readily attainable using the local value of the acceleration due to gravity, the ac calibrations were not used in conjunction with the operation of the road profilometer.

The implications of accelerometer uncertainties with regard to profile accuracy are discussed below.

Field Test

In addition to orientation and transducer errors, sources of error in the accelerometer results include noise and drift in the associated electronics.

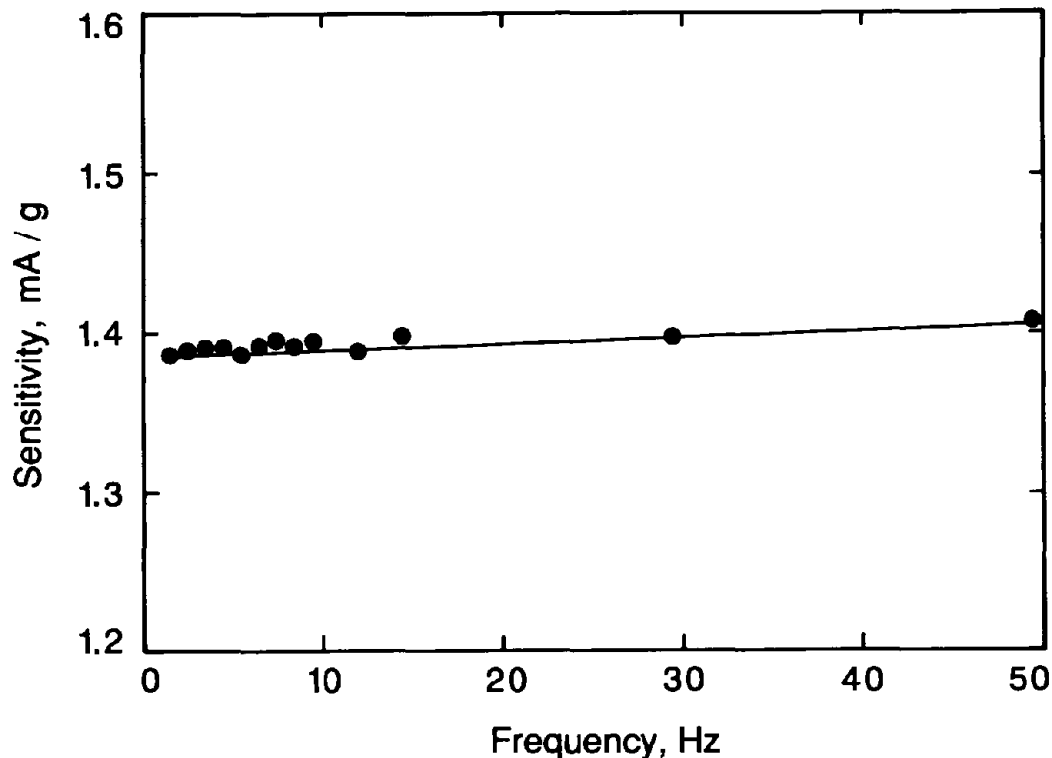


Figure 2. Sensitivity versus frequency for accelerometer S/N 236.

Therefore, field tests were performed on the complete accelerometer system to estimate the total magnitude of the accelerometer errors.

The accelerometer field test involves measurements to determine accelerometer scale factors (for both left and right channels) stored in a special disk file, SCALE.CAL, containing constants of the measurement system.

The procedure recommended by the manufacturer is as follows.

First, an accelerometer reading is taken that constitutes a measurement of the background accelerometer zero. Then a calibrated test current equivalent to a 1 g acceleration (32.17 ft/s^2) is injected into a special test port of the accelerometer, and the resultant accelerometer reading is measured. The difference between the two accelerometer readings is calculated, and used as an indicator of both functionality of the accelerometer and stability of calibration of the associated electronics.

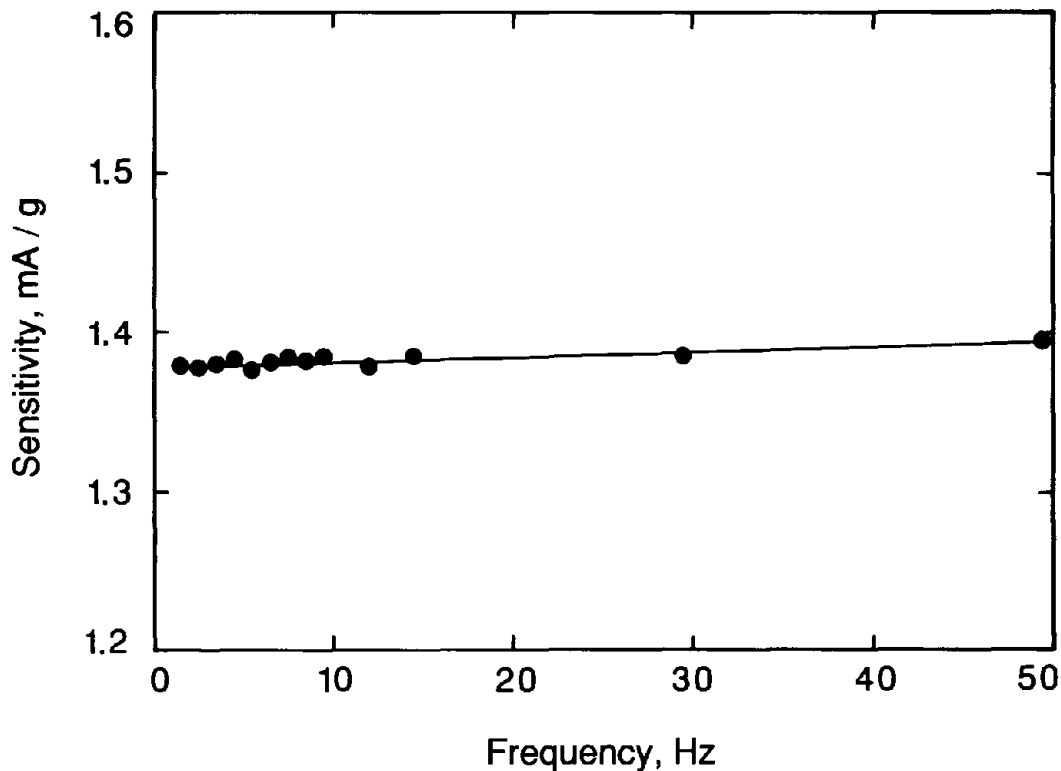


Figure 3. Sensitivity versus frequency for accelerometer S/N 237.

The field tests performed on the accelerometers include both the short-term and long-term variability of the measured g-value. The long-term results were measured between 4/22/87 and 8/31/87. For the right side accelerometer, the one-standard-deviation variability (1σ) was $\pm 0.022 \text{ ft/sec}^2$, which is 0.7 milli-g or 0.07 percent of the measured value; for the left side 1σ was $\pm 0.096 \text{ ft/s}^2$, which is 3 milli-g or 0.3 percent. This value is much higher than either the linearity, hysteresis, or alignment errors estimated above.

The short-term variability was considerably smaller. This was computed from a set of 10 measurements of g taken over a 10-minute period. The 1σ variability was $\pm 0.02 \text{ ft/s}^2$ or 0.6 milli-g for the right side and $\pm 0.01 \text{ ft/s}^2$ or 0.3 milli-g for the left.

Noncontact Sensors

Two important components of error in noncontact sensors are their repeatability and their linearity. The repeatability characterizes the variations in the measured height as a function of time, and the linearity characterizes the variations in the differential height measurements as a function of height itself. The testing procedures and results for these effects are described in the next two subsections, followed by a subsection containing a brief discus-

sion of the sensitivity of the noncontact sensor to variations in the surface material.

Repeatability

The repeatability may be measured by routine testing of the sensor calibration as a function of time. The test consists of measuring the height of a 1-in block positioned on a plate.⁽⁴⁾ The block has a measured height of 1.0004 ± 0.0016 in, as obtained with an interferometric dimensional gauge. Figure 4 illustrates the procedure for the repeatability test. First, the plate is leveled and its height is measured without the block in place. Then the block is slid into position on the plate and its height is measured. The heights of both the top of the block and the plate may be found from measurements of the angle of the rotating polygon mirror. The difference between them (t_b) should equal the 1-in thickness of the block. If the measured height is not equal to the known block height to within a desired tolerance, a calibration constant may be input to the computer so as to produce the correct result.

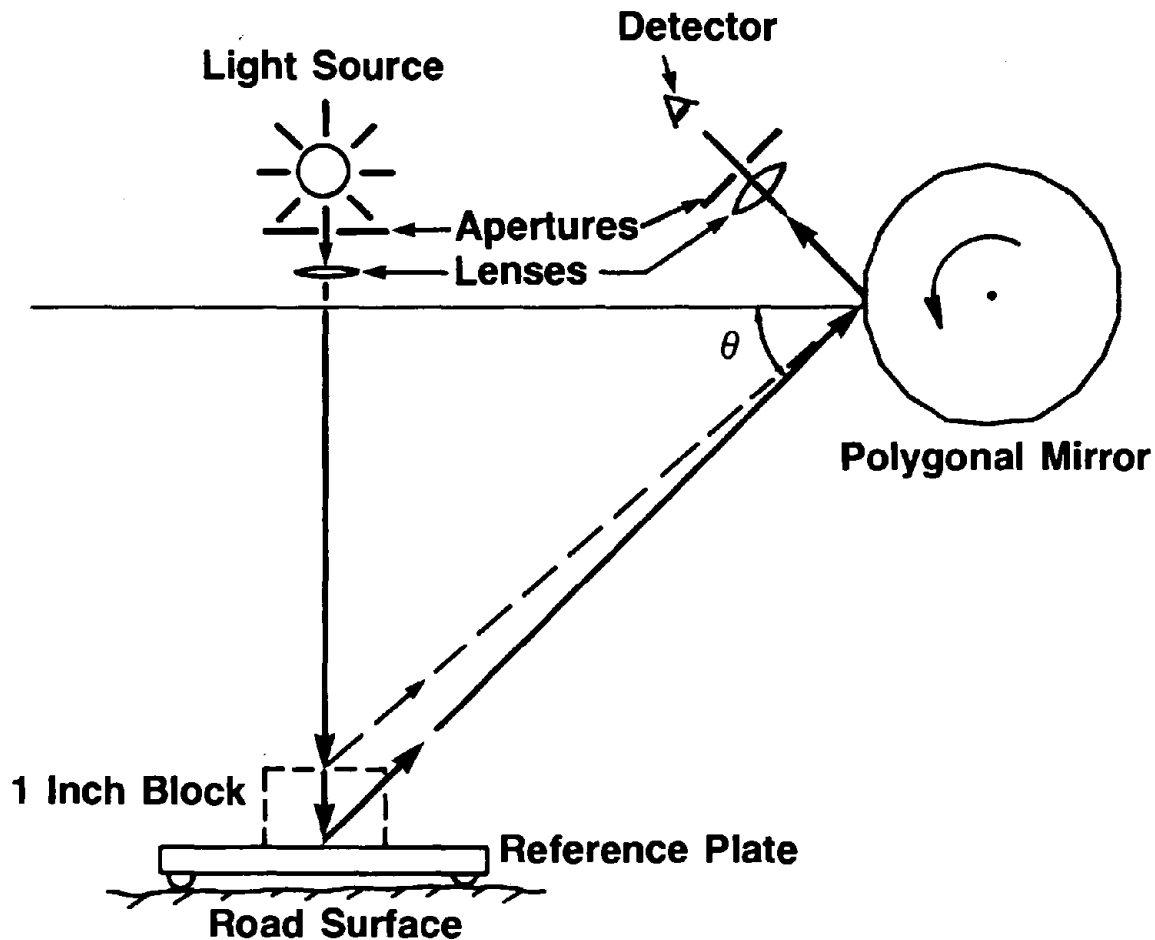


Figure 4. Optical setup of the noncontact sensor showing a measurement of the calibration block.

The measured height may vary for a number of reasons. One likely source of variation in the calibration is change in the alignment of the optical components of the sensor due to distortion of the assembly, either from thermal effects or its own mechanical instability. A second is variation in the properties of the analog elements in the electronics.

The repeatability of t_b was measured over both the short and long term. The short-term repeatability was measured by taking five successive measurements of t_b for each sensor over a period of about 10 minutes. The one standard deviation variability was 0.0007 in for the right-hand sensor and 0.0011 in for the left. Therefore, the short-term repeatability in the sensor calibration was not considered to be a significant source of error.

The long-term repeatability may also be held to a small value since the calibration constant may be changed to offset changes in the height sensitivity of the instrument. The results of the long-term measurements are shown in table 1 along with the calibration constants (scale factors) for both sensors. In some cases the scale factors were adjusted according to the manufacturer's procedure to keep the measured height t_b in good agreement with the calibrated value. In November 1987, the road profilometer was returned to the manufacturer where the right hand sensor was repaired. As a result, the sensitivity of that sensor was adjusted by several percent. Accordingly, the software scale factor was adjusted to compensate for the change in sensitivity in order that the measured t_b would remain close to 1.0 in. This is shown by the data of table 1.

Table 1. Noncontact sensor calibration data.

Date	Right		Left	
	Scale Factor	Calib Value	Scale Factor	Calib Value
4/22/87		0.9925		0.9999
5/11/87	0.2040	1.0024	0.1863	0.9966
5/12/87	0.2018	0.9957	0.1860	1.0051
5/13/87	0.2018	0.9836	0.1860	1.0062
5/14/87	0.2030	0.9987	0.1860	1.0056
5/15/88	0.2030	0.9834	0.1860	0.9890
8/31/87	0.2030	1.0075	0.1860	1.0013
12/11/87	0.2076	0.9976	0.1865	1.0026

The long-term repeatability is plotted in figure 5. One standard deviation of these data was 0.0085 in for the right sensor and 0.0058 in for the left. Therefore, it is clear that the static accuracy of the sensor over the height range represented by the sensor plate and its block can be well maintained with reasonable care by the operator. It appears that the accuracy of the block height measurement could be maintained within 0.005 in, or 0.5 percent, by appropriate adjustment of the calibration scale factor.

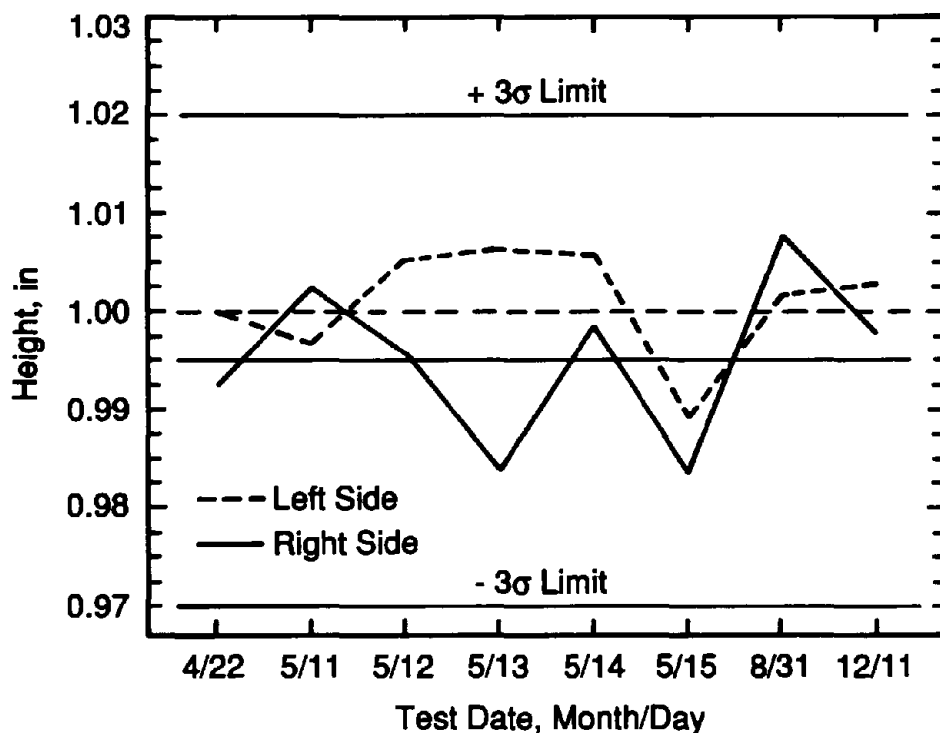


Figure 5. Variation in the measurement of the 1-in calibration block with the noncontact sensor between 4/22/87 and 12/11/87. (The central horizontal lines are the means of the two data sets. The control limits are $\pm 3\sigma$ of the right-side data.)

Linearity

The static accuracy of the noncontact sensors was measured as a function of height. This was done by raising the van on a garage lift and varying the height of the calibration plate with a lab jack. The sensor calibration check was then performed as a function of the height of the plate. The results of measured t_b vs. surface height are shown in figure 6. The abscissa zero is the estimated position of the pavement when the van is motionless on level pavement. In figure 6, the end points of the bars represent the lower and upper surfaces of the block for each height measurement, and the symbols (\bullet or \blacksquare) represent the nominal midpoint. The actual variation in measured height is plotted vertically. Over the 4.5-in range of data for the left sensor, the measurement t_b varies by 3.9 percent from 0.974 to 1.013 in. Over the 5.5-in range of data of the right sensor, the results vary by 3.5 percent from 0.976 to 1.011 in.

The expected variability shown by the theoretical curve of figure 6 agrees quite well with the data. The expected variability comes from the approximation formula for the tangent function in the software of the road profilometer. This formula is the polynomial,

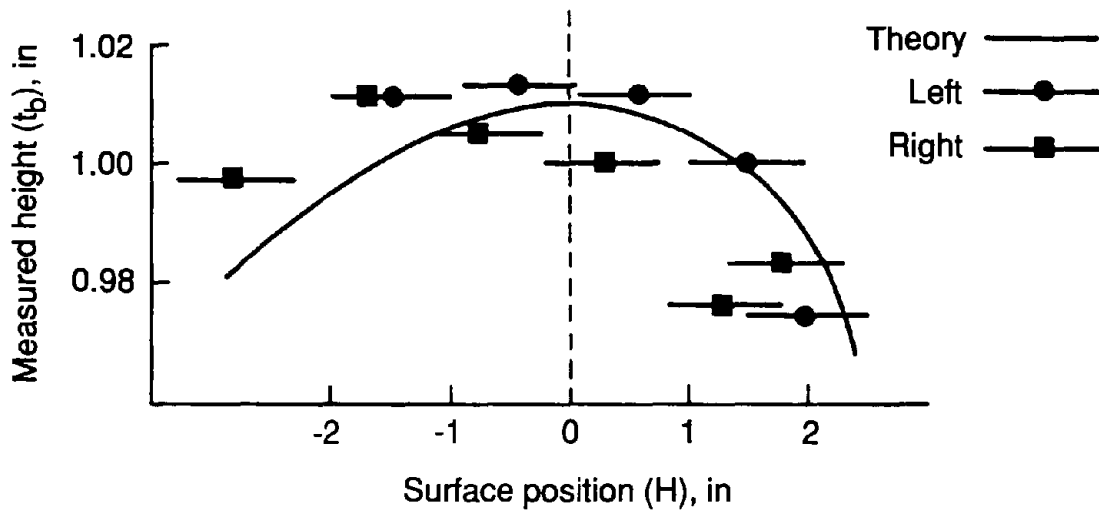


Figure 6. Measured t_b of a 1-in block versus surface height.

$$\tan' \theta = a_0 - a_1 \theta + a_2 \theta^2 = 0.662497 - 0.0202648\theta + 6.16998 \times 10^{-4} \theta^2, \quad (3)$$

where θ is expressed in degrees and \tan' is the symbol used to represent the polynomial approximation to the tangent function.

The accuracy of the above formula vis à vis linearity may be calculated by taking the ratio of its derivative to the derivative of $\tan \theta$ and plotting that ratio as a function of height. If it is assumed that the surface height zero is located at $\theta = 45^\circ$, then the actual surface height h and its derivative are given by

$$h = (1 - \tan\theta)L$$

$$dh/d\theta|_{\text{actual}} = -L \sec^2\theta(\pi/180), \quad (4)$$

when θ is expressed in degrees. However, in the road profilometer computer software,

$$dh/d\theta|_{\text{computed}} = L(a_1 - 2a_2\theta). \quad (5)$$

Therefore the differential sensitivity of the transducer as a function of height is given by the ratio of these two quantities:

$$\text{Sensitivity} = (2a_2\theta - a_1)(180/\pi)\cos^2\theta. \quad (6)$$

The resulting curve is shown plotted as theory in figure 6. Both the data and the theory show a maximum near the middle of the graph ($h = 0$) and both show that the sensitivity decreases more rapidly above the height zero than below it. Therefore, the departure from linearity of the noncontact sensor is largely explained by the approximation for the tangent function in the road profilometer software.

An estimate of the error caused by the sensor nonlinearity can be obtained by estimating the error in the measured height of a 2-in roughness asperity centered around the nominal zero ($\theta = 45^\circ$), assuming that the noncontact sensor has been calibrated using a 1-in block with its lower surface at a nominal height of 0.5 in. The 2-in height is a reasonable estimate of a peak-valley height that would be encountered by the sensor for a fairly rough road. The nonlinearity is introduced here by using the polynomial formula $\tan^2 \theta$ instead of the tan function itself. The resulting calculated value of asperity height is 2.008 in instead of the correct value of 2.000 in, corresponding to a 0.4 percent error due to sensor nonlinearity.

Contribution to Profiling Uncertainty

The profiling uncertainty due to the noncontact sensor can be estimated by quadratically adding the contributions from repeatability and linearity. The uncertainty is taken to be 0.7 percent for the repeatability component and 0.4 percent for the linearity component. The root-sum-square combination of these two components is 0.8 percent.

Signal Sensitivity to Pavement Reflectivity

The sensitivity of the sensor to pavement reflectivity was investigated by looking at the height and shape of the electronic road surface pulse that reproduces the pulse of light that occurs when the scattered light from the road is reflected into the detector by the rotating polygonal mirror.

For reflection from both the fairly light metallic surface of the calibration block and the fairly black anodized surface of the jack used in the linearity test, the road pulses were clean, with a single sharp peak, and well above the detection threshold. Therefore, any uncertainties due to pavement reflectivity are not expected to be significant.

Wheel Encoder

The road profilometer software includes a provision for adjusting the encoder scale factor (Δ) that represents the distance traveled for each encoder pulse. This calibration is done by manually indicating to the computer the beginning and end of a measured distance over which the van travels. Since Δ can change with such factors as tire wear, tire pressure, and tire temperature, it is important that the wheel encoder be calibrated frequently. The major source of error in calibration of the wheel encoder is probably the operator's ability to determine when the van crosses the beginning and end of the measured course. For example, if the van is traveling over a measured mile at 50 mph, an uncertainty of 10 ft at both the beginning and end of the course would correspond to an error of 0.4 percent in the wheel-encoder scale factor.

Expected Profiling Accuracy

The uncertainties in measurements of both profile amplitude and weighted root-mean-square acceleration (a parameter discussed later) are estimated in this subsection. These estimates are based on the errors in the three principal system components. The components of profiling error associated with the accelerometer system, the noncontact sensor, and the wheel encoder are, respectively, δP_{acc} , δP_{ncs} , and δP_{enc} . The corresponding components of error in rms acceleration are δA_{acc} , δA_{ncs} , and δA_{enc} .

Error Estimates for Accelerometer System

The uncertainty δA_{acc} in measurements of weighted rms acceleration due to errors in the accelerometer measurements themselves is estimated to be 0.3 percent (1σ) from the data previously discussed and is considered to be a conservative estimate of that source of error.

To estimate the uncertainty δP_{acc} in the measured profile due to errors in the accelerometer measurements, a random walk model was developed for the propagation of the accelerometer error when the accelerometer signals are doubly integrated to yield the road profile. This model yields an amplitude error proportional to $N^{3/2}$, where N is the number of data points in one cutoff length (300 ft). The model requires, as an input parameter, a measured result for short-term variability in the accelerometer data. Such results were obtained on 8/31/87. The resulting uncertainty (1σ) in profile amplitude due to the accelerometer system is $\delta P_{acc} = 0.028$ in.

Error Estimates for Noncontact Sensor

The estimated uncertainty in profile amplitude δP_{ncs} due to the noncontact sensor was calculated previously to be 0.8 percent (1σ) over a 2-in range of amplitude. This fractional uncertainty should propagate directly into an uncertainty δA_{ncs} of 0.8 percent in the calculation of weighted rms acceleration.

Error Estimates For Wheel Encoder

An error in Δ directly leads to a comparable error in the measured velocity V , a quantity raised to the second power in the second term of equation 1.

Sensitivity tests of the profile and parameter changes that occur when the scale factors for the accelerometer, height sensor, and encoder are systematically varied indicate that the overall amplitude of the profile is determined by low-frequency, high-amplitude structures in the profile sensed by the accelerometer, rather than by the high-frequency features measured by the height sensor. Therefore, the measurement of profile amplitude is highly dependent on the accuracy of the wheel encoder scale factor.

Errors in the sampling interval also affect the filtering term in equation 1, but the net result is to change the effective filter cutoff length by a small percentage. This is not a significant source of error in the measurement of profile height. Therefore, the fractional error in the profile due to the

encoder is estimated as

$$\frac{\delta P_{\text{enc}}}{P} = 2 \frac{\delta V}{V} = 2 \frac{\delta \Delta}{\Delta} = 0.8\% , \quad (7)$$

based on the fractional error in Δ , previously estimated to be 0.4 percent, and the quadratic dependence in the accelerometer term of equation 1.

The weighted rms acceleration, computed using the profilometer software, is affected differently. From a sensitivity analysis, it seems that this quantity is affected much more by the high frequency structure measured with the noncontact sensor than by the accelerometer readings. Therefore the changes in overall profile amplitude due to changes in the encoder scale factor do not lead to significant changes in the calculated rms acceleration. However, the calculation of rms acceleration involves the digital calculation of a second derivative with respect to lateral position. The calculated acceleration is therefore inversely proportional to the square of the lateral scale factor, Δ . The fractional error is estimated as

$$\frac{\delta A_{\text{enc}}}{A} \approx \frac{2\delta \Delta}{\Delta} = 0.8\% . \quad (8)$$

Combining Sources of Error

The errors estimated in the three preceding subsections are now combined to develop an uncertainty budget for measurement of both the amplitude of the road profile and the weighted rms acceleration. For measurement of profile, δP_{acc} , δP_{ncs} , and δP_{enc} are combined quadratically. The first term δP_{acc} is an additive error factor whereas the other two terms are better represented as percentages. Therefore the combination yields

$$\begin{aligned} \delta P_{\text{tot}} &= \pm \left[(0.028)^2 + (0.008P)^2 + (0.008P)^2 \right]^{1/2} \\ &= \pm \left[(0.028)^2 + (0.011P)^2 \right]^{1/2} \text{inch } (1\sigma). \end{aligned} \quad (9)$$

δP_{tot} is considered to be a 1σ uncertainty in the peak-to-valley height (P) measured over a sample 300 ft long. For road profiles with small amplitude, the uncertainty is limited by the first term (0.028 in). For profiles with peak-valley amplitudes greater than about 2.5 in, the second term becomes the larger factor.

For measurement of weighted rms acceleration, the three terms, δA_{acc} , δA_{ncs} , and δA_{enc} are combined to yield

$$\delta A_{\text{tot}} = \pm \left[(0.3\%)^2 + (0.8\%)^2 + (0.8\%)^2 \right]^{1/2} = \pm 1.2\% (1\sigma). \quad (10)$$

The above analysis shows a 1.1 percent scaling uncertainty in the direct measurement of profile heights, besides the 0.028 in additive uncertainty, and a 1.2 percent scaling uncertainty in measurement of the second derivative of height. Therefore, the uncertainty in the Mays index, as computed from a measured profile, would have a scaling component of 1.1-1.2 percent because the Mays index is essentially a slope parameter. That is, it represents the first derivative of profile height, intermediate between height itself and acceleration. The uncertainty in the Mays index should also include an additive component due to the single integration of the accelerometer reading, which is analogous to the first term in equation 9. However, this term is not expected to be significant because any error arising from the integration would be essentially a slow drift in the profile height, an error that is filtered out of both the Mays and acceleration calculations by the vehicle response functions to be described later.

Software

The signals from the hardware components discussed above are combined via the software to produce the profiling results, and the question now arises concerning whether or not errors, if any, or approximations in the software constitute a significant source of error in the results.

The software for profile measurement is a proprietary code named PROFILE written in assembly language. The sequence of operations that this software carries out is described below.

When the wheel encoder output indicates a forward travel of 1-in from that of the previous reading, the four channels of digitized information are read consecutively. These are the right-track accelerometer, left-track accelerometer, right-track noncontact sensor, and left-track noncontact sensor. The four data values are massaged and summed with previous readings using software described elsewhere, and a resulting, filtered value for profile height is computed.⁽²⁾ The individual height readings are then averaged in sets of 12 to produce values of profile height averaged over a 1-ft interval for each wheeltrack. These average values are recorded on magnetic tape at 0.5-ft sampling intervals.

Software errors could arise from the filtering and summing algorithms, from lack of simultaneity in the reading of the A/D signals, or from the quantization increment of the recorded data. The filtering algorithms are discussed later in this report and the conclusion reached there is that the software performs correctly. The quantization increment of the recorded data is 0.001 in, which is negligible compared to other potential sources of error and, in particular, to the difficulty of even defining where a road surface is to an accuracy approaching 0.001 in.

Review of the performance specifications for the minicomputer used in the road profilometer shows that the analog-to-digital conversions and the calculations required to compute the profile height are completed faster (within about 400 μ s) than the sampling interval for the noncontact height sensor.

Thus it is concluded that neither time synchronization of the data acquisition and analysis, nor other key aspects of the software, are significant sources of error in the profiling results.

Rocking Tests

The adequacy of performance for three elements of the road profilometer - the on-board computing system, inertial profile reference system, and noncontact sensors - should be periodically verified. A qualitative assessment of the sensitivity of the instrumentation package to undesired vehicle motions can be accomplished by observing the road profile while the vehicle is manually shaken (or rocked) to induce a roll, pitch, or yaw mode. The travel sensing system is not sensitive to these motions, and thus it suffices to conduct the rocking tests while the vehicle is standing still. This section describes such tests for the purpose of determining the limits of excursion for the observation profile in terms of two single-number roughness ratings, based on analyses of the recorded profile using the on-board computer and system software.

During initial tests, the profile output (figure 7a) was observed as a function of time for about 30 seconds in a quiet environment with no disturbances of the vehicle. This step was necessary in order to establish a noise and drift baseline for the subsequent motion tests. Ideally, the curves in figure 7a should be flat horizontal lines; the variations shown probably represent noise rather than drift. Typical average values for the Mays index and rms acceleration computed by the road profilometer software using the recorded profiles during these tests were 4.9 in/mi and 0.86 milli-g, respectively. Following the motion tests, these baseline values were found to be approximately the same as during the initial tests.

During rocking tests, the van was manually excited in a pitching, yawing, or rolling mode. The full (peak-to-peak) amplitudes were ≈ 2 in for the pitching motion as measured at the rear bumper, ≈ 1 in for the yawing motion as measured at one end, and $\approx 2\frac{1}{2}$ in for the rolling motion as measured at the running board. Typical profiles are shown in figures 7b, 8a, and 8b. For the two modes exhibiting the greatest motion and consequently the maximum recorded profile, namely pitching and rolling, typical computed values for the Mays index and rms acceleration were 10.6 and 6.6 in/mi and 2.3 and 1.3 milli-g, respectively.

The computed Mays index and rms acceleration for the smoothest road profiled during a field test program employing the road profilometer were on the order of 50 in/mi and 10 milli-g, respectively. For the test sites considered to have an average roughness, the corresponding values were approximately 160 in/mi and 40 milli-g.

Based on these tests and comparison of the single-number roughness ratings under various conditions, it is concluded that noise effects determined from rocking tests were negligible compared to the measured roughness statistics, assuming that the road profilometer system is linear. The typical values for these roughness statistics for even the smoothest road surfaces which were profiled were considerably larger than those values computed based on the maximum motion of the vehicle induced during rocking tests.

Profiling Consistency

There is a practical limit to the reproducibility in measuring road profiles because there is imprecision involved in locating the wheeltrack and in

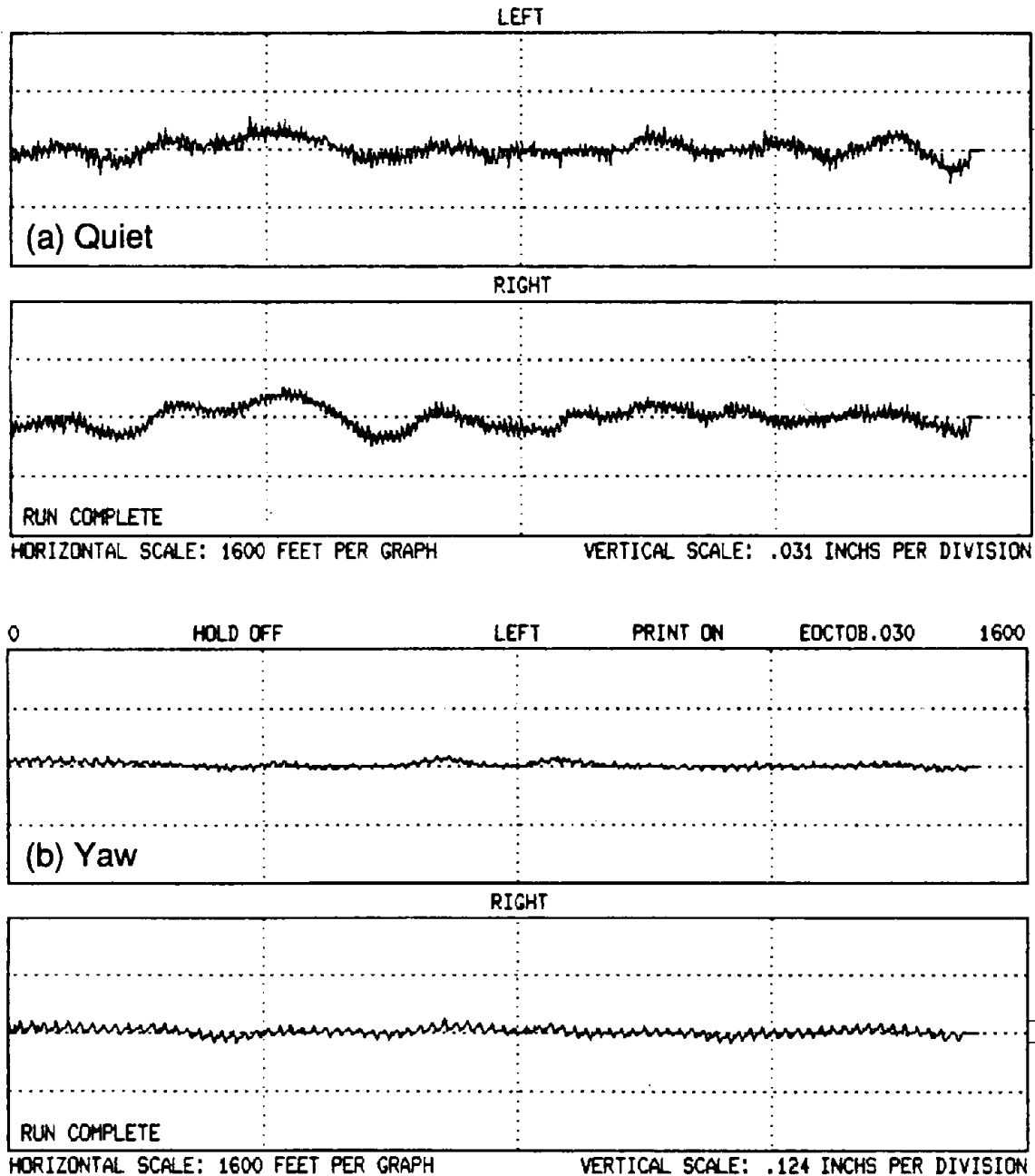


Figure 7. Typical recorded profiles for the road profilometer (a) while sitting completely still and (b) with a yaw excitation. (Note the change in vertical scale between the two profiles. The profiles were recorded for approximately 30 s; the horizontal scale is drawn assuming a speed of ~33 mph.)

initiating the beginning of a surface to be profiled. In this section, profile plots and computed single-number roughness ratings based on software analyses of the profiles are shown for repeated measurements on three road surfaces.

Figure 9 shows the agreement among three profiles measured with the road profilometer at a speed of 30 mph on South Drive, an asphalt road surface. The good agreement among these profiles for the right wheeltrack was also obtained

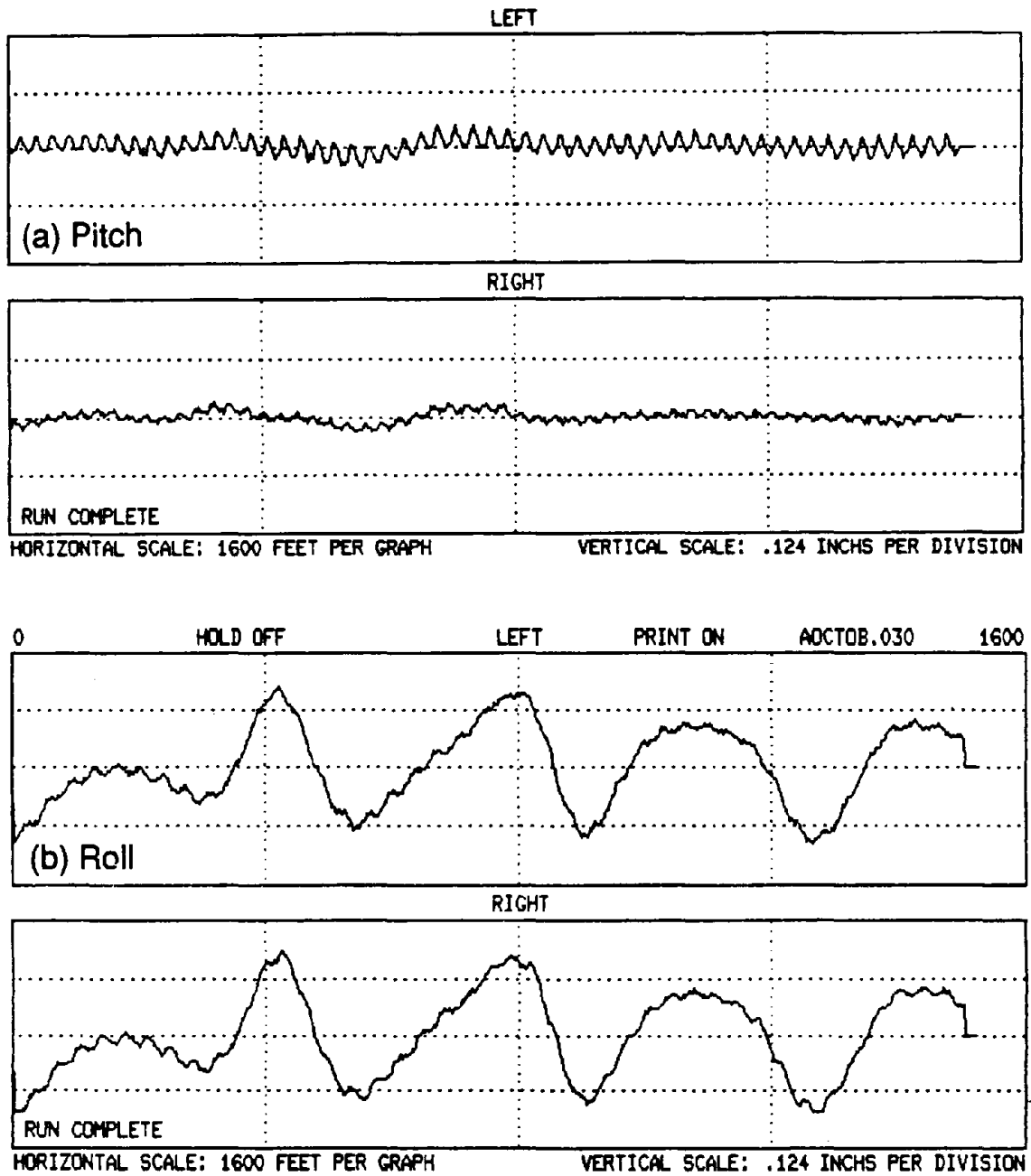


Figure 8. Typical recorded profiles for the road profilometer under (a) pitch and (b) roll excitations.

when visually comparing the left wheeltrack profile plots. The Mays indices computed for these three measurements, based on analyses of both wheeltrack profiles at a test speed of 30 mph over a profiled length of 1200 ft, were within 5.3 in/mi of each other. This variability was of the order of 3.6 percent of the average Mays index for this road surface.

The second comparison of profile plots recorded by the road profilometer during repeated measurements was made using data for a smooth bituminous concrete road surface. Figure 10 shows the agreement among eight profiles for the left wheeltrack measured with the road profilometer at a speed of 50 mph on the Blue Grass Parkway in eastern Kentucky. Good agreement among the right wheeltrack profiles was also obtained. The Mays indices computed for these measurements at a test speed of 50 mph over a profile length of 5280 ft were within 2.5 in/mi of each other. This variability was on the order of 5 percent of the average Mays index for this relatively smooth road surface.

A third comparison of profile plots recorded by the road profilometer was made for a relatively rough portland cement concrete road surface. Figure 11 shows the agreement among four measured profiles for the right wheeltrack measured at

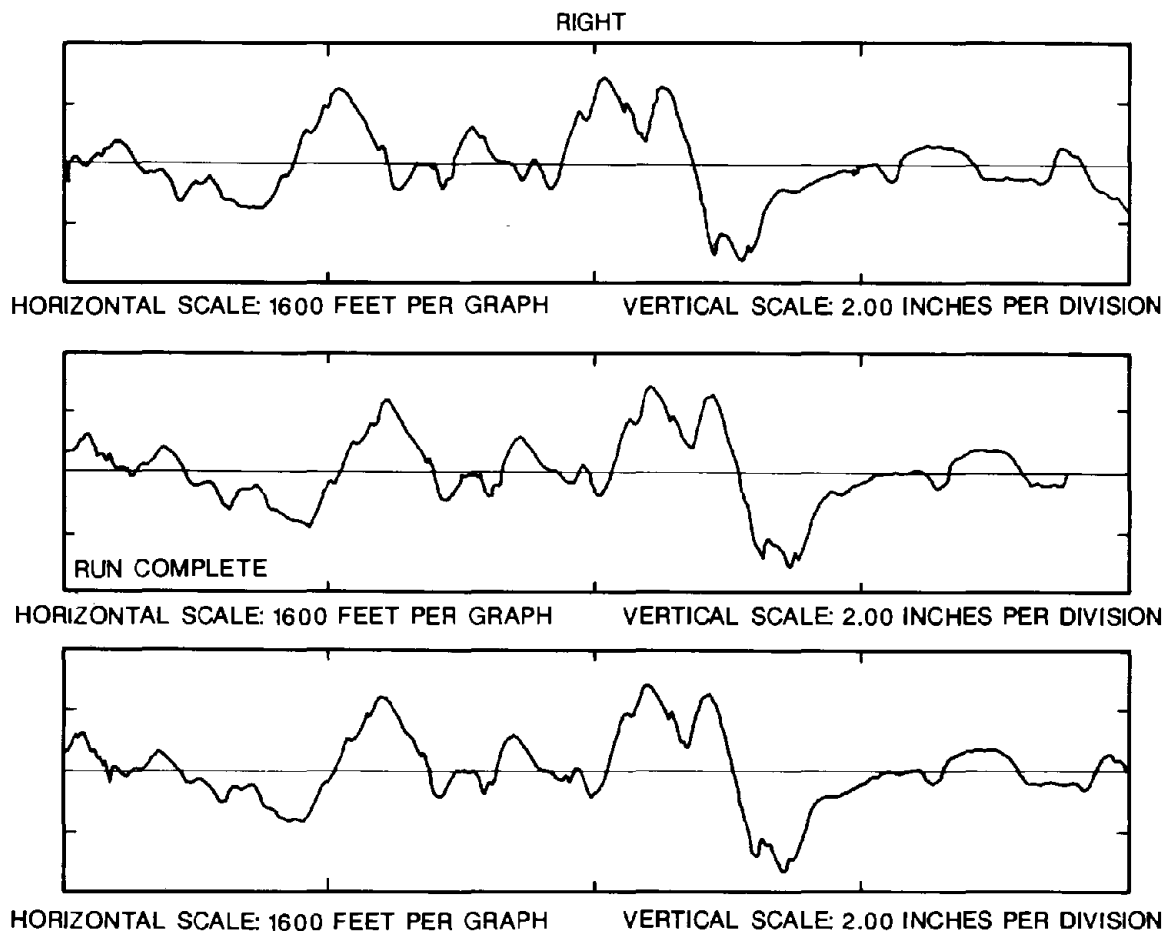
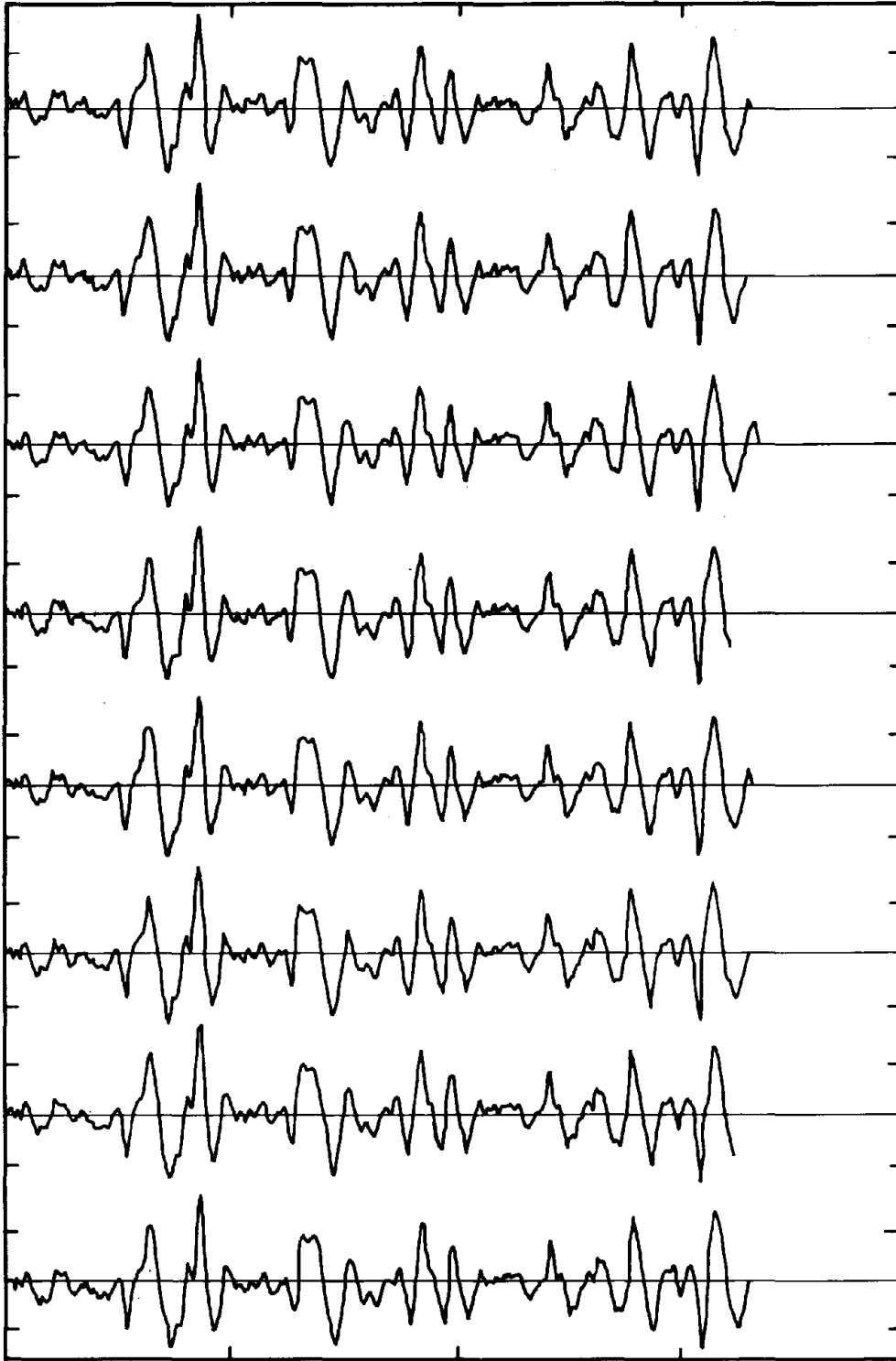


Figure 9. Example of the repeatability of the road profilometer during three measurements on South Drive.



HORIZONTAL SCALE: 6400 FEET PER GRAPH

VERTICAL SCALE: 1.00 INCHES PER GRAPH

Figure 10. Example of the repeatability of the road profilometer during eight measurements on the Blue Grass Parkway in Eastern Kentucky.

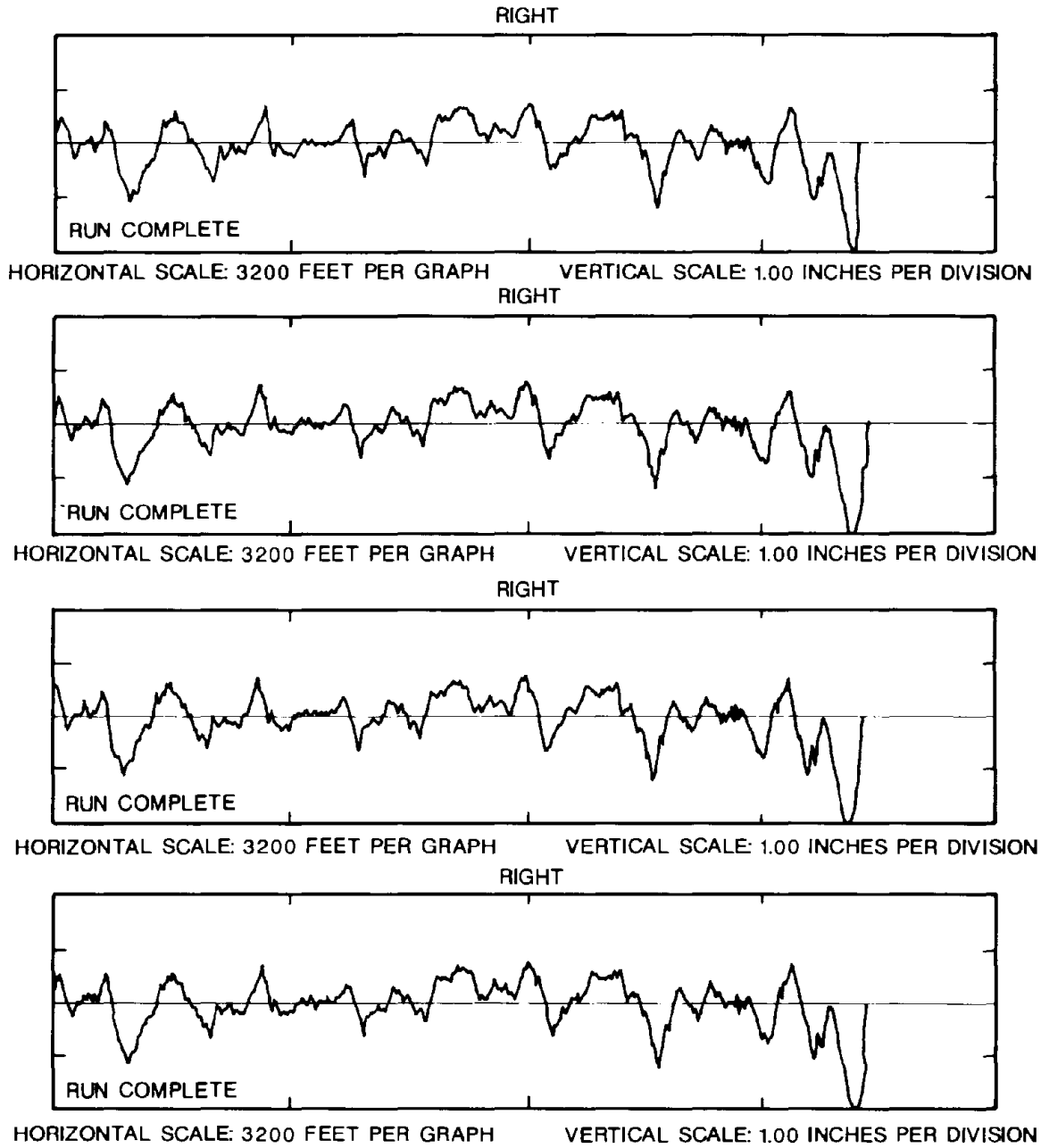


Figure 11. Example of the repeatability of the road profilometer during four measurements on Route 60 in Eastern Kentucky.

a speed of 50 mph on Route 60 in eastern Kentucky. Similarly good agreement was again found for the left wheeltrack. The Mays indices computed for these measurements at a test speed of 50 mph over a profiled length of about 2640 ft were within 5.9 in/mi of each other. This variability was of the order of 3.5 percent of the average Mays index for this road surface. The reproducibility levels in these examples were all obtained based on data recorded using the same vehicle operator, who attempted to drive in the same wheeltracks during successive measurements. The wheeltracks were not marked, and the variation associated with these measurements includes variability both in locating the start of a profile measurement and the lateral imprecision in the wheeltrack position.

Profiling Accuracy Tests

The present section discusses three tests of the overall accuracy of the road profilometer.

First, several road profiles obtained with the road profilometer were compared graphically with profiles obtained from rod-and-level measurements of the same roads. These graphical comparisons test the accuracy of the long wavelength response of the road profilometer, because it is the shapes and relative positions of the major peaks and valleys of the profile that show up on the profile graph.

Second, the short wavelength response of the road profilometer was tested by comparing profiles obtained for a sharp step input with those expected from the rated characteristics of the road profilometer.

Third, road statistics calculated from the road profilometer profiles were compared with those calculated from the rod-and-level profiles.

For the two profiling tests, an important consideration is the high-pass filter of the road profilometer. The raw rod-and-level profiles generally contain an overall slope from beginning to end and also the long-wavelength structure in the road. These features are attenuated in the road profilometer profiles by the high-pass digital filtering that takes place during measurement. Therefore, similar high-pass filtering of the rod-and-level profiles must be performed in order to compare them to the road profilometer results.

Rod-and-Level Testing

Four rod-and-level profiles were measured by two teams, one for the Maryland roads and one for the Kentucky roads.

The Maryland team measured a 1540-ft section of South Drive. The profile was taken on this road along a line of manhole covers located close to the right-hand wheel track in the eastbound lane. The sampling interval was 10 ft.

The Kentucky team measured three profiles. Their locations and specifications were:

- 1) The Blue Grass Parkway near milepost 48 on the eastbound direction in the right wheeltrack of the right hand lane. The profile length was 1056 ft and the sampling interval was 1 ft.
- 2) Kentucky State Route 151, just north of the Blue Grass Parkway, in the northbound direction, in the right wheeltrack. The profile length was 1056 ft and the sampling interval was 0.5 ft.
- 3) Same site as (2) but the left wheeltrack. The overall profile length was 1582.5 ft. The sampling interval was 0.5 ft for the first 1056 ft of profile and 1.5 ft between the 1056 and 1582.5 ft markers.

The four profiles were given the names: South Drive, Blue Grass, 151 Right, and 151 Left.

The two teams used similar procedures for the rod-and-level profiles. A geodetic level was set up and leveled on the side of the road section to be measured. Then, a tape was stretched along a 100-ft section of wheelpath to mark the correct sampling positions. For each data point a level rod was held parallel to the direction of gravity at each marked sampling position. The level was sighted on the rod, and the height on the rod that was coincident with the cross hair in the leveled telescope was measured. By subtraction, the height of the road with respect to the cross hair could be determined.

For each setup, a 100-ft long section of road was measured. For lengths longer than this, errors due to the varying index of refraction of the air path between the level and the rod can become significant. The relative heights of the 100-ft sections were tied together by careful measurements of the beginning and ending points from adjacent setups. In addition, the Kentucky team placed the rod on fixed features near to the road and sighted on these from two adjacent setups.

Certain details of the equipment were different between the two teams. The Maryland team used a metric rod with smallest line spacing of 1 cm and a micrometer comparator with a least count of 0.0001 m. The bottom end of the rod was spherical and about 1-inch in diameter. The Kentucky team used a rod with line spacings of 0.01 ft which they interpolated to 0.001 ft. The bottom end was slightly convex. Its shape in the horizontal plane was elliptical with approximate dimensions of 1.5 in by 2.5 in.

The repeatability of the rod-and-level data was measured separately by the Kentucky team. Five profiles were taken along a 50-ft tape laid out on a flat parking lot. For each profile, 50 points were taken, one at every foot marker along the tape. Thus, each profile point was measured five times. The first profile is inconsistent with the other four. The cause is not known, but it was likely some human error in the setup of the first run. The other four runs are quite consistent. The standard deviation of the four readings averaged over the 50 profile points is ± 0.0026 ft. This figure serves as a good estimate of the repeatability of the rod-and-level data.

South Drive, in Maryland, was chosen because of its convenience to home base. It was envisioned that its profile could be used as a sort of check standard of

the operation of the road profilometer from time to time. The Kentucky roads were part of a cooperative survey between NIST, the Kentucky Department of Highways (KY DOH), and Surface Dynamics, Inc., to test the accuracy of the road profilometer as well as the repeatability of KY DOH Mays meters. The Blue Grass Parkway (BGP) site was the smoothest asphalt concrete section in the survey. The KY 151 site was one of the rougher sites in the survey.

The four rod-and-level profiles are shown plotted on figure 12. Their total amplitudes, from highest point to lowest point, range from about 6 ft for the BGP site to about 22 ft for the left wheeltrack of the KY 151 site. For a proper comparison with the road profilometer results, the very-low-frequency information shown in figure 12 must be filtered out to get at the higher-frequency road roughness information that is obtained with the road profilometer.

A subroutine was written in BASIC to simulate the high-pass digital filter of the road profilometer. The input data were the unfiltered rod-and-level profiles, and the output results were filtered profiles that should look like the ones measured with the road profilometer.

The filtering subroutine was one component of a data analysis program to analyze rod-and-level profiling data. This software is outlined in appendix A. The algorithm is based on the one developed for the road profilometer itself.⁽²⁾

A flow chart of the filter drawn up along the lines of the Spangler patent is shown in figure 55 of appendix A.⁽²⁾ It is a standard 3-pole Butterworth high-pass filter. The nominal cutoff length L was set at 300 ft to match the filter cutoff of the road profilometer measurements. Prior to the digital filter itself, the subroutine also included a straight-line fit to minimize initial transients in the data. First the data were pinned by subtraction so that the first point in the profile was identically equal to zero. Then the value of the slope of a straight line was calculated to minimize the least-squares deviations between it and the data. The single-parameter straight-line fit should also minimize the initial transients.

The filtered rod-and-level profiles resulting from this procedure are shown in figures 13 to 16 along with the corresponding road profilometer profiles as output directly on that instrument's printer. The rod-and-level profiles have been shifted upward from the road profilometer profiles to make for a clear comparison between the two. For all of these figures, the major features of the rod-and-level profiles are duplicated very well by the road profilometer.

Figure 13 shows the road profilometer results for South Drive, compared with the filtered rod-and-level profile measured along the right hand wheeltrack there. The major features of both profiles are strikingly similar, indicating that the road profilometer accurately measures the larger features of the road surface profiles in accordance with its stated filtering characteristics. The road profilometer data are smoother than the filtered rod-and-level data because the sampling interval of the road profilometer is 0.5 ft, whereas the interval for this set of rod-and-level data is 10 ft.

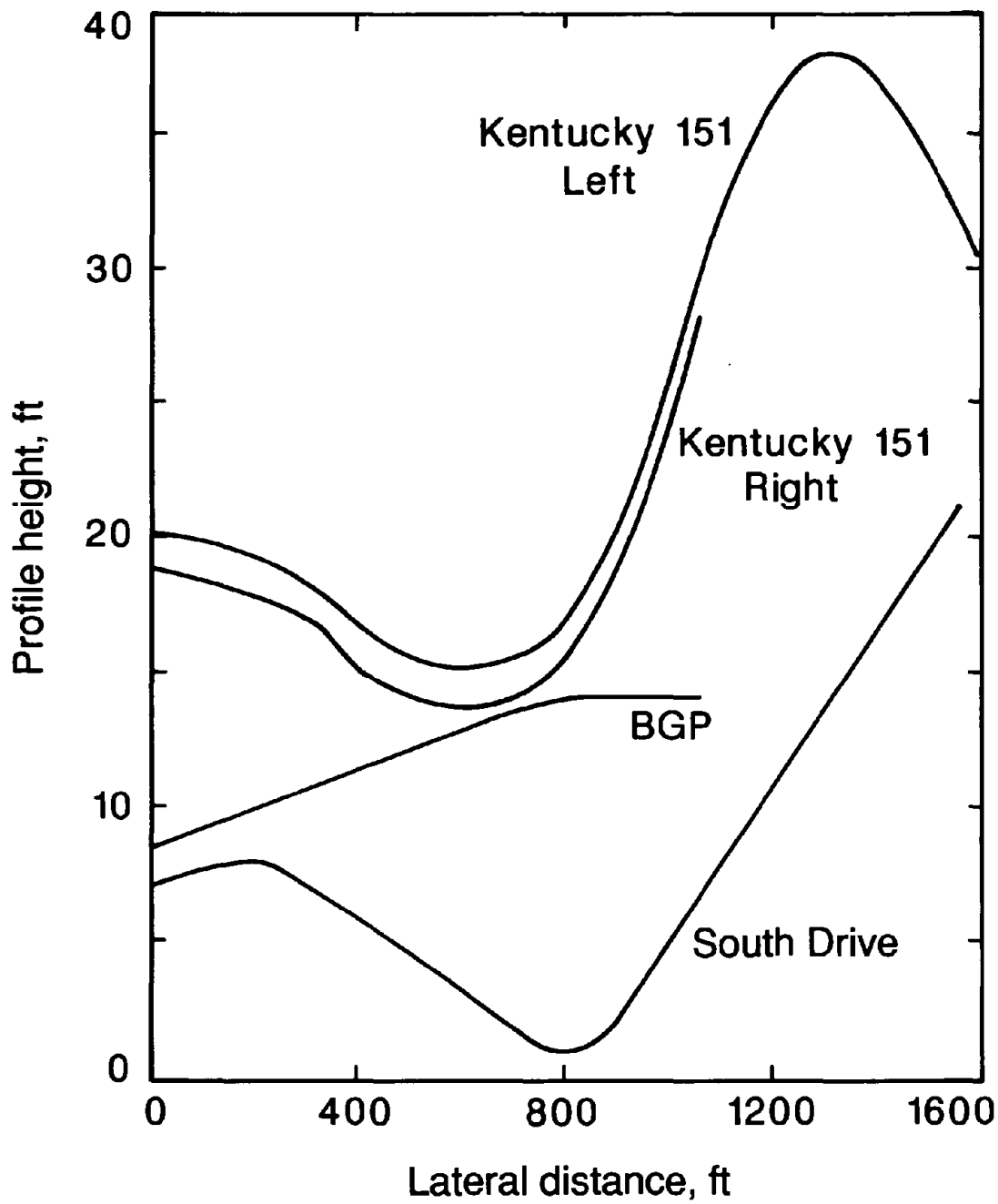


Figure 12. Unfiltered rod and level profiles of four roadways. (The profiles have been displaced vertically for clarity.)

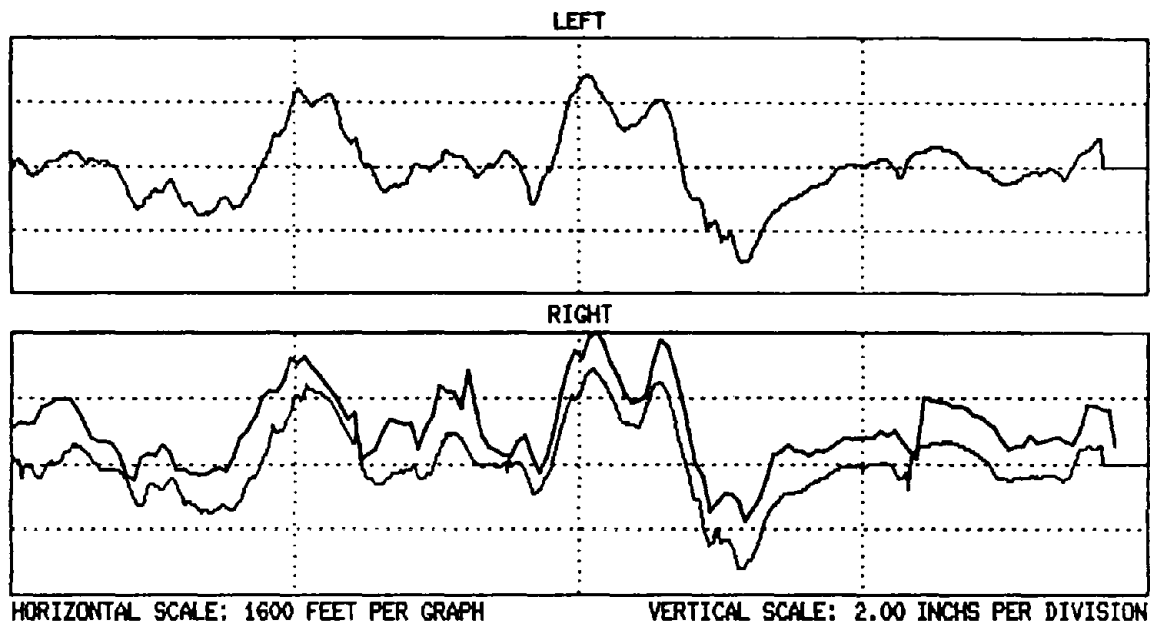


Figure 13. Road profilometer results for South Drive compared with filtered rod-and-level data taken along the right wheeltrack. (The rod-and-level data form the upper curve shown for the right wheeltrack.)

Figure 14 reveals similar results. The upper curve is for a 1056-ft segment of the Blue Grass Parkway. The rod-and-level profiles of figure 14 are smoother than those of figure 13 because the sampling interval of these data is 1 ft instead of 10 ft. Once again the features of the road profilometer profiles match those of the rod-and-level profiles very well. This observation holds even when the profiles are examined with higher resolution. The lower curve of figure 14 shows the initial 400-ft length of profile at four times the scale of the upper curve. The major features of the two types of profiles agree quite well, but there is some disagreement for the finest features, probably due to aliasing errors and wheelpath deviations. These effects are discussed in detail below.

The Blue Grass Parkway site of figure 14 was a comparatively smooth road. Figure 15 shows the profiles for both wheeltracks of the KY Rte. 151 site, which was significantly rougher. As in figure 14, the profile length was 1056 ft, but the sampling interval was 0.5 ft. Once again, the major features of the rod-and-level profiles are duplicated in the road profilometer profiles. However, there are several apparent outlier points in the rod-and-level data that are probably due to human error in the rod-and-level observations.

The rod-and-level data taken on the left wheeltrack on KY Rte. 151 were also extended to 1582.5 ft with a sampling interval of 1.5 ft. That entire length of profile for the left wheeltrack is plotted in figure 16, once again revealing good agreement with the road profilometer but also showing evidence of a few discrete outlier points in the rod-and-level data.

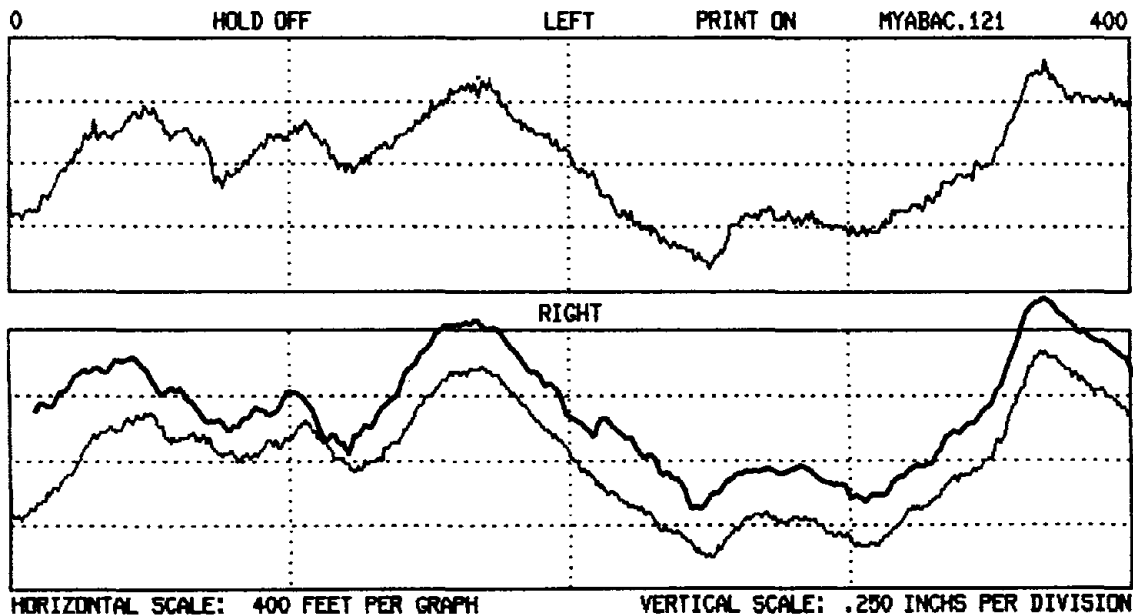
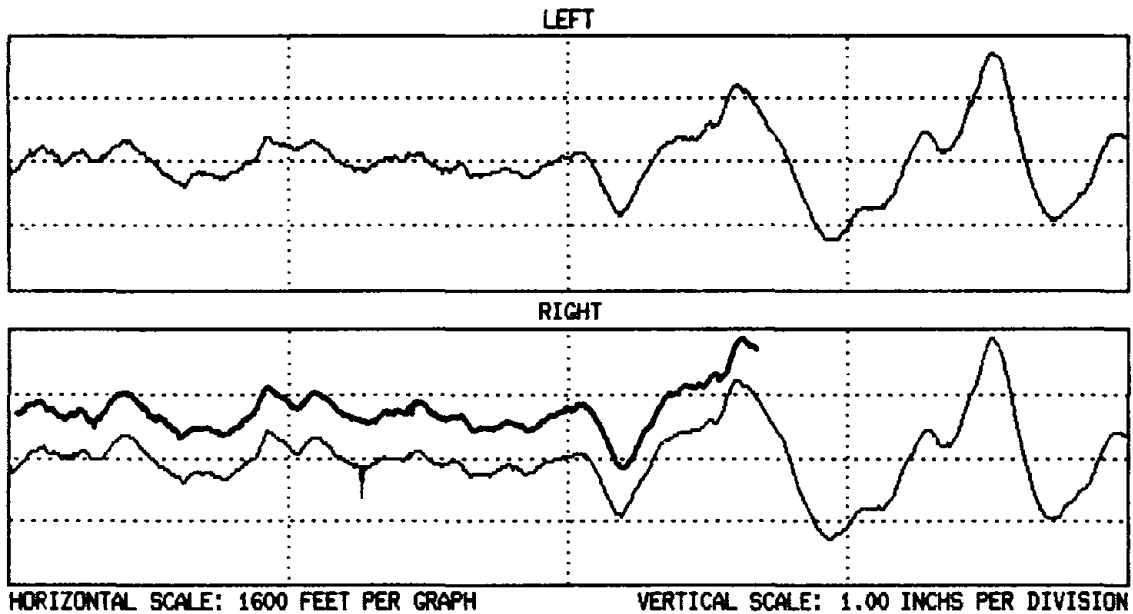


Figure 14. Road profilometer results for the Blue Grass Parkway compared with rod-and-level data taken along the right wheeltrack. (Data are displayed with two scales; the lower graph is a magnified rendition of the first 400-ft section of the upper graph. For each graph, the rod-and-level data form the upper curve for the right wheeltrack.)

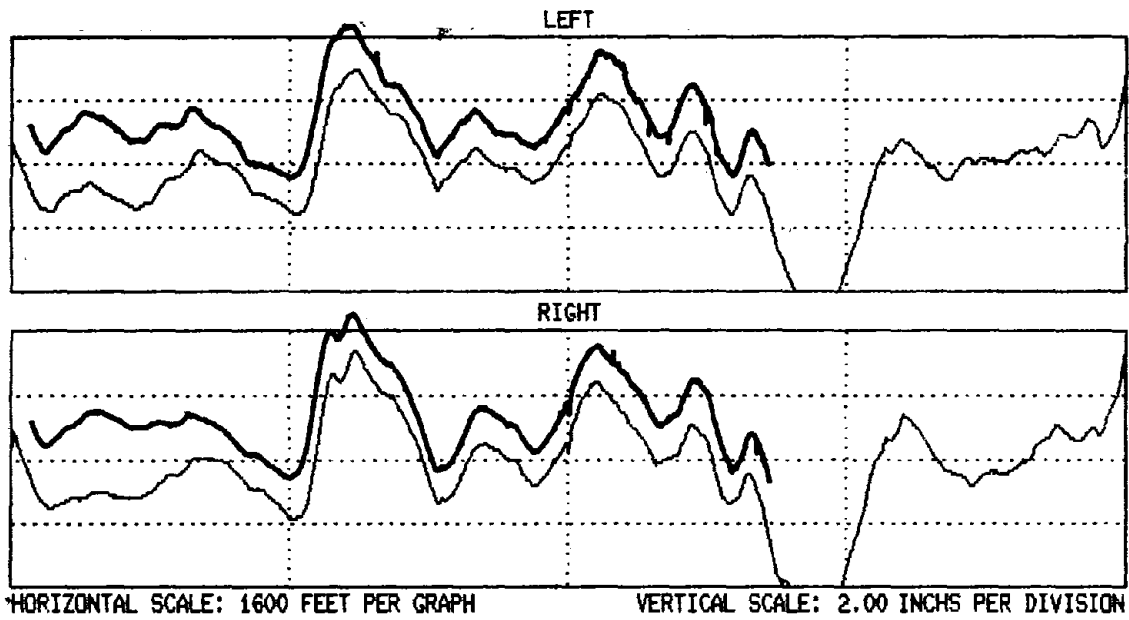


Figure 15. Road profilometer results for Kentucky Rt. 151, Northbound, with filtered rod-and-level data for both wheeltracks. (The rod-and-level data are the heavier curves that have been shifted upward for clarity.)

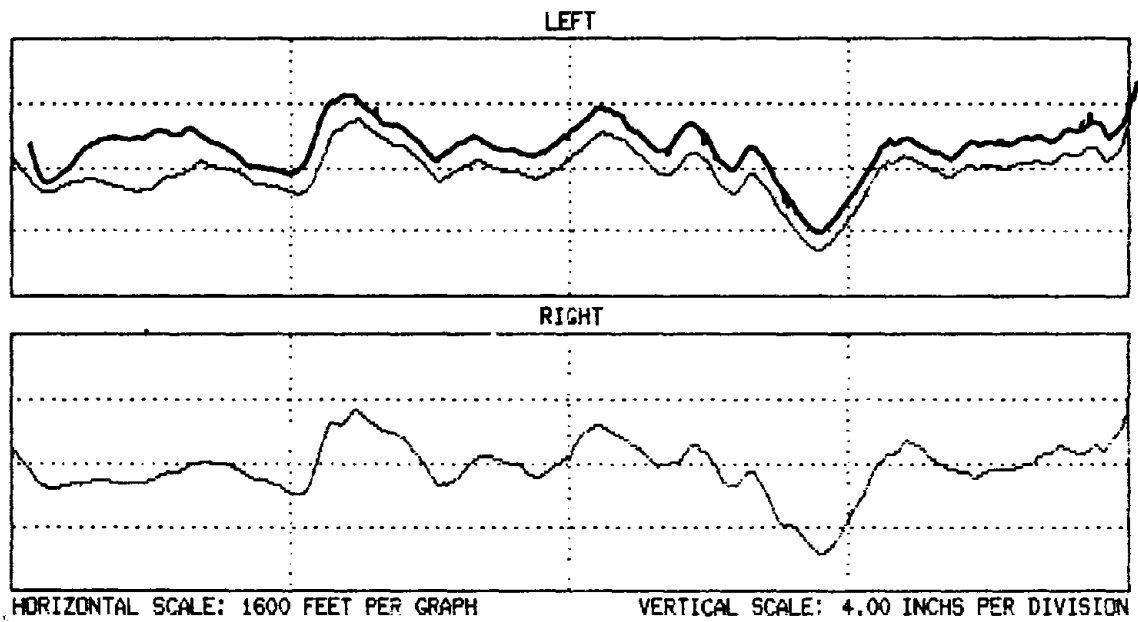


Figure 16. Road profilometer results for Kentucky Rt. 151, Northbound, with filtered rod-and-level data for the left wheeltrack measured over 1582.5 ft. (The rod-and-level data form the upper curve shown for the left wheeltrack.)

In general, the two types of profiles agree very well. However, there are several sources of error that cause deviations between them. Those effects that arise in connection with the rod-and-level profiles are initial transients, outliers, and aliasing. Two additional sources of deviation are the variation of the wheelpath and the longitudinal (i.e., in the direction of travel) scale calibration. Each of these components is discussed below.

Initial Transients

If the initial height and slope of the rod-and-level profile are not equal to zero, the filtering procedure leaves an initial transient signal in the filtered profile. In order to minimize this effect, the initial point of the rod-and-level profile is assumed to begin at the origin and a best line is fitted to the data as described before. However, if the fitted rod-and-level data have a steep initial slope, there may be a significant, but decaying, transient that occurs in the first 300 ft of the filtered profile.

In contrast, the road profilometer profiles were initiated after an appreciable start-up distance during which data were measured, integrated, and filtered. Any initial transients had decayed by the beginning of the data record.

The initial transient in the rod-and-level data is most clearly shown in figure 16. The trends in the rod-and-level profile over the first 300 ft are slightly different from those of the road profilometer profile. The initial transients are not as apparent in the other three graphs because the initial slopes of the raw rod-and-level profiles match the overall slopes fairly well.

It should be particularly noted that the initial transient in the filtered rod-and-level data of figure 16 is significantly different from that of the left wheeltrack of figure 15, although the raw data were identical. This happens because the slopes of the fitted best lines are different for the two data sets. The best line for figure 15 is fitted over the first 1056 ft of profile, whereas the best line for figure 16 is fitted over the full 1582.5-ft profile (see figure 12). The data in figure 16 therefore have a higher slope and the initial transient has a deeper minimum than in figure 15.

Outliers

The rod-and-level data are subject to human error, because the observer must repeatedly read and interpolate a linear scale sighted through the telescope of the level. The errors that occur can sometimes be easily recognized since they show up as single points significantly above or below neighboring data points in the profile and differing from them by discrete amounts such as 1 ft, 0.1 ft, or 0.05 ft. The most obvious ones in the raw rod-and-level data have been corrected by interpolating between adjacent readings. However, less obvious outliers appear when the rod-and-level data are filtered. Examination of the data revealed a single outlier in figure 14, at least seven in the data for figure 15, and seven in the data for figure 16.

These outliers do not affect the major features of the filtered profiles. However, they should be removed from filtered profile data prior to any subsequent statistical analysis.

Aliasing

The outliers discussed above would present less of a problem were it not for aliasing in the rod-and-level profiles. Aliasing occurs because the resolution of the rod-and-level profiles is limited by the point spacing, as discussed below. As stated previously, the low-frequency limits of the two types of profiles are nearly identical because the same high-pass digital filter has been applied to both types. At the high-frequency end of the spectrum of road wavelengths, the sensitivities of the two types of methods are quite different.

The short wavelength limit of the road profilometer measurements is approximately 1 ft. The initial sampling interval of the measurements is 1 in, but these measurements are processed so that the sampling interval of the recorded data is 6 in and each recorded point represents an average of 12 readings. That is, the data are smoothed over 1-ft intervals of travel. This procedure improves the signal-to-noise ratio of the data for the desired measurement bandwidth of 1-300 ft and simulates the smoothing function of tires for shorter road wavelengths. It is also an anti-aliasing procedure that limits the bandwidth of measured wavelengths to be consistent with the sampling interval.

There is no such anti-aliasing smoothing for the rod-and-level data. The short wavelength limit of these measurements is determined by the size of the base of the rod which is approximately 2 in. However, the sampling interval for these data is 6 in or more. Therefore, the bandwidth of the measurements is wider than the spatial bandwidth determined by the sampling interval. That means, for example, that the rod can rest in a narrow, deep hole in the road at one of its sampling positions. The hole may be only a few inches wide, but in the rod-and-level profile it would appear to be equal to the sampling interval. For the road profilometer, the presence of such a hole would be largely attenuated by the smoothing routine. As a result, the finest structures appearing in the rod-and-level profiles are likely to be quite different from their counterparts in the road profilometer profiles.

Longitudinal Scale Calibration

Figure 14 seems to exhibit a small difference between the longitudinal scales (i.e., the x-axis direction) of the two types of profiles. The rod-and-level profile appears longer than its counterpart. The distance encoder of the road profilometer can be calibrated to a few tenths of a percent by careful measurement of the 1540-ft surveyed length of South Drive. However, the encoder may drift in calibration by a few tenths of a percent due to variations in tire pressure or tire wear. Therefore the uncertainty in the longitudinal scale (along the road) is estimated to be approximately 0.5 percent.

The sampling interval of the rod-and-level measurements is determined by the markings on the measuring tape. Therefore, the accuracy of sampling intervals depends on how smoothly the tape is stretched along the roadway. Any errors in this procedure likely tend to reduce the actual sampling interval and make the measured profile appear longer than it should. This is the effect seen in figure 14. However, experienced rod-and-level surveyors can hold the longitudinal error to less than 0.1 percent.

Wheeltrack Differences

The sideways positions of the rod-and-level profiles in the lanes were precisely measured. However, this was not the case for the road profilometer profiles. The positioning of the road profilometer was estimated on the fly by the driver. Based on measurements taken early in the project, we estimate that a skilled driver can hold the tracking variation to ± 8 in. However, since the two kinds of profile tracks are not identical, the finest structures appearing in the resulting profiles are likely to be different.

In spite of these sources of error, the graphical comparisons described above indicate that the road profilometer is capable of accurate measurements of the larger road features (for wavelengths from, say, 10 to 300 ft) within the stated limitations of its high-pass filter. Wheeltrack differences and aliasing effects limit the ability to test its accuracy for profiling smaller features (size < 10 ft). To accomplish this, some tests using flat plates were performed, as discussed below.

Some preliminary testing was also performed on a slightly different profiling system, developed by the University of Michigan Transportation Research Institute (UMTRI).^(5,6) Like the other road profiling system, this system uses accelerometers to measure the motion of the van and optical noncontact sensors to measure the distance between the van and the road. However, the noncontact sensors in this instrument sense riding height with a position-sensitive array detector instead of with a rotating mirror and timing circuitry. The system also has a third sensor located between the other two, so that it can measure the rut depth of wheeltracks in addition to road profile.

For road profiling, the biggest difference between the two systems is the high-pass digital filter. The UMTRI system uses a phase-corrected, moving-average filter whereas the road profilometer uses a 3-pole, Butterworth filter. The two different filters yield different profiles over the same stretches of road.

One example of these differences is shown in figure 17. Here the profile of South Drive as obtained with the UMTRI system differs from the one obtained with the road profilometer, figure 13.

Nevertheless, it should be possible to simulate the UMTRI profile from the rod-and-level data by applying the moving-average filter. This was done and the resulting filtered profile is shown in figure 17 above the measured profile. The moving-average baseline was 300 ft for both. All of the features in the rod-and-level profile match ones in the UMTRI data. However, there is evidently a systematic difference in height calibration for the two sets of measurements. The peak-to-valley amplitude of the UMTRI profile is approximately 11.8 in, but that of the filtered rod-and-level profile is approximately 16.2 in, suggesting a difference in calibration of about 25 percent between the two systems. Additional measurements would need to be performed to trace the actual source of the apparent difference.

Flat Plate Tests

The short wavelength response of the road profilometer was determined by mea-

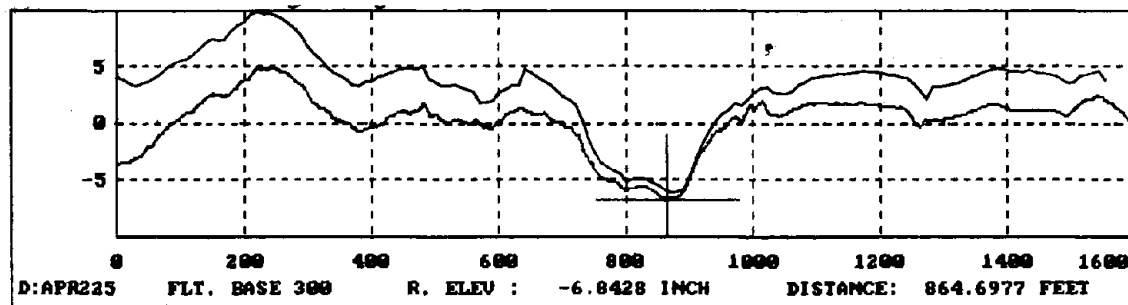


Figure 17. Road profiling results obtained by the UMTRI system compared with rod-and-level data filtered by a moving average, high-pass digital filter. (The rod-and-level data form the upper curve.)

suring profiles of flat plates. The flat plates served to generate sharp-pulse inputs to the sensing system. The response of the system to such an input should be predictable based on its rated characteristics.

Sketches of the flat plates are shown in figure 18. They are of rectangular shape with dimensions 18 by 24 by 5/8 in thick. The plates are rounded at the edges to prevent damage to the tires of the road profilometer. Two identical plates were fabricated so that the output response could be measured for three types of inputs: a single pulse input on one wheeltrack, simultaneous pulse inputs on both wheeltracks, and two sequential pulse inputs on one wheeltrack.

It was envisioned that such a plate might be useful in field checks of the road profilometer impulse response, because it can be set down in a protected area, such as a parking lot, and profiled at low speeds. The plates are portable. Each one weighs about 26 lb. In retrospect, it seems that only one plate is needed for field testing, rather than two.

The plates had through holes for bolting them to inserts in the road, but for the tests described here, they were fastened down with thick, double-sided foam tape. They were profiled at speeds less than 10 mph to prevent them from rebounding from the road and colliding with the underside of the van or with the noncontact sensor during measurement.

The standard profiling software (PROFILE) in the road profilometer will not accept speeds less than about 11 mph. Therefore, to profile at speeds less than this, a second program, TSTFIL, must be used that simulates the wheel encoder pulse rate at approximately 34 mph. When it measures the profile, this program is useful for testing the transducers both at slow speed and while the van is motionless. However, longitudinal distance on the output profile must be reckoned by means other than the (incorrect) scale on the profile graphs.

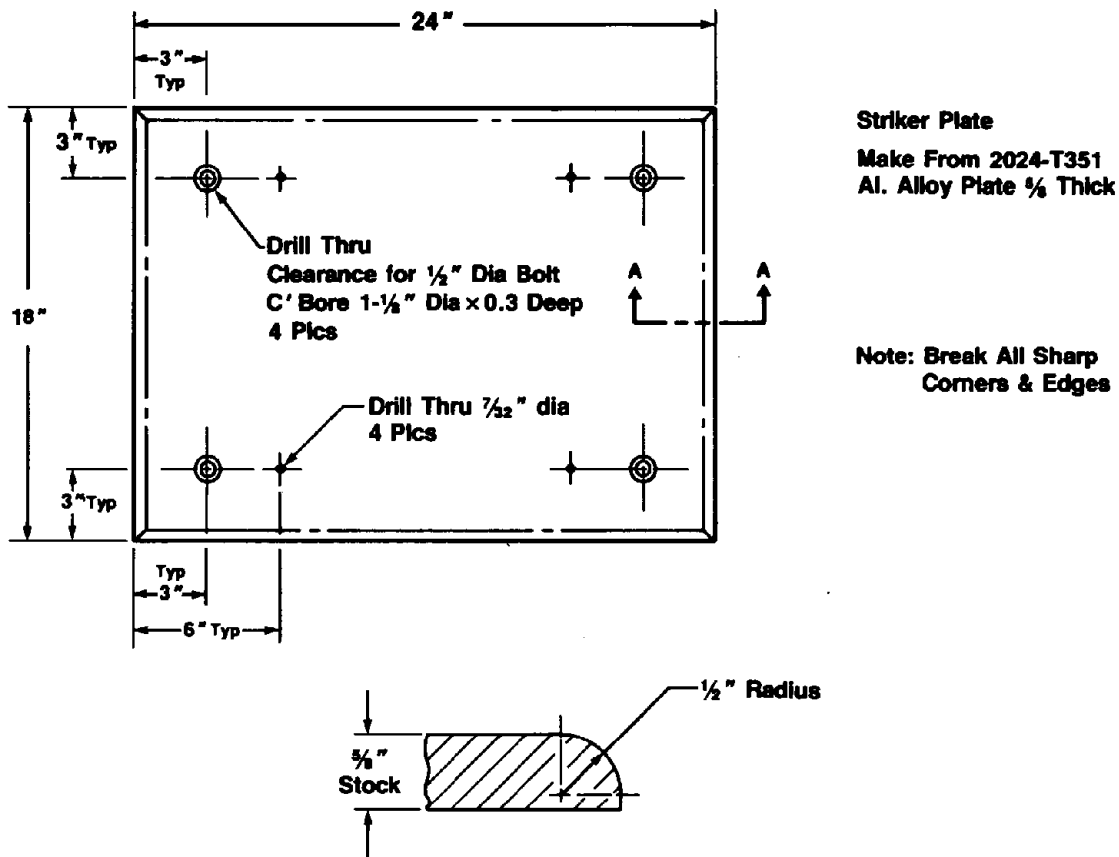


Figure 18. Design sketch of a road plate for testing the short-wavelength response of road profiling vehicles.

A typical profile for two plates placed sequentially along the wheeltrack is shown in figure 19. The first plate was placed so that its short dimension (1.5 ft) was parallel to the direction of travel. The other was placed so that its long dimension (2 ft) was parallel to the direction of travel.

The data were taken at an approximate speed of 8.4 mph, whereas on the graph the simulated speed is 34.1 mph. Hence the lateral scale is distorted by a factor of 4.1. The leading edges of the plates were actually 21.5 ft apart. Using that figure as a scaling factor, the two pulses shown on the graph have widths of 1.7 and 2.6 ft, values within reasonable limits of the actual ones, given the uncertainties in determining the edges of the transient pulses on the profile and the rounding of the plate edges. The heights of the leading edges of the profile traces are 0.67 and 0.70 in, once again within experimental error of the true value of 0.625 in. The decay of each pulse is due to the filtering algorithm in the data-taking procedure. The filtering cutoff length was a nominal 300 ft, but in reality scaled down by a factor of 4.1 to 73 ft.

Another profile (figure 20) emphasizes the effect of the filter. Here the 2-ft length of plate was measured at a speed of approximately 5.1 mph. The filter

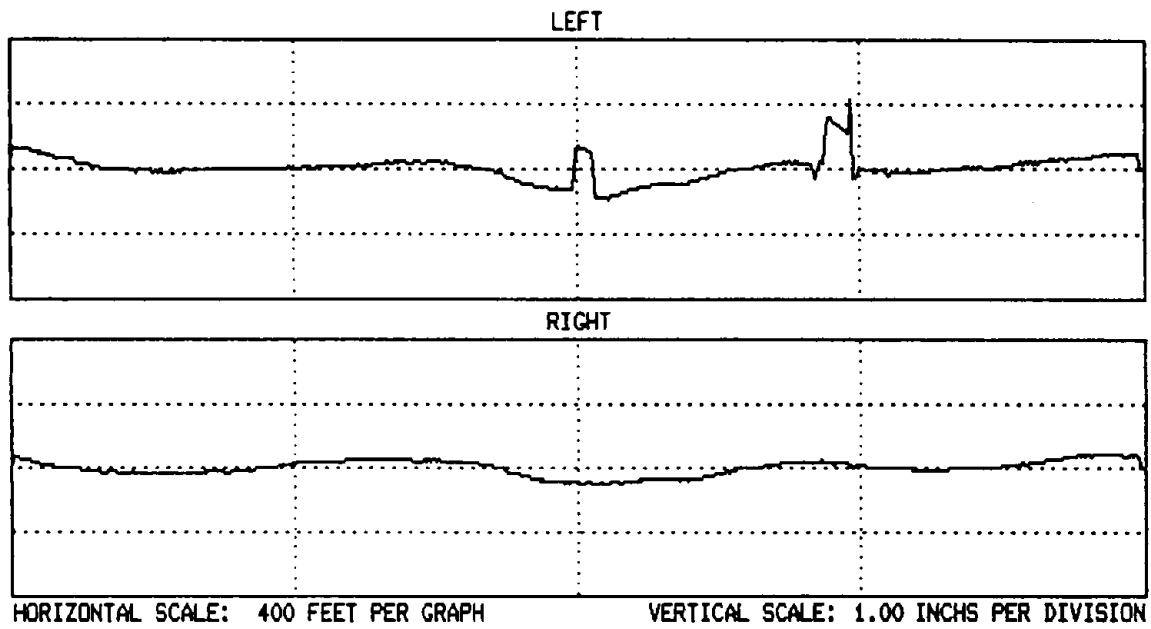


Figure 19. Road profiles obtained when two test plates are positioned along the left wheeltrack of the road profilometer. (The horizontal scale is distorted by a factor of 4.1; the spacing between the leading edges of the plates is actually 21.5 ft.)

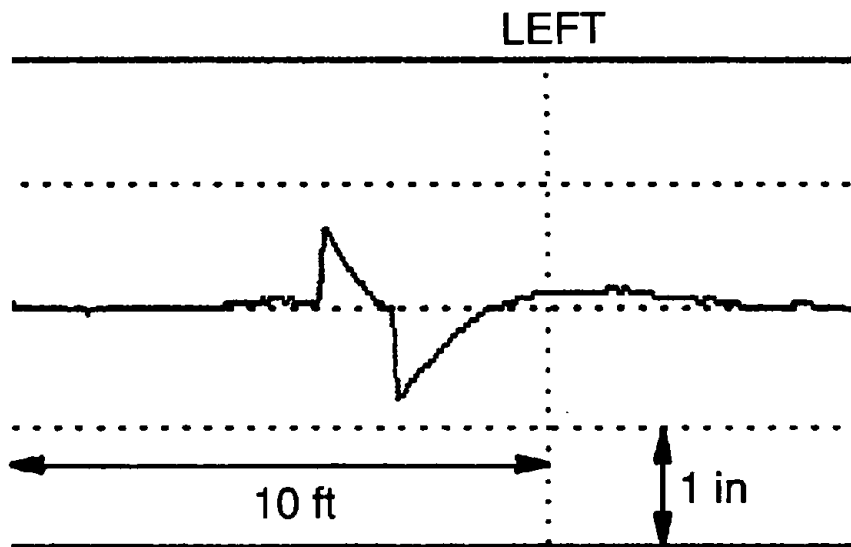


Figure 20. Detail of a profile for a single plate. (The units shown are corrected ones; the filter cutoff here was 14.8 ft to emphasize the decay of the square pulse.)

cutoff was nominally 100 ft, but was actually about 14.8 ft when the longitudinal scale-distortion factor is taken into account. The substantial decay of the pulse over the 2-ft length of the plate is clearly evident here.

A simulation of the filtering algorithm was performed with a cutoff length of 14.8 ft, assuming a profile with a pulse input of 0.625-in height and 2-ft length. The result is shown in figure 21. All of the features of the measured pulse profile are duplicated very well by the simulation. From these data it is concluded that the road profilometer is capable of an accurate response to short road wavelengths, as well as long ones, within the resolution limits of its sensor.

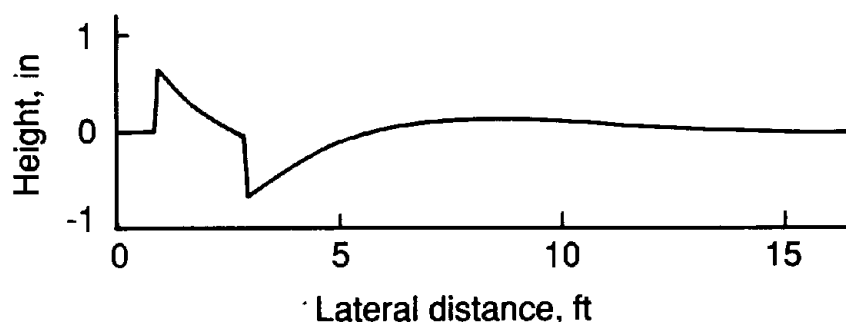


Figure 21. Mathematical simulation of road profilometer response to a square pulse input with height of $5/8$ in and width of 2 ft. (The filter cutoff was 14.8 ft.)

Two types of profiling errors were encountered while measuring these plates. First, an anomalous pulse sometimes appears on the trailing edge of the plate profile (see figure 19). The probable cause is stray reflection from the plate edge. As the illumination spot passes over the rounded edge, the light specularly reflected from the edge at a certain instant can be directed into the noncontact sensor and cause a spurious pulse of light that precedes the actual measurement pulse, and hence makes the measured profile point appear higher than it really is. It might be worthwhile to apply a finish to the plate that would reduce such specular reflections.

The second error is an apparent waviness that can show up when the profile is measured at a low speed. The probable cause of this is acceleration and pitching of the van at slow speeds, because of the difficulty of maintaining a constant speed less than 10 mph. This error can probably be corrected by using a long enough distance from the starting position to the plate position and by taking special care to maintain a constant speed over the plate with no pitching, acceleration, or deceleration.

Single-Number Roughness Ratings

The profile graphs are indicators of the accuracy of the long-wavelength response of the road profilometer, and the plate measurements are indicators of its short-wavelength response under controlled measurement conditions. To supplement these measurements, two single-number roughness ratings calculated from the rod-and-level profiles were compared with those calculated from the road profilometer profiles measured under typical conditions.

These parameters are the Mays index and the weighted rms acceleration. Their values are primarily sensitive to the short wavelength features of the road profiles with spacings on the order of 2-50 ft. Therefore, these two parameters are indicators of the accuracy of the road profilometer for measuring road features in a wavelength range important to ride quality.

The Mays index is an estimator of the total, absolute vertical travel of the vehicle body with respect to the axle.⁽⁷⁾ This single-number rating may be measured directly with an instrument installed in a car, or it may be simulated by an appropriate calculation from the measured road profile. Such a calculation includes a standard automobile simulation, known as the quarter-car model to estimate the motions of both the body and the axle that are excited by the road profile.^(7,8) The quarter-car model is shown in figure 22. It assumes

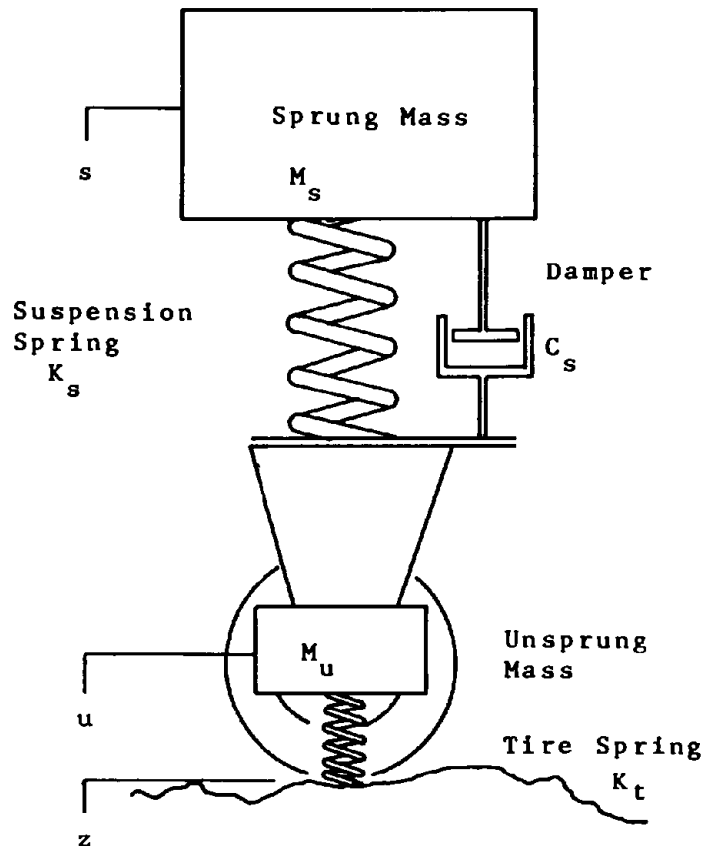


Figure 22. Quarter-car model of vibrational response to road excitations.

that the car axle is set off from the road by an undamped (tire) spring and that the body is supported on the axle by a suspension spring and damper combination.

The coupled differential equations describing the vertical motion of the unsprung and sprung masses are:

$$\ddot{s} + C(\dot{s} - \dot{u}) + k_2(s - u) = 0 \quad (11)$$

and

$$\ddot{s} + \mu\ddot{u} + k_1u = k_1z \quad (12)$$

where $z = z(t) =$ road elevation (in),

$u = u(t) =$ position of the unsprung mass (in) with respect to its initial equilibrium position,

$s = s(t) =$ position of the sprung mass (in) with respect to its initial equilibrium position,

the single and double dots represent, respectively, first and second order time differentiation and, for simulation of a Mays meter, the normalized model parameters are

$$k_1 = K_t/M_s = 653 \text{ s}^{-2},$$

$$k_2 = K_s/M_s = 62.3 \text{ s}^{-2},$$

$$C = C_s/M_s = 6.0 \text{ s}^{-1}, \text{ and}$$

$$\mu = M_u/M_s = 0.150.$$

The road profilometer software computes the road elevation, $z(t)$, as a function of time from the known road profile, $z(x)$, and an assumed vehicle speed. The vertical motion of the axle and the body are then calculated by integrating the differential equations, equations 11 and 12, over small increments of distance. For a road profile that is digitized over a series of road positions, i , the Mays index (MI) is given by

$$MI = \frac{5280}{L} \sum_{i=1}^N |(s_i - u_i) - (s_{i-1} - u_{i-1})|, \quad (13)$$

where L is the length of road over which the index is calculated (expressed in feet), N is the number of digitized points in the road length L , and $(s_i - u_i)$ is the relative displacement of the body with respect to the axle at position i . The values of $(s_i - u_i)$ are obtained from z_i by integrating the differential equations of motion over the successive positions i . As can be seen from equation 13, the Mays index is proportional to the average absolute slope of the relative-displacement profile. It is normally expressed in units of in/mi.

While the road profilometer software carries out the Mays index calculation in the time domain, it is instructive to look in the frequency domain at the transfer function between the body-to-axle displacement and the road profile. The transfer functions between the body and the road and between the axle and the road are given, respectively, by

$$\frac{s}{z} = \frac{\dot{s}}{\dot{z}} = \frac{\ddot{s}}{\ddot{z}} = \frac{k_1(k_2 + j\omega C)}{D} \quad (14)$$

and

$$\frac{u}{z} = \frac{\dot{u}}{\dot{z}} = \frac{\ddot{u}}{\ddot{z}} = \frac{k_1(k_2 - \omega^2 + j\omega C)}{D} \quad (15)$$

where $\omega = 2\pi f$ is angular frequency and the denominator is given by

$$D = \mu\omega^4 - [k_1 + k_2(1 + \mu)]\omega^2 + k_1k_2 + j\omega C[k_1 - (1 + \mu)\omega^2] \quad (16)$$

The transfer function between the body-to-axle motion and the input motion due to the road profile,

$$\frac{s - u}{z} = \frac{\dot{s} - \dot{u}}{\dot{z}} = \frac{\ddot{s} - \ddot{u}}{\ddot{z}} = \frac{k_1\omega^2}{D} \quad (17)$$

is plotted as a function of frequency in figure 23. It is seen that this transfer function goes through a sharp maximum near 1.4 Hz and through a broader, slightly higher maximum at 9.7 Hz.

As indicated following equation 13, in the spatial domain, the Mays index is proportional to average absolute slope, $|z'|$. In the time domain, it is proportional to $|\dot{s} - \dot{u}|$ and hence, from equation 17, to $|\dot{z}|$. Thus the slope of the road profile (in/ft) should be multiplied by the vehicle speed (ft/s) to obtain the vertical velocity, \dot{z} , at the tire-road interface. This velocity should be used in conjunction with the transfer function, equation 17, to obtain the Mays index.

The spectral density of the slope of an "average road" is approximately

$$G_z(\nu) = G_0 [1 + \nu_0^2/\nu^2] \quad (18)$$

where ν is the wave number (cycles/ft), G_0 is a scaling factor, and the parameter $\nu_0 = 0.05$ cycle/ft for bituminous concrete roads and $\nu_0 = 0.02$ cycle/ft for portland cement concrete roads.⁽⁷⁾ For a vehicle speed of 50 mph, the corresponding power spectral densities of $\dot{s} - \dot{u}$, arbitrarily normalized, are shown in figure 24. A second abscissa axis shows the wavelength corresponding to a given frequency for a speed of 50 mph. It is seen that at this speed the Mays index is controlled by contributions from the frequency range 0.5 to 15 Hz.

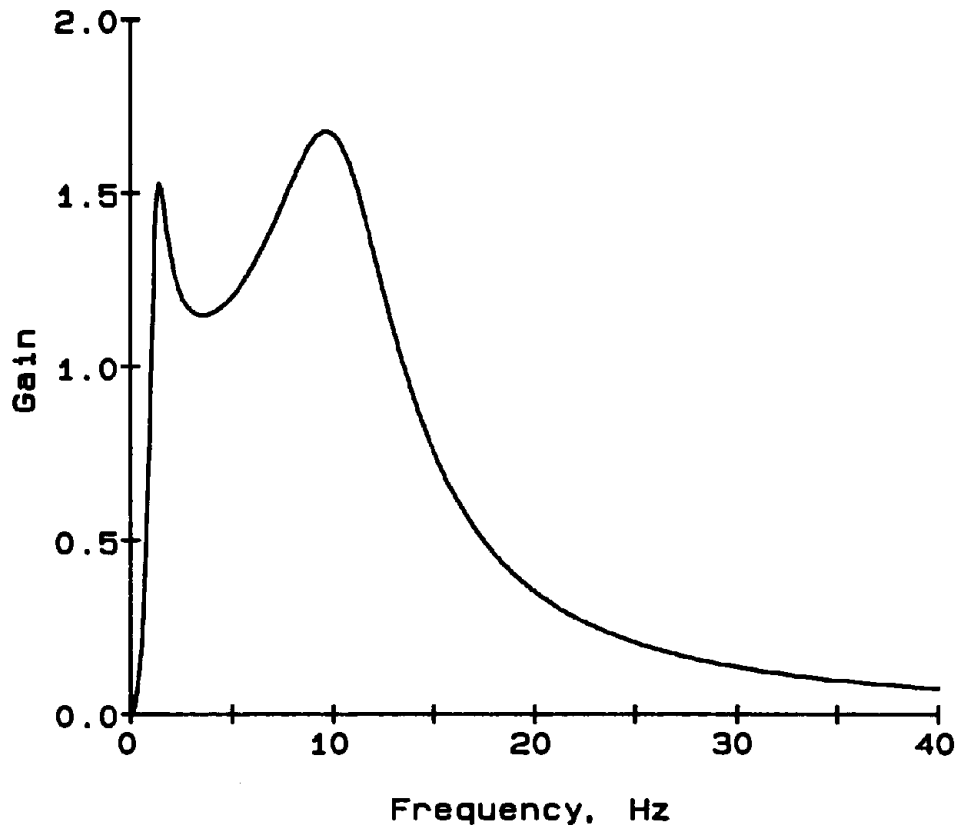


Figure 23. Magnitude of the transfer function, equation 17, between the body-to-axle motion and the input motion due to the road profile.

The software for the road profilometer also computes the weighted rms vertical acceleration, A_{rms} , of the vehicle body. The weighting, which is intended to approximate human sensitivity to vertical acceleration components of different frequencies, is shown by the solid curve in figure 25. Note that in this figure the frequency scale is logarithmic and the gain of the weighting filter is expressed in decibels. Also shown in figure 25 are the inverse of the internationally standardized (ISO 2631) contour for equal human response to vertical acceleration (dashed curve) and the proposed international standard filter (dotted curve) to approximate that contour.^(10,11) The inverse equal response contour has a slope of +3 dB/octave below 4 Hz, is flat from 4 to 8 Hz, and rolls off at -6 dB/octave above 8 Hz. The internationally proposed filter conforms closely to the earlier contour shape. Above 4 Hz, the filter used in the road profilometer software is very similar to the ISO contour and proposed filter shape. Below 4 Hz, however, the filter in the road profilometer has a slope of +6 dB/octave so that it gives less weight to the low frequencies than does the proposed ISO filter.

The transfer function from vertical velocity at the tire-road interface to vertical body acceleration is, from equation 14,

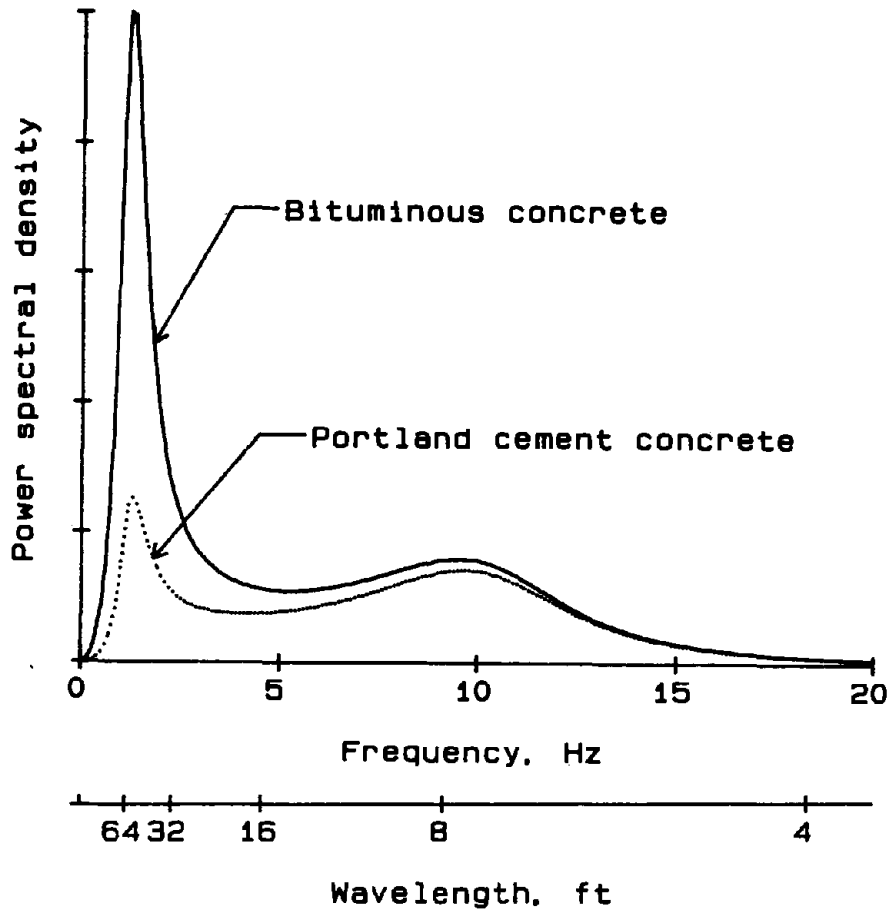


Figure 24. Normalized power spectral densities for the velocity of the body relative to the axle. The vehicle is assumed to be moving at 50 mph over "average" roads.

$$\frac{\ddot{s}}{z} = \frac{j\omega k_1 (k_2 + j\omega C)}{D} \quad (19)$$

In the frequency domain, the human response filter used in the road profiler software has the form

$$W(\omega) = \frac{j\omega}{8\pi + j\omega - \omega^2/16\pi} \quad (20)$$

Application of the transfer functions of equations 19 and 20 to the spectral density of the slope of "average roads," per equation 18, yields the results shown in figure 26 for the spectral density of the weighted vertical acceleration of the vehicle body. The frequency range for contributions to this single-number rating is seen to extend from about 0.5 to 15 Hz, with relatively larger contributions from the 3 to 10 Hz range than is the case for the Mays index.

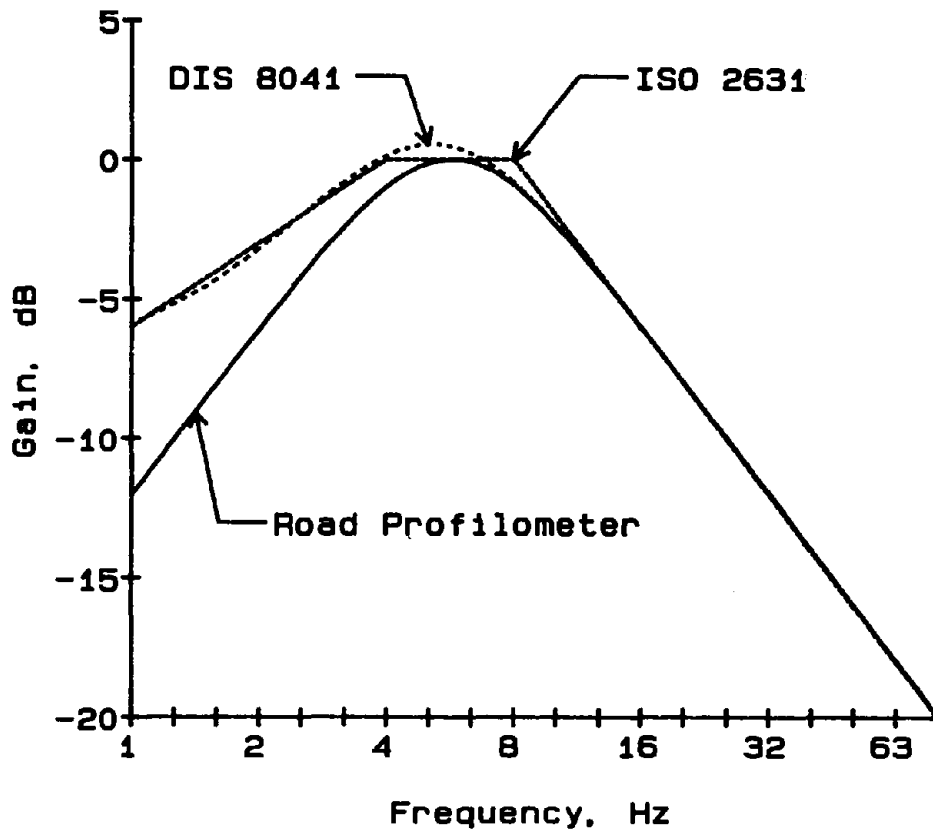


Figure 25. Frequency weighting to simulate human sensitivity to vertical acceleration. (The three curves are identified in the text.)

The road profilometer software computes the weighted root-mean-square acceleration, A_{RMS} , of the simulated vehicle body in the time domain, by numerical integration of equations 11 and 12 and of the differential equation for the human response filter.

The values of MI and A_{RMS} obtained from the road profilometer profiles were compared with those obtained from the rod-and-level profiles. In the case of the road profilometer, the algorithms are contained in a FORTRAN program called SDYNOO that executes on the road profilometer computer. For the rod-and-level data, the algorithms are contained in one routine of a BASIC program, described in appendix A, that uses the rod-and-level profiles as input data. These algorithms are essentially translations into BASIC of the FORTRAN algorithms, along with some simplifications of the procedures. The first simplification in the BASIC software is that only one wheeltrack may be analyzed at a time, whereas the FORTRAN software allows for the analysis of both right and left wheeltracks together.

The second simplification has to do with the assumed initial conditions of the van motion. In the BASIC routine, it is assumed that the initial displacement and velocity of both masses in the quarter-car model are equal to zero. In the FORTRAN routine, it is assumed that the initial displacements of the axle and

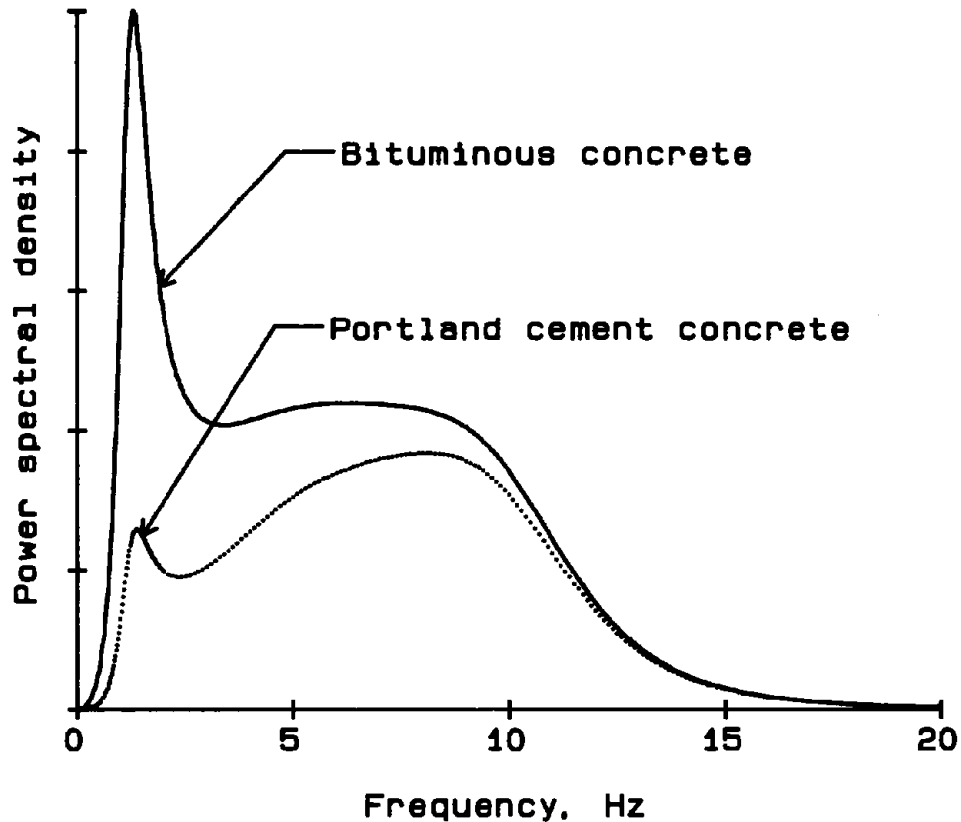


Figure 26. Normalized power spectral densities, weighted for human sensitivity, for vertical acceleration of the vehicle body. The vehicle is assumed to be moving at 50 mph over "average" roads.

the body and the velocity of the body are all equal to zero, but that the velocity of the axle is equal to the initial height difference between the first two points of the digitized profile, divided by the time increment between digitized points. The difference between these two sets of initial conditions should not introduce any significant differences between the two sets of calculations (see discussion below).

Values of MI and A_{rms} were computed over each tenth-mile section for four road profiles as shown in table 2. The sampling intervals for the rod-and-level data were 0.5 ft, 1.0 ft, or 1.5 ft, depending on the measured profiles. As discussed before, the left track of Rt. 151 was measured with two sampling intervals. Hence, there are two entries in the table for this profile. The sampling interval on the calculations for the road profilometer profiles was 0.5 ft in all cases.

Each result for the rod-and-level data was calculated from a single profile, whereas the road profilometer results represent averages taken from a number of measured profiles, 20 for the Blue Grass Parkway and 10 for KY 151. Therefore each result quoted on the right hand side of the table includes the standard deviation as well.

Table 2. Mays index (MI) and rms acceleration (A_{rms}) calculated from profiles generated with both rod and level and road profilometer. (Each section was 528 ft (0.1 mi) long. The sampling intervals for the rod-and-level data are shown in column 3. The sampling interval for the road profilometer was 0.5 ft. There were 20 sets of road profilometer data for the Blue Grass Parkway (BGP) and 10 for Kentucky Route 151. The uncertainties shown are equal to ± 1 standard deviation of these sets.)

Site	Section	Rod and Level			Road Profilometer	
		Sampling Interval (ft)	MI (in/mi)	A_{rms} (milli-g)	MI (in/mi)	A_{rms} (milli-g)
BGP	1	1.0	58.4	13.3	53.8 \pm 2.5	12.6 \pm 2.2
	2		57.5	13.6	50.1 \pm 1.0	9.9 \pm 2.8
	avg		57.9	13.4	52.0	11.2
Route 151 Right	1	0.5	110.7	22.6	103.3 \pm 3.0	22.4 \pm 0.7
	2		129.6	34.4	138.8 \pm 6.4	33.5 \pm 0.8
	avg		120.1	28.5	121.0	28.0
Route 151 Left	1	0.5	104.9	19.6	84.5 \pm 1.6	15.9 \pm 0.2
	2		136.7	29.0	112.0 \pm 1.2	22.6 \pm 0.5
	avg		120.8	24.3	98.2	19.2
Route 151 Left	1	1.5	121.0	27.0	84.5 \pm 1.6	15.9 \pm 0.2
	2		126.4	33.3	112.0 \pm 1.2	22.6 \pm 0.5
	3		137.0	36.5	124.1 \pm 4.6	24.2 \pm 0.7
	avg		128.1	32.3	106.6	20.9

The data from table 2 are plotted in figures 27 and 28 for the Mays index and the root-mean-square acceleration, respectively. On the average, the values of the single-number ratings calculated from the rod-and-level profiles are about 20 percent larger than those calculated from the road profilometer data. Part of this difference may be due to the fact that the rod-and-level results were calculated from only one profile and hence represent only a single sample of the random road profile.

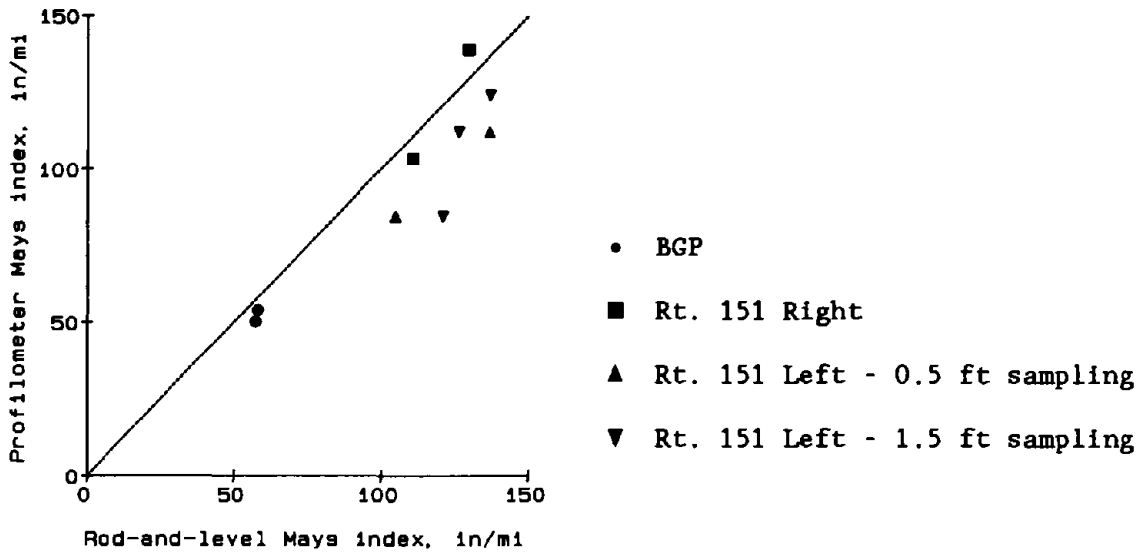


Figure 27. Comparison of the Mays indices computed from profilometer data with those computed from rod-and-level data.

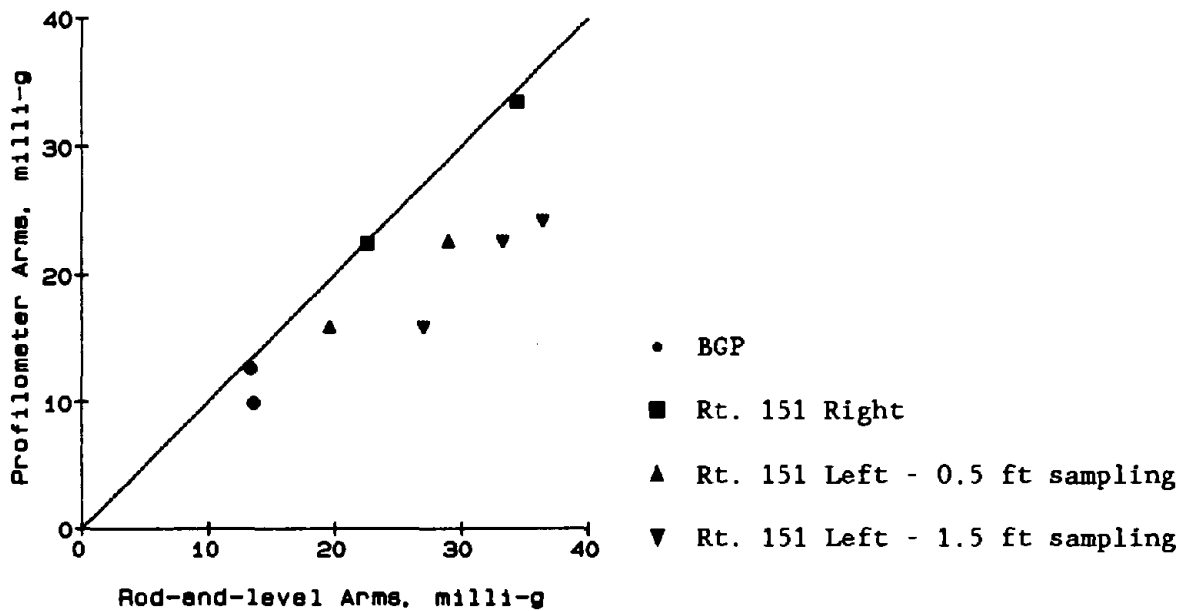


Figure 28. Comparison of root-mean-square accelerations computed from profilometer data with those computed from rod-and-level data.

There are numerous causes of differences between the rod-and-level and the road profilometer results. Three principal ones discussed before - aliasing, outliers, and wheel-path differences - are discussed again in terms of the single-number ratings of road roughness. Other concerns are the software and random errors in the rod-and-level data.

Aliasing

The rod-and-level data, unlike road-profilometer data, are not smoothed. Hence, they contain more short wavelength features. The MI and A_{rms} parameters are sensitive to such features, and one would expect, as is observed, that the values of these parameters calculated from the rod-and-level profiles should be larger than those calculated from the road profilometer profiles.

To reduce the effect of aliasing, the data underwent a three-point smoothing before the statistical processing, but this was evidently not sufficient to simulate the twelve-point smoothing of the road profilometer data. On the other hand, if a twelve-point smoothing procedure were used on the rod-and-level data, larger features in the rod-and-level data, corresponding to ones actually measured with the road profilometer, would be excessively attenuated. Because the 2-in footprint on the rods is smaller than the 0.5 to 1.5 ft sampling interval, there is no way, for example, to distinguish between features with widths of twice the sampling interval and those with widths significantly less than the sampling interval in these rod-and-level profiles .

One method to prevent aliasing in the rod-and-level profiles would be to use a rod with a long compliant base that effectively averages the height of a 1 ft section of road. However, the compliance of such a device might lower the precision of the rod-and-level measurements because the measured heights would be sensitive to any changes in vertical force on the rod. An alternate approach would be to take rod-and-level data with a sampling interval of, say, 1 in and then average 12 readings over a 1-ft interval, as is done with the road profilometer. This procedure would make the rod-and-level procedure about an order of magnitude more tedious than it is. It would also increase the number of outlier points entering the rod-and-level data due to human error.

Outliers

The outliers are a significant source of error in the statistical calculations. As discussed previously, they probably arise from human error in reading the rod. The most obvious outliers were removed when the unfiltered profiles (figure 12) were plotted. Then, more were removed after the filtered profiles were plotted and a first cut at the parameter calculations was performed.

Figure 15, for example, shows the rod-and-level points for the 1056-ft stretch of KY 151. A cursory examination of the original plots shows approximately 6 outlier points in the left hand profile and three in the right hand profile. Further inspection of the profiles strongly suggests that there are at least 11 outliers for the left and five for the right wheeltrack of figure 15. When these points are reinterpolated between their nearest neighbors, the calculation yields the parameter values shown in table 2.

These results are, on the average, about 8 percent lower than those calculated before the outliers were corrected. Outliers obviously have a significant effect on the calculation of MI and A_{rms} . They tend to increase the values of the results. If it is assumed that undetected outliers still present in the data cause errors in the statistical results equal to about half the average correction detected so far, a possible four percent error in the MI and A_{rms} values due to outliers in the rod-and-level data is estimated.

Random Error

The random error in the rod-and-level data also tends to increase the values of the calculated parameters. A 1-standard-deviation variability of this component was estimated as ± 0.003 ft from the rod-and-level repeatability runs. However, errors in the statistics due to this component of error are expected to be small because the random error of the rod-and-level readings would be added quadratically to the random variations of the road in any statistical calculation.

Wheelpath

Another source of error between the rod-and-level and the road profilometer data is path deviation. The path of the rod-and-level profiles was carefully measured, whereas the path of the road profilometer could only be controlled approximately by the driver. However, the road profilometer results in Table 2 represent an average of 10 or 20 runs. The variability of these values is at least partly due to the variation in the wheelpath of the road profilometer. Therefore one could say that the 1- σ variation in table 2 accounts for wheelpath error. However, there may be a systematic wheelpath error as well. Although the driver attempted to follow the unmarked path made by the rod-and-level team, it is possible that all of the road profilometer runs were displaced to one side or the other of the rod-and-level path, and that none of them overlapped the rod-and-level path. If road conditions were significantly different between the two paths, systematic differences in MI and A_{rms} values, calculated from road profilometer versus rod-and-level data, could result.

Software

The accuracy of the BASIC program was tested by performing the program calculations with sinusoidal road profiles as the simulated input data. The results were then compared with those obtained by analytical solutions of the quarter-car response to sinusoidal inputs. In the latter approach, the differential equations describing the quarter-car and the human response were solved analytically for sinusoidal input data, in order to calculate the displacement and accelerations of the various masses.

For this purpose, the road profile was assumed to have the digital form:

$$z(i) = A \sin (2\pi iS/\lambda), \quad (21)$$

where S is the sampling interval,

λ is the wavelength,

i is the digital index along the profile, and

A is the amplitude.

For these calculations, A was set equal to 0.01 ft, and the simulated speed of the vehicle, upon which the solution of the differential equations depends, was equal to 50 mph. Values for MI and A_{rms} were then calculated for three wavelengths λ equal to 53, 21, and 7.5 ft. At 50 mph, these road wavelengths yield driving frequencies of 1.4, 3.5, and 9.7 Hz, which correspond closely to the first maximum, the minimum, and the second maximum, respectively, of the quarter-car response as a function of frequency [see figure 23].^(11,12) The digital results were obtained for three sampling intervals of 0.5, 1.0, and 1.5 ft, corresponding to various sampling intervals of the rod-and-level files. The digital calculations were also performed over successive tenth-mile (528 ft) integration lengths corresponding to those of the rod-and-level profiles. For the 0.5-ft and 1-ft sampling intervals, two sections were used. For the 1.5-ft sampling interval, three sections were used.

The analytical and digital results are compared in table 3. The calculated values of MI and A_{rms} are shown there for the three surface wavelengths and the three sampling intervals. The values represent the averages over the 0.2-mi or 0.3-mi sections.

Table 3. Comparison of analytical and computer results for MI and A_{rms} for three sinusoidal road profiles with varying wavelength (λ). (In addition, three different sampling intervals were tried for the digitized sine wave.)

λ (ft)	Frequency @ 50 mph (Hz)	Analytical Results	Computed Results		
			Sampling Interval (ft)		
			0.5	1.0	1.5
			Mays index (in/mi)		
53	1.4	73.0	72.8	73.5	74.6
21	3.5	137.1	137.5	137.7	137.8
7.5	9.7	561.0	518.1	470.5	418.3
			A_{rms} (milli-g)		
53	1.4	9.51	9.56	9.71	9.95
21	3.5	29.5	29.4	29.3	29.2
7.5	9.7	107.	114.	125.	137.

In general, the analytical and computed results agree best for the two longer wavelengths. For $d = 7.5$ ft, the agreement is reasonable for the shortest sampling interval of 0.5 ft but degrades as the sampling interval increases. In particular, the results for MI decrease and those for A_{rms} increase as the sampling interval increases.

It is clear that the response of the quarter-car is not modeled well by the digital calculation for short road wavelengths and long sampling intervals. For an accurate digital calculation, the sampling interval should be short for two reasons. First, it should be much smaller than the road wavelength that is being sampled. Second, the corresponding sampling frequency should be much greater than any resonances in the mechanical structure. The wavelength of 7.5 ft corresponds to a frequency of 9.7 Hz at 50 mph. This is the upper resonance frequency in the quarter-car model (see figure 23). As the sampling interval increases above 7.5 ft, the calculation does not converge.

To test this observation, the digital calculation was performed on a mathematical profile with a sampling interval of 10 ft. All the points $z(i)$ in the data set were equal to zero except for the point at $i = 0$ representing a single pulse disturbance. When the digital calculation was attempted for this profile, the calculated amplitudes increased monotonically without bounds. Therefore, it is important that the sampling interval be kept small. Sufficient calculations were not carried out to establish the shortest wavelength, and the corresponding sampling interval, that should be used to obtain valid Mays indices, in general.

The results for each of the various 0.1 mi integration lengths are in good agreement with one another and with their averages shown in table 3. The largest differences between individual calculated values are only three percent of the values themselves. That level of agreement suggests that differences in the initial conditions do not significantly affect the accuracy of the calculations, because the initial conditions for the tenth-mile segments were different. As stated before, the initial values of displacement and velocity were equal to zero for the first tenth-mile segment. But the initial displacement and velocities for the successive tenth-mile segments were set equal to the final ones in the preceding segments. Since the differences between the calculated values for the segments are small, it is concluded that the differences in initial conditions between the BASIC and FORTRAN programs do not significantly affect the calculated values of the parameters over tenth-mile segments.

The main conclusion concerning the digital algorithms is that the 1.5-ft sampling interval can lead to errors in the calculated parameters as large as about 30 percent for surface wavelengths as short as about 7.5 ft. The digital algorithms themselves do not cause the large differences seen between the road profilometer and rod-and-level statistical calculations of the data with sampling intervals of 0.5 and 1.0 ft.

The accuracy of the BASIC software in the rod-and-level program was checked against the analytical solutions as described above. There was no similar direct check made of the FORTRAN software used by the road profilometer. However, the BASIC software is a translation and an adaptation of the FORTRAN

software so that significant errors would not be expected in the FORTRAN code when none appear for the BASIC code.

In summary, there is a high degree of correlation between the MI and A_{rms} values obtained with the rod-and-level data and those obtained with the road profilometer data. However, differences were observed that are about 20 percent on the average but that in some cases were as large as 50 percent. Such differences are believed to be primarily due to a higher spatial frequency content in the rod-and-level profiles than in the profilometer profiles and to approximations inherent in the digitized calculations. Improving the agreement between road profilometer measurements and rod-and-level measurements would likely involve a significantly more elaborate procedure for rod-and-level measurements of road profile.

3. RESPONSE-TYPE ROAD ROUGHNESS MEASUREMENT SYSTEM TEST RESULTS

A response-type road roughness measurement (RTRRM) system is defined as "any device that measures the relative motion of a sprung mass system in response to traveled surface roughness where the mass is supported by automotive type suspension and tires."⁽¹⁴⁾ Measurements made by RTRRM systems involve interactions among the road, the vehicle, and the road meter instrument. Such systems are not stable over time because the properties of vehicles change, and differences among vehicles result in roughness data that are not reproducible by similar systems.

The test apparatus for an RTRRM system may include: (1) devices for measuring the axle-body displacement of an automobile and a displacement accumulator, (2) devices for measuring the vertical acceleration of the vehicle body, (3) devices for measuring the vertical acceleration of the vehicle's axle, (4) a distance measuring system, and (5) a recording system mounted in a vehicle. The response of the vehicle to road roughness is dependent on speed and vehicle properties in addition to the roughness characteristics of the road surface. Vehicle response to traveled surface roughness is normally made while traveling at constant speed, and the vehicle is "either a suitable passenger automobile with four wheels or a suitable single-axle, two-wheel trailer towed by a vehicle."⁽¹⁴⁾

Most roughness-related measurements have been made using RTRRM systems which were installed in a passenger car or single-axle trailer. For this project, the road profilometer was temporarily modified by the addition of a commercial RTRRM (a Mays Ride Meter, manufactured by the Rainhart Co., in Austin, Texas), a linear potentiometer to indicate the displacement between the vehicle body and the rear axle (specifically the differential housing), and two accelerometers, one to measure the vertical acceleration of the rear axle and the other to measure the acceleration of the vehicle body directly above the rear axle. (Care was taken to ensure that these modifications did not interfere with the normal operation of the road profilometer.) An FM tape recorder, with appropriate signal conditioning, was used to record the signals from the linear potentiometer and auxiliary accelerometers.

Mays Ride Meter Testing

Static Tests of Rotary Encoder

In this section, a description is given of a laboratory evaluation of a Mays Ride Meter. As noted in reference 7, RTRRMs such as Mays Ride Meters are not ideal but only follow the gross axle-body motion. The signals from these transducers are modified by various effects such as hysteresis and quantization; the latter can be eliminated or minimized by using transducers that continuously measure motion.

Static laboratory, or proof, tests of the rotary encoder in the Mays Ride Meter were performed to determine the magnitude of the meter's hysteresis and quantization errors.

The Mays Ride Meter rotary encoder assembly is rigidly attached to a vehicle's body immediately above the differential housing. Normally, the vertical motion of the solid rear axle is imparted to the input pulley of the encoder by a swivel-ended rod with an attached parallel wire rope. The taut cable, with both ends secured to the rod, loops around the encoder's pulley and provides positive drive.⁽¹⁵⁾

Early experience with this arrangement in the laboratory, together with the manufacturer's warning about possible slippage of the drive pulley due to slack in the drive cable, led to the design of an alternative method for transferring axle motion to the encoder. A continuous displacement transducer was selected to measure axle-body displacement, in order to circumvent several of the well-documented limitations of the Mays Ride Meter, such as quantization. The continuous displacement sensor uses a multiturn potentiometer coupled to a reel driven by a stainless steel cable. Cable tension is maintained by a constant force spring within the cable take-up reel inside the transducer case.

The cable for the displacement transducer had a tension of 4 lbf, and a means was developed for calibrating the transducer and evaluating the Mays Ride Meter nonlinearity errors with the same test arrangement. The displacement sensor was calibrated by recording its output voltage, which corresponded to known increments of linear translation. The moveable head of a milling machine allowed displacement of the cable in increments known within 0.001 in. Based on the maximum deviations from a best-fit straight line over the full range, the worst-case error of the displacement transducer was found to be 0.25 percent of full scale, or 0.025 in.⁽¹⁶⁾ The output of the continuous displacement sensor was then used to generate a continuous record of the motion of the input pulley for the evaluation of the rotary encoder quantization and hysteresis errors, as shown schematically in figure 29. A long steel cable was attached to the end of the displacement cable, and the long cable was then routed over the rotary encoder pulley and attached to the milling machine cross slide as shown in the figure. The cable tension provided by the constant-force spring within the transducer case was sufficient to ensure that there was no slippage between the cable and the encoder pulley.

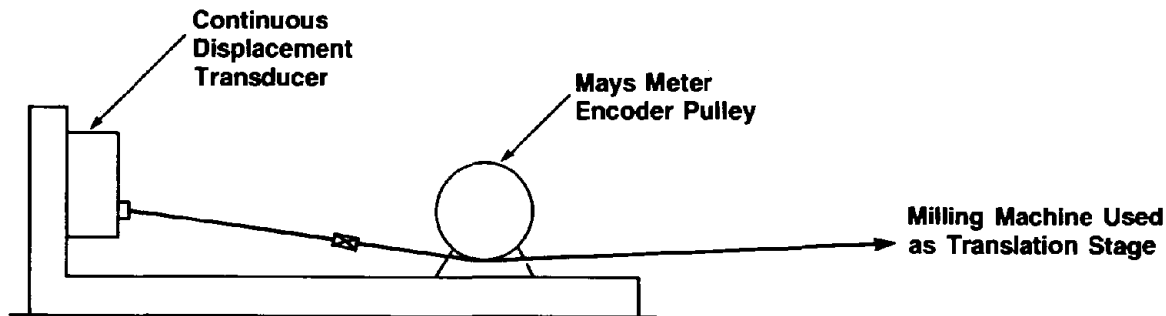


Figure 29. Schematic of laboratory test arrangement for determination of Mays Ride Meter quantization and hysteresis.

A Honeywell 5200C X-Y recorder was connected such that the X-axis was driven by the displacement sensor output voltage and the Y-axis was driven by the pulsed voltage applied internally to the chart drive stepper motor of the Mays Ride

Meter. This setup allowed the operations of the rotary encoder and the chart drive assembly to be evaluated independently.

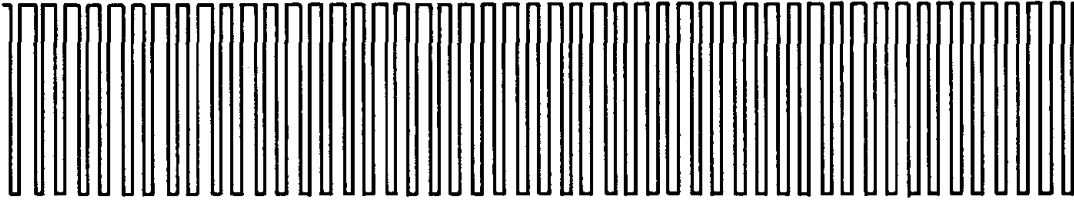
In reference 7 it is shown that the Mays Ride Meter hysteresis may be determined by measuring the difference in axle-body positions when the meter registers an increment of motion in one direction (i.e., it "clicks"), and then registers motion in the other direction. Data obtained using the just-described setup were used to evaluate the hysteresis of a specimen Mays Ride Meter over typical ranges of body-axle excursion. When a displacement range of 1 in was investigated, the hysteresis was determined to be approximately 0.034 in. When the quantization level was determined for a larger displacement range corresponding to axle-body motion of ± 2.5 in, the hysteresis was found to be 0.022 in. The two values are consistent with the average value of 0.027 in for six Mays Ride Meters reported in reference 7.

The rotary encoder comprises four photocells and a cylindrical binary-coded film strip illuminated by an incandescent lamp of the type ordinarily used in automobile dome lights. Since the lamp socket is adjustable to accommodate variations in position of the filament within the envelope of replacement lamps, the possibility exists that misadjustment of the lamp position could adversely affect encoder performance.

Prior to the determination of the Mays Ride Meter quantization error, the sensitivity of the operation of the rotary encoder to internal lamp position had been examined by first displacing the bulb 0.25 in to the right of the slit which focuses the light onto the encoder film. After the change in the electrical output waveform was recorded, the bulb was repositioned so the lamp filament was located directly over the slit as specified in the meter's operating manual.⁽¹⁵⁾ A plot of the rotary transmitter output voltage for the light bulb centered relative to the slit, and for the bulb displaced 0.25 in to the right of the slit, is shown in figure 30. Each transition from a high to a low voltage or from a low to high voltage causes the Mays chart recorder to advance by one increment. Thus, to interpret the effect of the bulb location relative to the slit in the rotary transmitter, it is necessary to look at the edges of the square wave pulses shown in the figure. The center of the tracing represents the equilibrium position for the transmitter. For the upper trace, which corresponds to the bulb center position, the distance between the transitions is uniform for all positions of the transmitter input pulley. However, the spacing between the waveform edges is nonuniform with the bulb displaced relative to the slit; this is shown in the lower trace. Such distortion might be significant for small displacements about the transmitter equilibrium position when, for example, axle-body motions on smooth roads are recorded.

In the determination of quantization error, the previously described X-Y recorder arrangement was used to obtain data for a range of ± 2.5 in of input displacement. From these data, the average meter step size was determined for pulley motion about the equilibrium position, corresponding to both upward and downward motion of the push/pull rod in a typical installation. The average step size was 0.09969 in, or within 0.3 percent of the specified Mays quantization level. A summary of these test results is shown in table 4. A principal result is that the average measured quantization level was uniform for all four ranges of encoder input.

Bulb centered relative to slit:



Bulb displaced 0.25 in to right of slit:

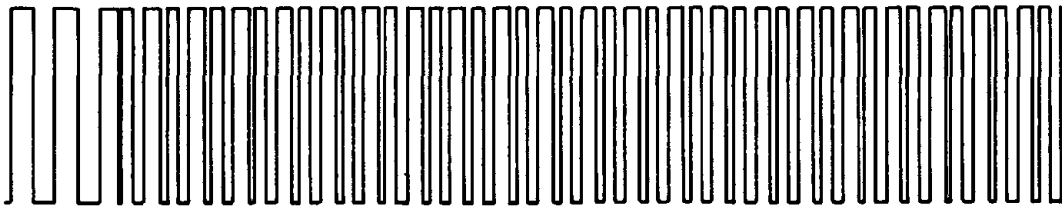


Figure 30. Rotary transmitter output voltage for the light bulb in two positions relative to the transmitter optical slit.

A potentially significant problem with the Mays recorder system was encountered during the laboratory tests; namely, an occasional failure of the chart drive mechanism to advance the chart paper. This problem could be alleviated by applying, by hand, a small tension to the chart paper. In view of the obvious impracticality of this remedy, it is not surprising that many users of the Mays Ride Meter system have devised alternative methods of recording the accumulated axle-body displacement data.^(17,18)

Table 4. Quantization levels of Mays Rotary Encoder.

Mays Ride Meter Displacement	Range of Encoder Input Displacement (in)	Average Increment (in)	Standard Deviation (in)
Rod Upward	-2.5 to 0	0.0993	0.0131
	0 to +2.5	0.0994	0.0110
Rod Downward	-2.5 to 0	0.09997	0.0063
	0 to +2.5	0.1001	0.004
Average	---	0.09969	---

The specification for the Mays Ride Meter chart motion was checked by providing a total displacement of 28.1 in with the milling machine. The Mays chart drive for this displacement moved 4.35 in, or 0.01548 in per count, since the chart paper moves one step for each 0.1 in of rotary encoder input motion. The rated value for the roughness summation is 1 in chart motion for 64 impulses or 0.015625 in per count. Thus, the measured value for chart motion per count (representing 0.1 in axle vertical travel) was approximately 0.93 percent lower than the rated value.

Tests to determine the Mays recorder sensitivity to power supply voltage indicate that the manufacturer's specification of a minimum of 13 volts is conservative. For the single Mays Ride Meter unit whose voltage sensitivity was investigated, normal recorder performance was observed as the supply voltage was changed from about 11 to 14 V.

Installation of RTRRM in Road Profilometer Van

Based on the successful results of the laboratory proof tests, a further evaluation of the Mays Ride Meter was planned as part of the field test program required to develop calibration procedures for profilometers and field test procedures for response-type road roughness measuring systems.

The test arrangement for the Mays Ride Meter and the continuous displacement transducer was based on the laboratory test setup, modified in order to measure the axle-body motions of the FHWA profilometer vehicle.

An aluminum plate with dimensions 9 by 18 by 0.5 in was securely bolted to the floor of the profilometer. A 1-in diameter hole was cut in the floor panel above the axle housing and a steel cable was attached to a bracket clamped on the housing. This cable was connected to the end of the displacement transducer cable and routed over the Mays Ride Meter encoder pulley located above the hole in the floor, as shown schematically in figure 31. The point of tangency of the drive cable and the pulley lay on the centerline of the hole. The rotary encoder housing and its connection to the aluminum base plate is omitted in the schematic drawing for clarity.

The useful service life of the continuous displacement transducer is limited by the number of extension and retraction "cycles" of the transducer spring. In order to extend the sensor's life the displacement sensor input cable was disconnected when data were not being collected. Even with this precaution, the transducer cable failed during on-the-road operation so that Mays and displacement roughness data could not be obtained for one of the test sites.

The continuous displacement transducer used embodies a high-resolution multi-turn potentiometer which, when connected to a highly regulated dc power supply, produced a voltage proportional to the length of cable unwound from the helically-grooved pulley inside the transducer housing. This voltage, proportional in this application to the distance between the mounting plate and the axle housing, was recorded, using a Honeywell 5200C FM tape recorder, for later analysis.

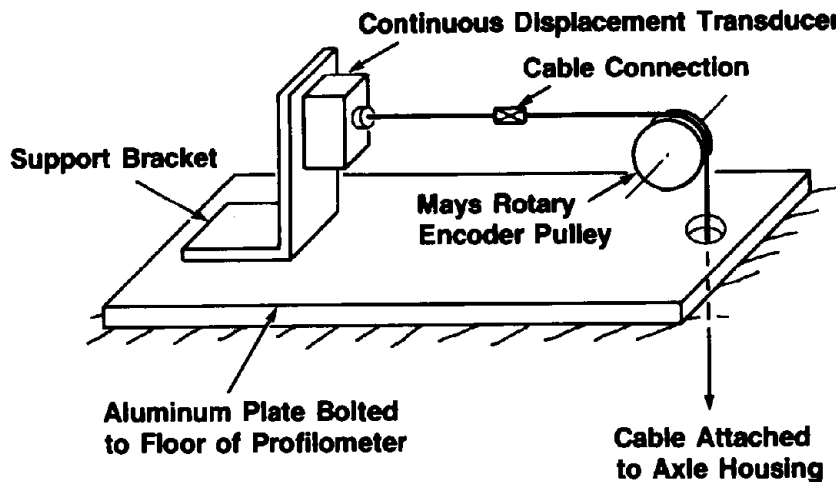


Figure 31. Schematic of the installation of the Mays Ride Meter and the continuous displacement transducer in the road profilometer.

Field Tests

The results of field tests of RTRRM systems for a synthetic sinusoidal surface in Pennsylvania, for 2 smooth pavement surfaces in Maryland, and for 14 pavement sections in Kentucky are described below. The ASTM Draft Standard for the calibration of RTRRM systems was reviewed in light of the field test results. Sections of the calibration procedure which were scrutinized include characterization of the ridemeter vehicles, pavement calibration sections, comparison of roughness indices measured by ridemeters with those computed by profilometer, measurement reproducibility, and determination of a RTRRM system's calibration equation. Based on this examination, a field test procedure for Mays Ride Meters was developed and is included in volume II of this report.

Experimental investigation of test procedures for the field calibration of Mays Ride Meters was initially made using the FHWA's road profilometer as the host vehicle for the Mays Ride Meter system. The Mays Ride Meter was installed in the road profilometer, as previously described. Pavement profiles of the sinusoidal surface were measured and Mays indices were computed from the profiles based on the quarter-car model as embodied in road profilometer software.⁽⁷⁾ This surface is made from a series of sinusoidal surface concrete blocks, and the tires of a vehicle running on the track are subject to sinusoidal excitation at frequencies ranging up to 40 Hz, depending on the vehicle test speed.⁽¹⁹⁾ A series of tests was conducted at different vehicle speeds on this test track, during which pavement profiles were measured using the road profilometer and, simultaneously, Mays Ride Meter roughness values were determined. A linear regression analysis was made of the paired measured indices and the computed Mays index values for several test speeds up to 27 mph. The principal result of this evaluation is that the measured and computed roughness indices show a high degree of correlation for all test speeds. The results were somewhat inconclusive, however, since the sinusoidal test track

was not a typical road surface and the road profilometer vehicle dynamic parameters are not well simulated by the "golden car" parameters used in the quarter-car model.

Subsequently, profiles were measured for two smooth pavement surfaces in Maryland in April, 1987, during which the rod-and-level survey was made for one road section. In addition, a comparison was made of the Mays index roughness statistic computed by the road profilometer and by a second FHWA-owned profilometer designed by UMTRI.^(5,6) When the static rod-and-level data were suitably filtered, i.e., using the same filter algorithm as the profilometer, very good agreement was found between the profile measures produced by the road profilometer and the rod-and-level reference, as discussed earlier. The UMTRI inertial road profiling system computes roughness statistics only for separate wheeltracks, and uses a different filter algorithm than does the FHWA's Law road profilometer.^(5,6) Nonetheless, the Mays indices obtained by the FHWA/Law profilometer and the UMTRI profilometer, for a given wheeltrack, were in good agreement. The systematic difference between the profiles obtained with the two profilometers (see figures 13 and 17) and was primarily a long-wavelength effect and appears not to have affected the Mays indices significantly.

An extensive field test program was then planned and conducted in cooperation with Surface Dynamics, Inc., and the Kentucky Department of Highways (KY DOH).

Three IRPSs and 5 Mays Ride Meters were used to measure profiles of 14 pavement test sections in eastern Kentucky during May 1987. For this test program, a comparison was made of the Mays index statistic computed from profiles measured by the FHWA/Law road profilometer and a second Law 690DNC road profilometer owned and operated by the Ohio Department of Transportation. The profiles measured by the FHWA/Law profilometer were also compared with the results of a rod-and-level survey, and were found to agree closely when the same filtering was employed. After the basic repeatability of the road profilometers was established, the FHWA/Law system was employed to calibrate five Mays Ride Meters and to generate data for correlation with data from several other response-type and roughness measurement systems, as described below.

The RTRRM systems investigated during the field test program included five KY DOH Mays Ride Meter vehicles and the Mays Ride Meter installed in the FHWA/Law Profilometer. In addition, the latter system was instrumented with body and axle accelerometers and a continuous displacement transducer to record body-axle motions. Data recorded during the field test program and later analyzed have provided a basis for the examination of various features of the proposed ASTM draft standard for the calibration of RTRRM systems.

During the first 2 days of the field test program, repeated runs were made on selected pavement sections using all the test vehicles. These data were used to establish the reproducibility for all measurement systems and thereby to determine the minimum number of repeated runs necessary to obtain accurate profiles and single-number roughness ratings.⁽²⁰⁾ All three IRPSs demonstrated good reproducibility, and a high degree of correlation was found between the two nominally identical Law 690DNC profilometers. The latter result was considered to reinforce the concept of calibration of RTRRM systems by correlation with an IRPS, since the Ohio profilometer obtained profile measurements

considered valid for all the test runs during the road profilometer meeting held in Ann Arbor, Michigan at 27 test sites. (21)

The Kentucky ridemeters employed Mays Ride Meters conventionally installed in sedan-type automobiles. The roughness data were recorded by use of an onboard printer in lieu of using the standard Mays chart drive. Roughness data were also recorded by the Mays Ride Meter installed in the FHWA/Law profilometer, using the Mays chart recorder. It should be noted that the unique installation of this measurement system in the profilometer was designed for purposes other than calibration, as discussed earlier, and the quarter-car parameters in the computer simulation are not characteristic of the profilometer vehicle used as a platform for the Mays Ride Meter.

In the vicinity of Frankfort, Kentucky, 14 pavement test sections were selected as candidate sites for the calibration of KY DOH Mays Ride Meters. Of the pavement test sections, seven were portland cement concrete (PCC) and seven were bituminous concrete (BC). Six of the test sites, three for each surface material, were judged to be most suitable for Mays Ride Meter calibration sites, based on multiple roughness measurement data discussed below. Proper selection of calibration sites requires the use of these data and the imposition of additional criteria covering the roughness range for the various pavement types. (21)

Most of the field roughness measurements were made at vehicle speeds of 50 mph on pavement test sections 1 mi in length. However, several of the test sections were about half that length, and speeds were limited to 30 or 40 mph for safety. Vehicle speeds were varied from 30 to 60 mph when multiple profiles could be measured conveniently on the same 1-mi pavement section.

Recorded signals from the continuous linear-displacement transducer were digitized and an analysis was carried out to look at the effects of quantization and hysteresis when a (simulated) Mays index was computed from data that originally were essentially free of the quantization and hysteresis that are inherent to the design of the Mays Ride Meter. The results of this analysis confirmed the findings of reference 7 with regard to the effects of quantization and hysteresis on the Mays index.

Comparison with Road profilometer

The repeatabilities of the FHWA profilometer and the Ohio DOT profilometer were first established by making measurements from 10 to 20 times on 2 bituminous concrete pavement surfaces. After this repeatability was established, a smaller number of repeat measurements was made of the elevation profiles of the remaining 12 pavement test sections. The computed Mays indices, based on the quarter-car model, and the standard deviation for the multiple measurements for each of the 14 Kentucky test sites are shown in table 5. Of the test sites, six, including three PCC pavements and three BC pavements covering the desired roughness range in each pavement type, were judged to be suitable for Mays Ride Meter calibration sites.

Table 5. Inertial profilometer measurements.

Kentucky Test Site No.	Number of Repeat Profile Measurements	Standard Mean Mays index (in/mi)	Standard Deviation
<u>PCC</u>			
101*	9	75.0	0.34
102	5	82.4	2.52
103	6	100.5	0.82
104*	5	103.0	0.57
105*	9	144.1	1.38
106	5	151.4	1.57
107	5	160.7	2.71
<u>BC</u>			
201	20	47.1	0.56
202*	5	49.4	0.45
203	5	63.3	0.42
204	6	57.5	1.04
205	5	83.5	0.93
206*	10	111.4	1.03
207*	6	133.9	1.38

*Selected for calibration test sites

At each of the selected calibration sites, the five KY DOH Mays Ride Meter vehicles were used to obtain the Mays index values marked with an asterisk in table 5. Each of the test sites was measured at least 10 times by each Mays Ride Meter system. The repeat measurements were made to compute a mean Mays index and a standard deviation about the mean for each Mays Ride Meter system for each test site.

The computed Mays index values from the FHWA profilometer were then used with the computed mean Mays index for each Mays Ride Meter system to compute the least-squares best-fit linear relationship between the two data sets. This relationship for one of the Mays Ride Meter vehicles is shown graphically in figure 32. The computed slope and intercept were then used to develop a calibration equation between the Mays index values obtained with the KY DOH Mays Ride Meter system and the Mays index value computed from the profilometer profile measurements.

The experience gained during the field test program suggests several recommendations relating to the calibration of Mays Ride Meter Systems:

1. Because of the high standard deviation for typical Mays Ride Meter systems, calibrations should normally be made by averaging multiple repeat measurements for each test site. For one of the test sites where a rod-and-level survey was conducted, special procedures were used to align all of the Mays Ride Meter vehicles and the FHWA profilometer, insofar as possible, in the

same wheeltrack. Procedures could be developed to assist operators of Mays Ride Meter vehicles to maintain improved wheeltrack alignment for calibration by comparison with an IRPS, to determine if such control measures can be considered to be effective.

2. Normally, the calibration equation is determined from a regression analysis of all paired reference roughness values and RTRRM system roughness values. A linear regression model is specified for standardization and comparison purposes, with a proposed criterion for the regression standard error.⁽⁷⁾ For one of the pavement materials investigated during the field test program, the standard error was much reduced by use of a nonlinear regression model. This result suggests that judgment in the selection of calibration sites may be required to comply with the standard error specification, i.e., to ensure the adequacy of the linear regression model. No attempt should be made to use the resultant calibration models outside the range of roughness values used to determine the particular model.

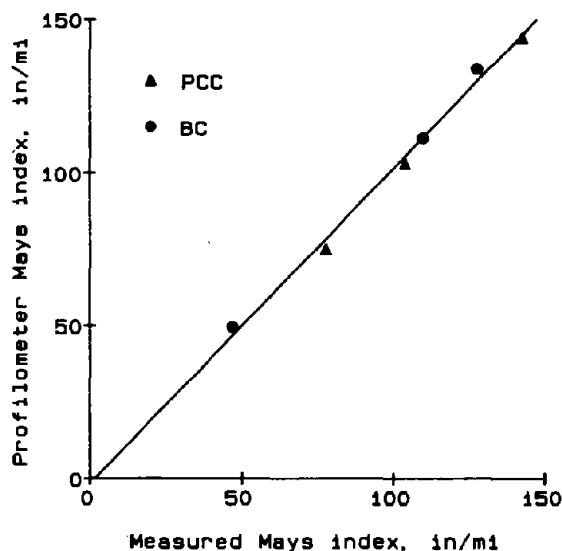


Figure 32. Example of Mays Ride Meter calibration by regression with calculated Mays indices from road profilometer.

Accelerometer Testing

Description of Sensors and Instrumentation

Two Sundstrand QA-1400-AA03-1 servo-accelerometers were temporarily installed in the FHWA/Law road profilometer in order to measure the vertical acceleration of the vehicle body and of the rear axle. (These accelerometers were in addition to the accelerometers that are normal components of the road profilometer.) The body accelerometer was bolted directly to the aluminum plate, shown in figure 31, that was used to install the Mays Road Meter and the

continuous linear displacement transducer in the profilometer van. The axle accelerometer was mounted, with a special fixture, to the differential housing. The fixture utilized RTV silicon rubber potting material to isolate and protect the accelerometer from high-frequency components of mechanical shock while still allowing it to follow faithfully the vertical acceleration of the differential housing over the low-frequency region of interest.

The FM tape recorder, mentioned earlier, was used to record the analog signals from the two accelerometers. A Norwegian Electronics Type 830 Real-Time Analyzer was used to obtain the 1/3-octave band vibration levels at band center frequencies from 0.8 to 315 Hz.

Spectral Analysis

The accelerometer signals were recorded and analyzed for at least one run of the road profilometer over each of the roads measured in the field trip to Kentucky, described earlier. The 1/3-octave-band root-mean-square accelerations of the profilometer van axle and body for four of these roads are shown in figures 33 through 40. In these figures, the solid circles represent the "raw" measured accelerations, while the open circles represent accelerations that were adjusted, as described below, for the estimated component of acceleration arising from sources other than road roughness.

For 12 sets of data, representing 10 different roads, the measured accelerations for each 1/3-octave band were plotted versus A_{rms} , the root-mean-square accelerations which were weighted for human response and computed using the quarter-car model from the profiles obtained by the road profilometer. As examples of this process, figures 41 and 42 show the measured 1/3-octave-band accelerations of the van body for the 2- and 4-Hz band, respectively, plotted versus the A_{rms} values for the road profilometer. Although the data exhibit scatter, it is evident that there would be significant vertical acceleration of the vehicle body even for $A_{rms} = 0$. Extrapolation of plots such as figures 41 and 42 to $A_{rms} = 0$ enabled inference of the approximate root-mean-square vertical acceleration that would be expected if driving the vehicle over a perfectly smooth road, i.e., the residual acceleration due to vibrations induced by the engine and drive train, rather than by road roughness. The residual acceleration was so obtained for each 1/3-octave band from 0.8 to 315 Hz. The data represented by the open circles in figures 33 through 40 were obtained by subtracting the mean-square residual acceleration from the mean-square measured accelerations and taking the square root of the answer so obtained. This procedure implicitly assumes that the residual acceleration and the acceleration due to road roughness add incoherently on a power basis.

In figures 33 through 40, it should be noted that the vertical scale for axle acceleration differs by almost an order of magnitude from that for body acceleration. Inspection of these figures reveals that, as might be expected, the engine and drive train produce quite significant vertical axle accelerations over the frequency range from about 16 to 315 Hz, but the vehicle's springs and shock absorbers attenuate the higher frequency components so that the vertical acceleration of the body of the vehicle is much lower at high frequencies than is the axle acceleration. As discussed previously, the major contributions to both the Mays index and to A_{rms} are from frequencies below about 16 Hz. As

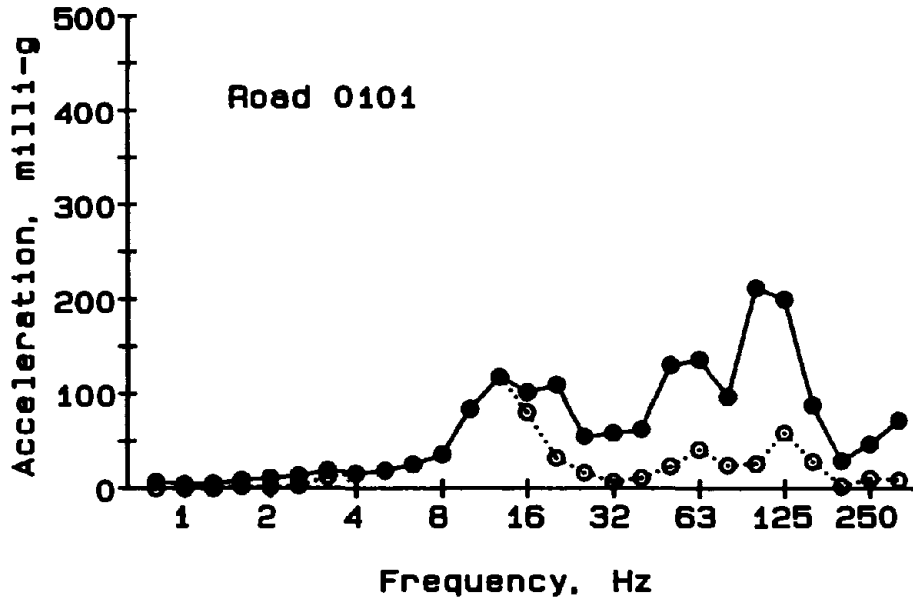


Figure 33. Measured 1/3-octave-band acceleration of the road profilometer axle for a 50-mph run at Test Site 101 (PCC).

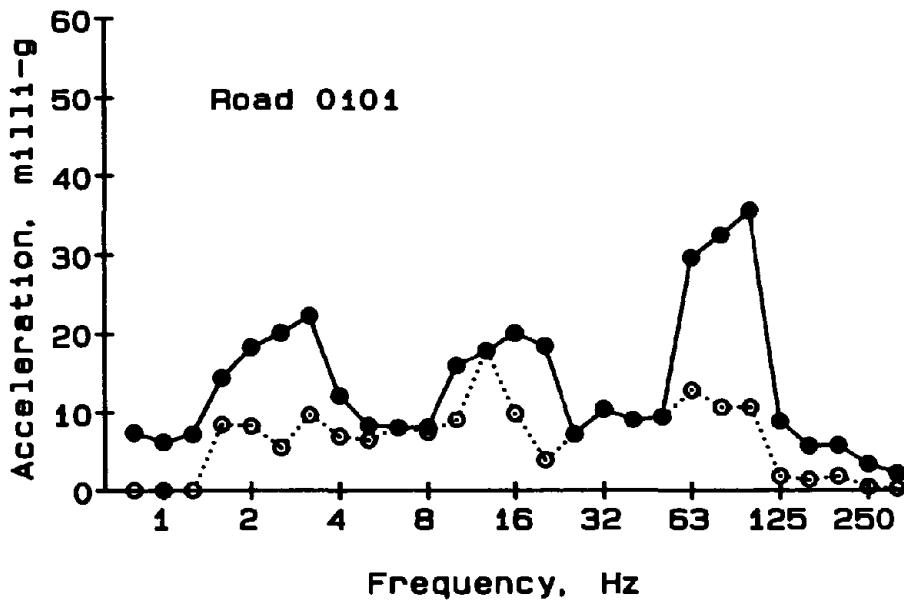


Figure 34. Measured 1/3-octave-band acceleration of the road profilometer body for a 50-mph run at Test Site 101 (PCC).

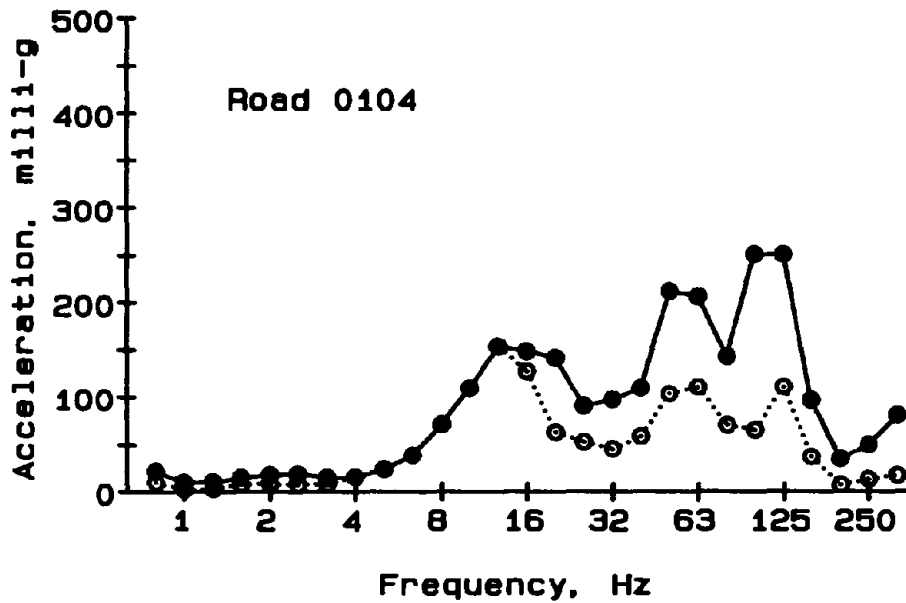


Figure 35. Measured 1/3-octave-band acceleration of the road profilometer axle for a 50-mph run at Test Site 104 (PCC).

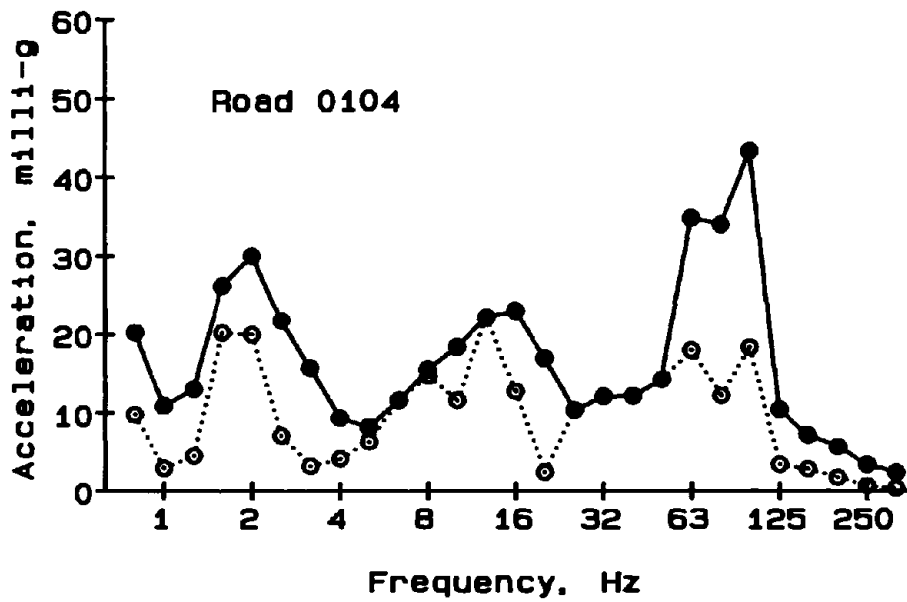


Figure 36. Measured 1/3-octave-band acceleration of the road profilometer body for a 50-mph run at Test Site 104 (PCC).

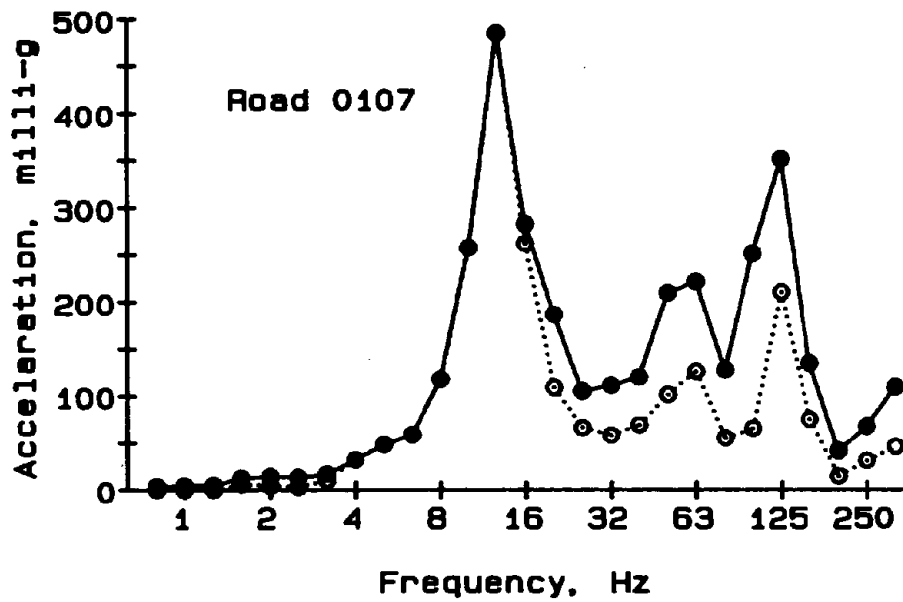


Figure 37. Measured 1/3-octave-band acceleration of the road profilometer axle for a 50-mph run at Test Site 107 (PCC).

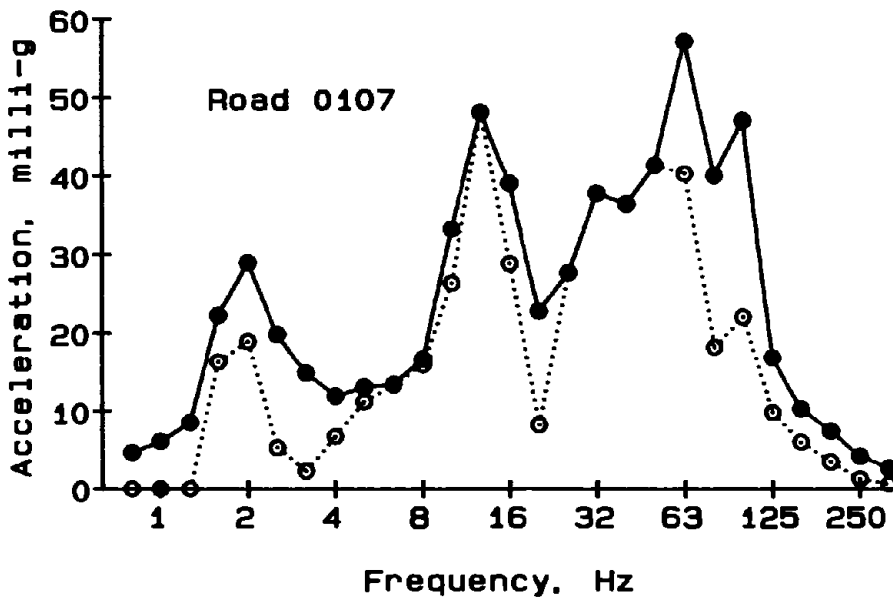


Figure 38. Measured 1/3-octave-band acceleration of the road profilometer body for a 50-mph run at Test Site 107 (PCC).

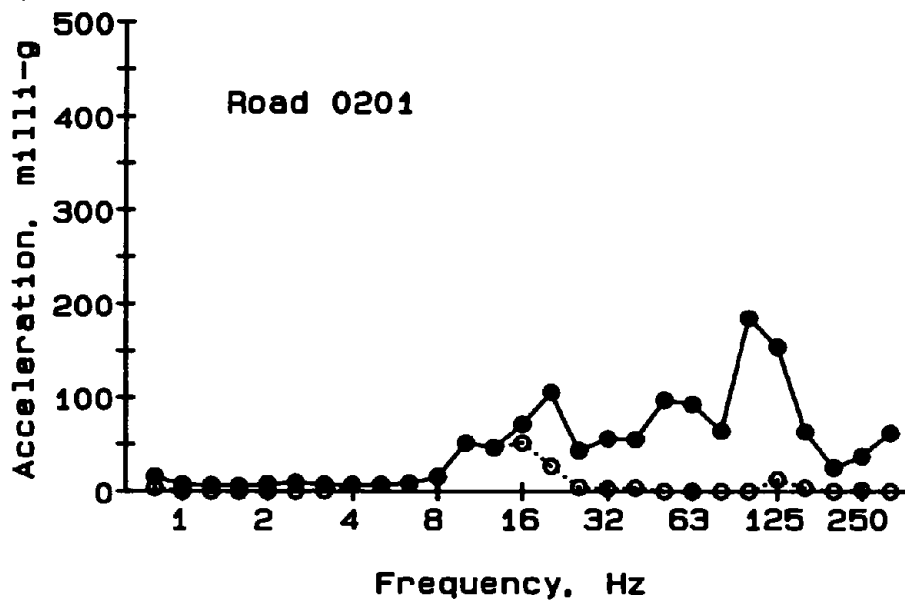


Figure 39. Measured 1/3-octave-band acceleration of the road profilometer axle for a 50-mph run at Test Site 201 (BC).

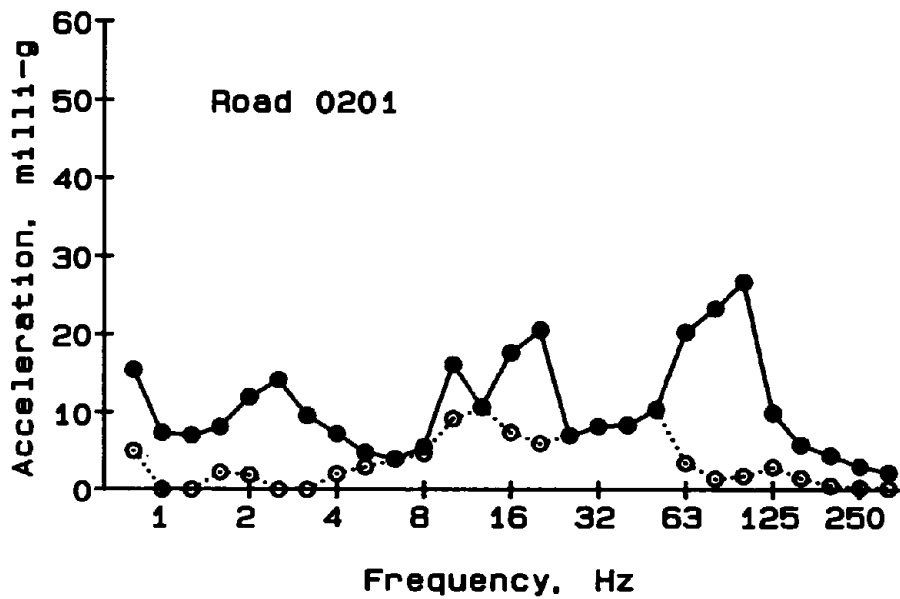


Figure 40. Measured 1/3-octave-band acceleration of the road profilometer body for a 50-mph run at Test Site 201 (BC).

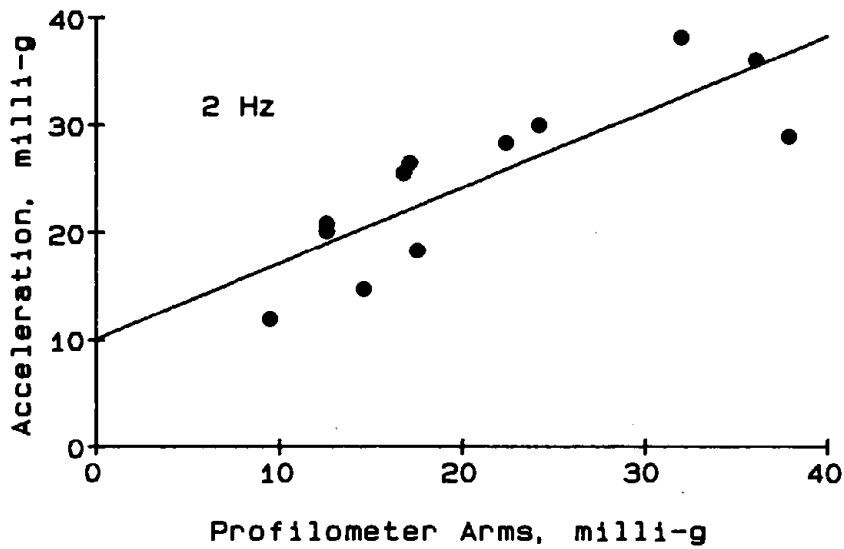


Figure 41. Measured 1/3-octave-band acceleration, for the 2-Hz band, of the vehicle body plotted versus A_{rms} computed from road profilometer profiles .

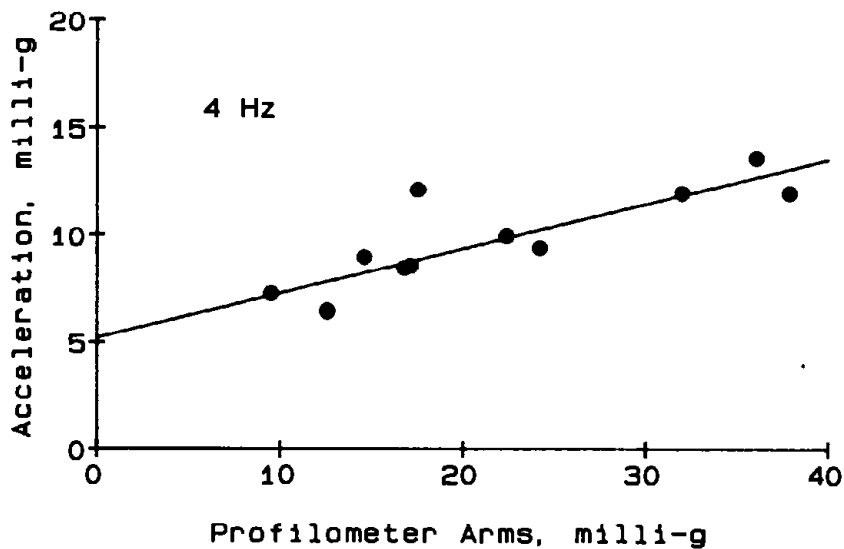


Figure 42. Measured 1/3-octave-band acceleration, for the 4-Hz band, of the vehicle body plotted versus A_{rms} computed from road profilometer profiles.

will be seen below, the observed vertical accelerations above 16 Hz correspond to small vertical displacements, of the order of less than 0.001 in. Thus, even though the suspension of the profilometer van is somewhat stiffer than is the suspension assumed in the quarter-car model, one would not expect contributions from frequencies above about 16 Hz to affect ride quality significantly. It should be noted that the corrections for residual (engine and drive train) vertical body accelerations are quite significant for the critical frequency range from 0.8 to 6.3 Hz. This has important implications with regard to any proposed methods for using accelerometers to obtain "absolute" roughness ratings since the residual acceleration components may swamp the acceleration contributions due to the roughness of the traveled surface. A dramatic illustration of this effect can be seen in figure 40, which corresponds to a rather smooth road. (Note that engine and drive-train-induced body vibrations do not affect the accuracy of data obtained using an inertial road profiling system since the purpose of the accelerometers in a profilometer is to establish an inertial reference frame and there is no assumption that the body acceleration is due to road roughness alone.)

Although the vertical scale of the figures does not enable detailed inspection of the effect of residual contributions to axle acceleration, the effect is similar to that which can be seen for body acceleration since the transfer function from the axle to the body is close to unity at low frequencies.

The solid curve in figure 43 is a plot of the transfer function from the axle to the body of the quarter-car model (i.e., the transfer function obtained by taking the ratio of equations 14 and 15). The data points (solid circles) were obtained from data on a single, rather rough road (0107) by dividing the uncorrected rms accelerations for the body (see figure 37) by the uncorrected rms accelerations for the axle (see figure 38). The apparent transfer function represented by the data points is higher than that for the quarter car over most of the frequency range shown. At 16 Hz and above, this difference is probably primarily due to engine and gear train vibrations that are coupled directly into the body without having to be transmitted through the rear springs and shock absorbers. At the lower frequencies, the increased apparent transfer function may be partly due to the reason just stated, but probably is also partly due to the suspension parameters for the profilometer van differing from those assumed in the quarter-car model.

Figures 44 through 47 represent the spectra of the rms vertical displacement of the Profilometer van body, as obtained from the uncorrected rms vertical body acceleration spectra for the same four roads (the solid circles in figures 34, 36, 38, and 40). The vertical motion of the van body is not large. The importance of the accuracy of the accelerometers used to establish the inertial reference frame of the road profilometer can be seen to decrease with frequency until, above about 16 Hz, the vertical displacement is so small that the measured road profile, for these frequencies, does not depend upon the road profilometer's accelerometers at all.

Figures 48 through 51 represent spectra of the profiles of these four roads, as obtained by two very different methods. The solid triangles were obtained by first carrying out a Fourier analysis of profiles obtained by the road profilometer and then computing the 1/3-octave band root-mean-square displacements.

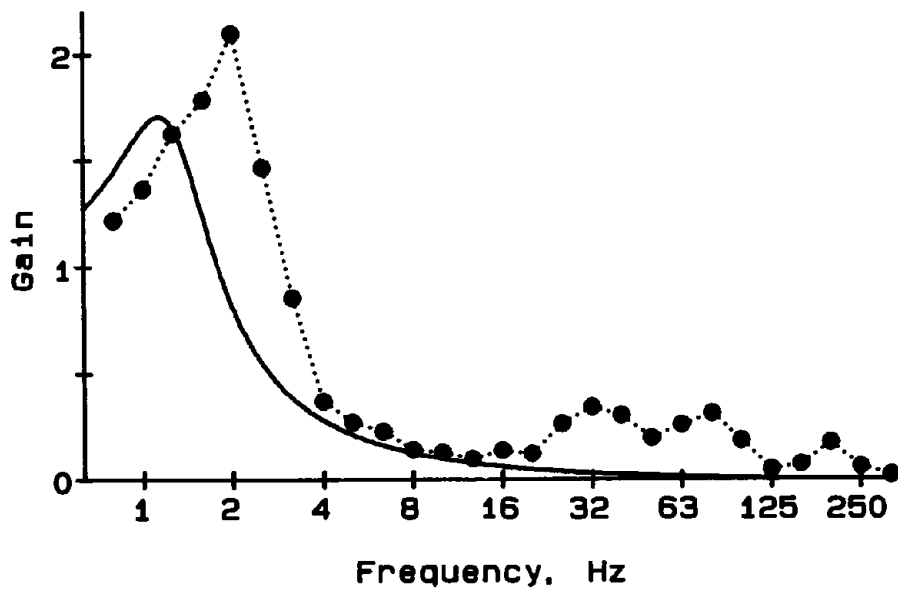


Figure 43. Axle-to-body transfer function for the quarter-car model (solid curve) and for the road profilometer (solid circles) traveling at 50 mph over Road 0107.

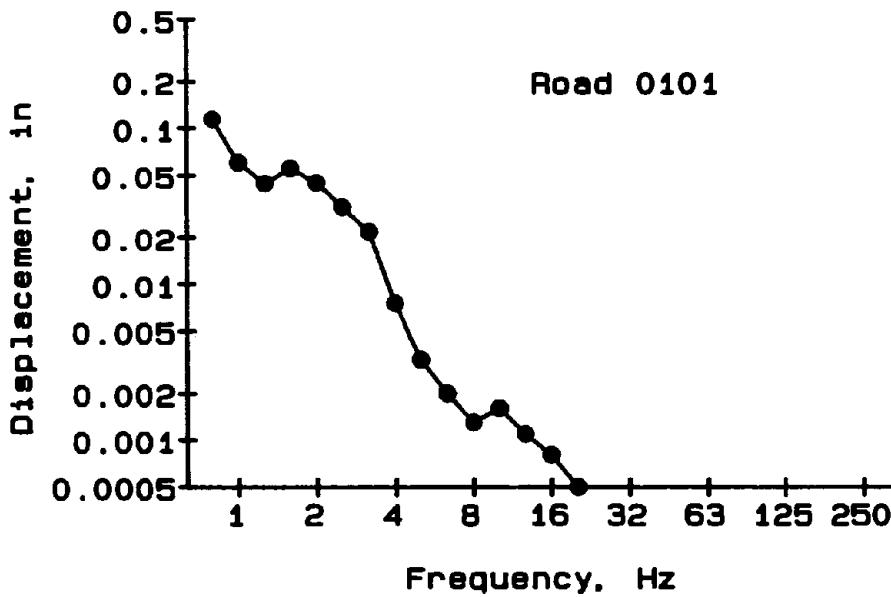


Figure 44. Root-mean-square vertical displacement of the body of the road profilometer while traveling at 50 mph over Road 0101.

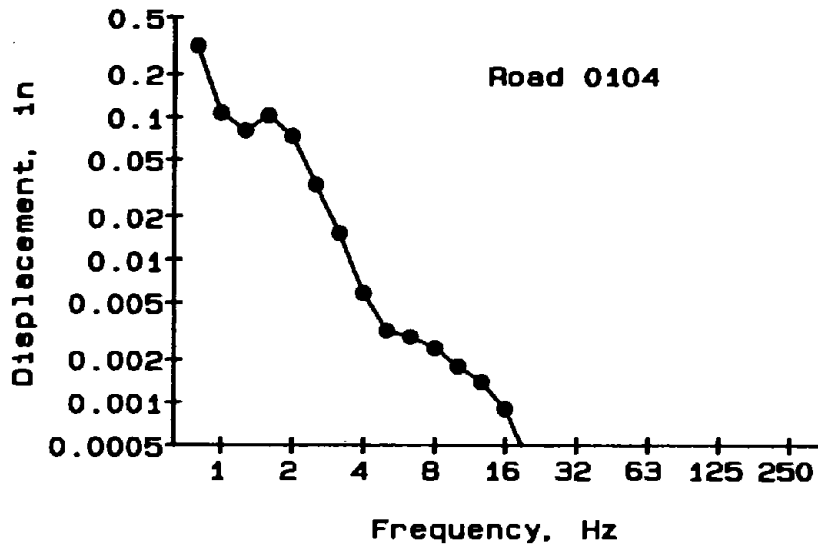


Figure 45. Root-mean-square vertical displacement of the body of the road profilometer while traveling at 50 mph over Road 0104.

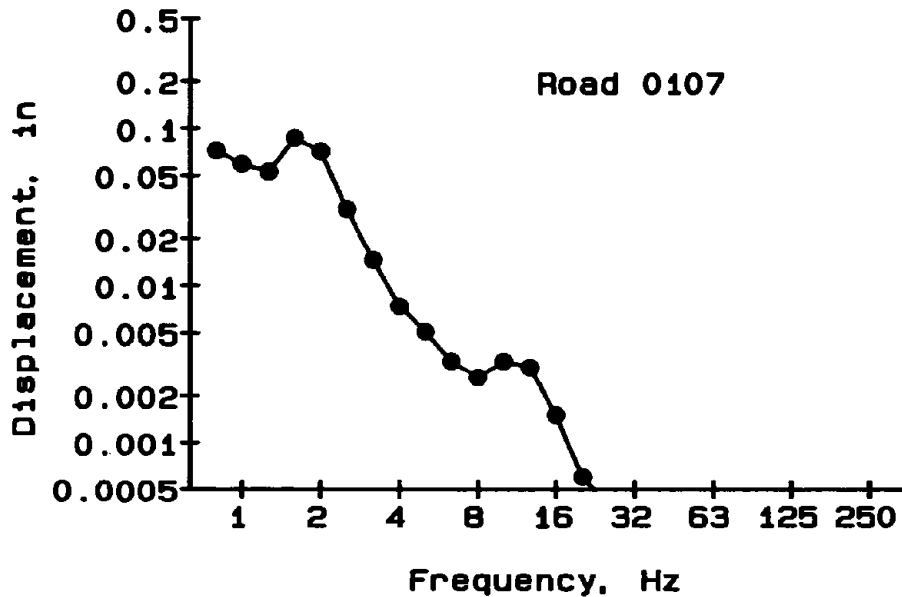


Figure 46. Root-mean-square vertical displacement of the body of the road profilometer while traveling at 50 mph over Road 0107.

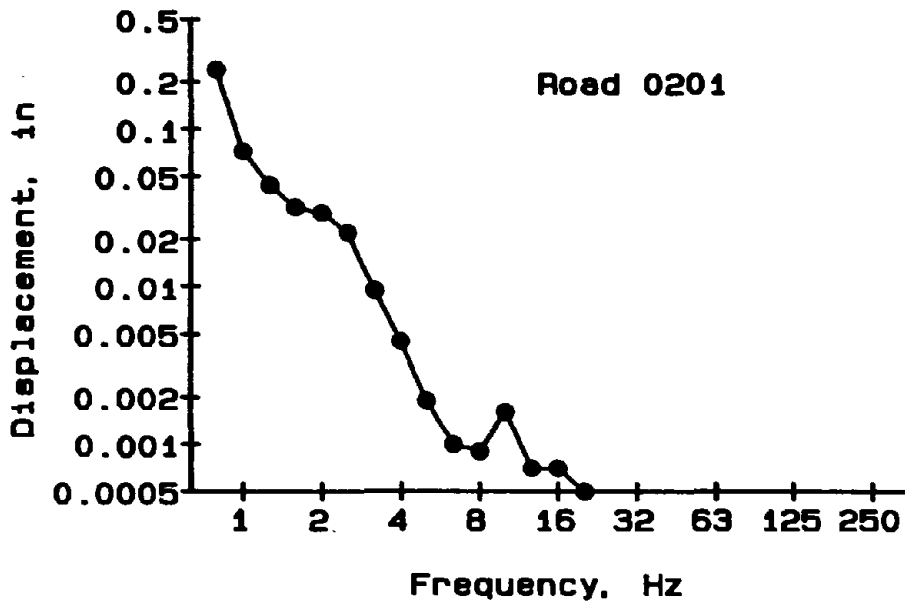


Figure 47. Root-mean-square vertical displacement of the body of the road profilometer while traveling at 50 mph over Road 0201.

From equation 15, for the quarter-car model, the transfer function from vertical displacement at the tire-road interface to vertical axle acceleration is

$$\frac{\ddot{u}}{z} = \frac{-\omega^2 k_1 (k_2 - \omega^2 + j\omega C)}{D} \quad (22)$$

The measured rms axle accelerations were divided by this transfer function to obtain the displacements plotted as solid circles in figures 48 through 51. The displacements plotted as open circles in these figures were similarly obtained from the axle accelerations that had been corrected for "residual acceleration," as described above. Inspection of these figures shows qualitative agreement between the profile spectra obtained from axle accelerations and those obtained from road profilometer data. Somewhat surprisingly, over the frequency range from about 2 to 10 Hz, the profile spectra obtained from the unadjusted axle-accelerometer data are generally lower than the spectra obtained from road profilometer data. The agreement between these two sets of data is generally rather good over the frequency region from 0.8 to 2 Hz which makes the major contributions to single-number ratings of road roughness at speeds near 50 mph (e.g., see figures 24 and 26). At the highest frequencies shown, the unadjusted axle-accelerometer data yield significantly higher spectral values, presumably due to acceleration contributions from the engine and drive train, than do the road profilometer data. The "adjustments" to the axle-accelerometer data make things worse, rather than better, over the frequency region of most interest, i.e., below 20 Hz.

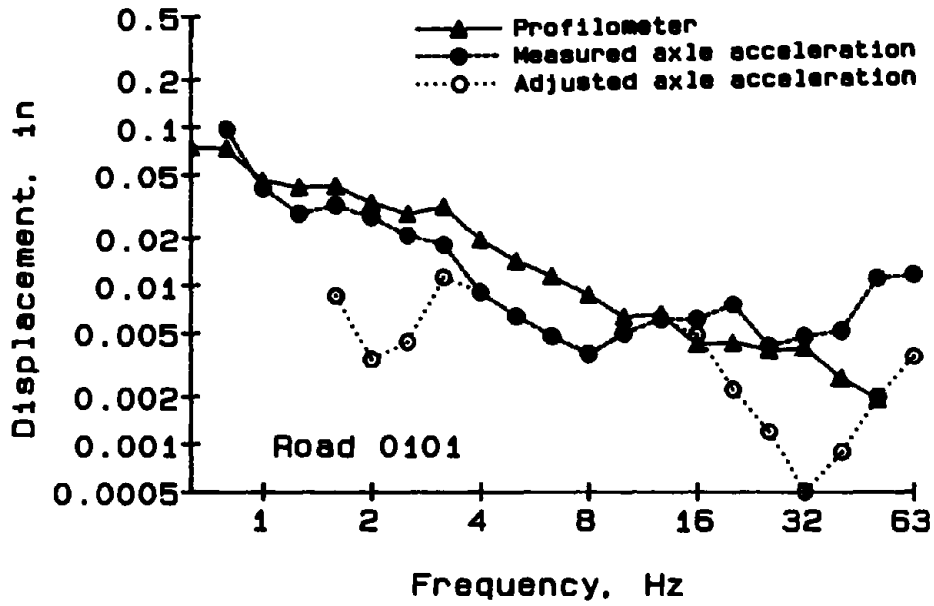


Figure 48. Spectra of the root-mean-square vertical displacement for Road 0101 as functions of frequency for 50 mph travel.

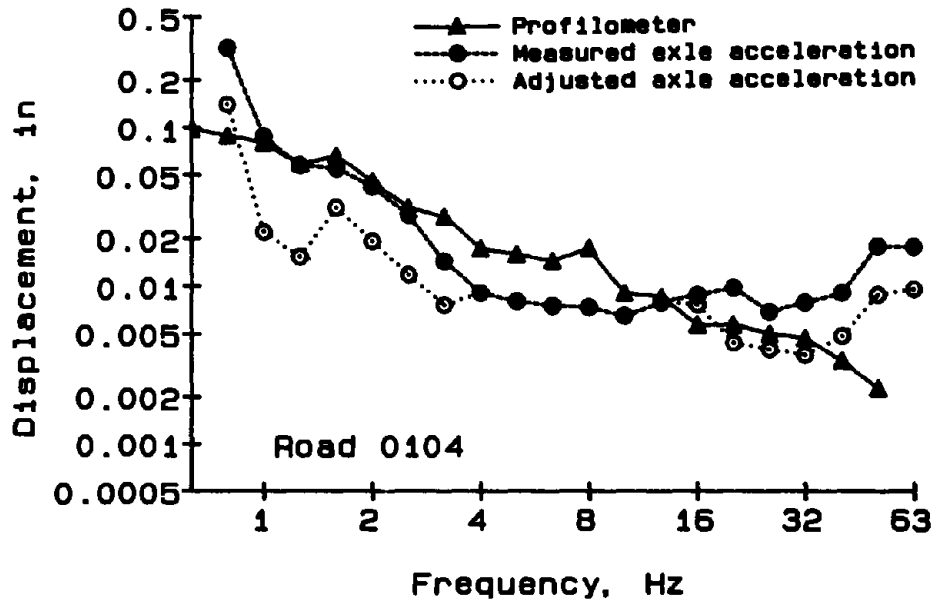


Figure 49. Spectra of the root-mean-square vertical displacement for Road 0104 as functions of frequency for 50 mph travel.

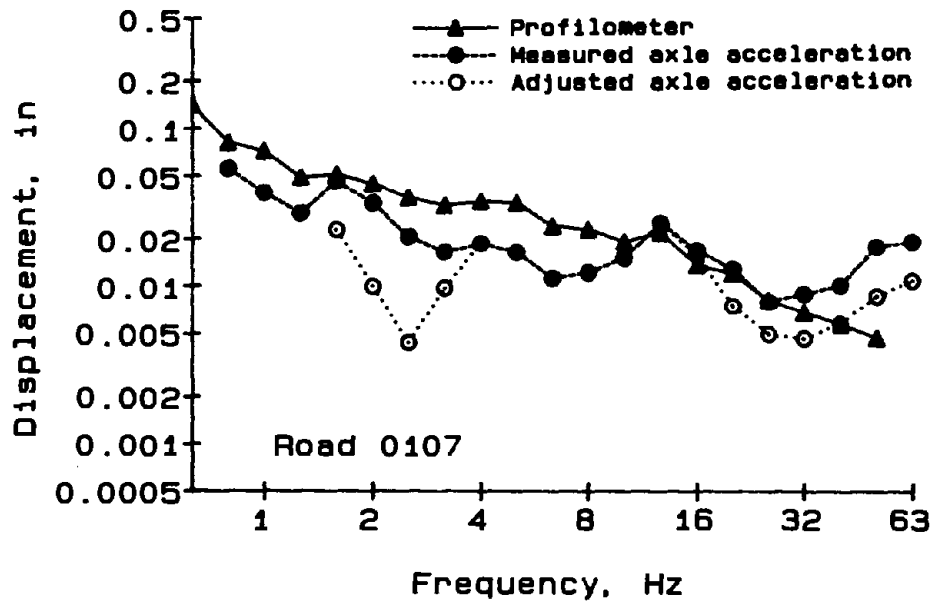


Figure 50. Spectra of the root-mean-square vertical displacement for Road 0107 as functions of frequency for 50 mph travel.

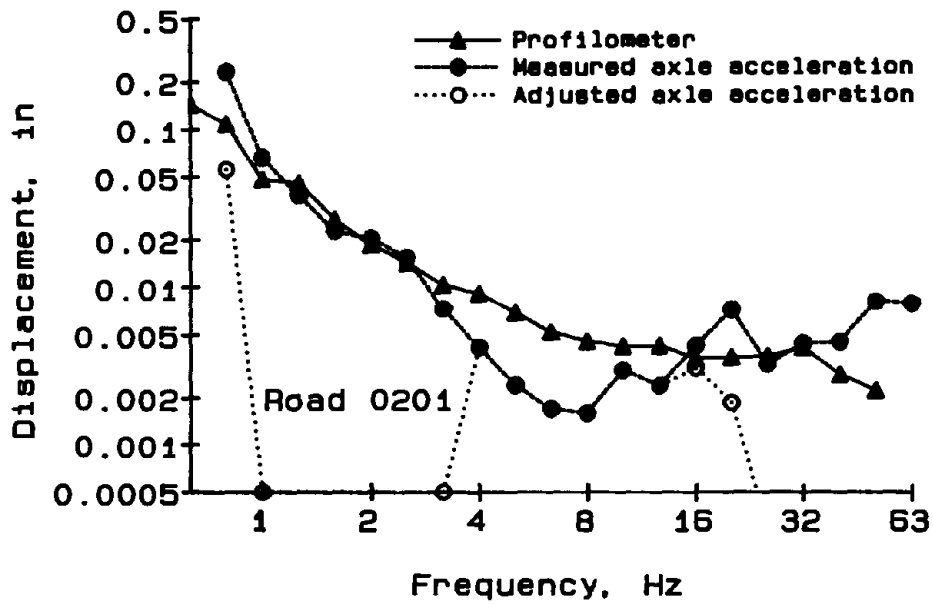


Figure 51. Spectra of the root-mean-square vertical displacement for Road 0201 as functions of frequency for 50 mph travel.

Part of the disagreement between the profile spectra obtained by Fourier analysis of road profilometer data and those obtained from accelerometer data may be due to the road-to-axle spring constant for the road profilometer van being different from that which is assumed in the quarter-car model and which was used in the calculations for figures 48 to 51. In retrospect, it would have been worthwhile to measure the spring constants and damping coefficient for the profilometer van and to use these measured values in calculations. However, the major cause of the discrepancies seen is probably vibrations of the axle due to the engine and drive train rather than due to the road profile. The results just discussed further support the caution given previously regarding the use of accelerometers to obtain "absolute" roughness ratings.

Comparison with Road profilometer

For 12 50-mph runs over roads on the Kentucky field trip, the root-mean-square vertical acceleration of the road profilometer van body was computed by weighting the rms acceleration for each 1/3-octave band by the "human response" frequency weighting used in the road profilometer software (the solid curve in figure 25) and summing the band contributions on a mean-square basis. The values of A_{rms} thus obtained from the measured body acceleration are shown plotted in figure 52 versus the values of A_{rms} obtained from the road profilometer profiles and software. The correlation is good ($r^2 = 0.991$), indicating

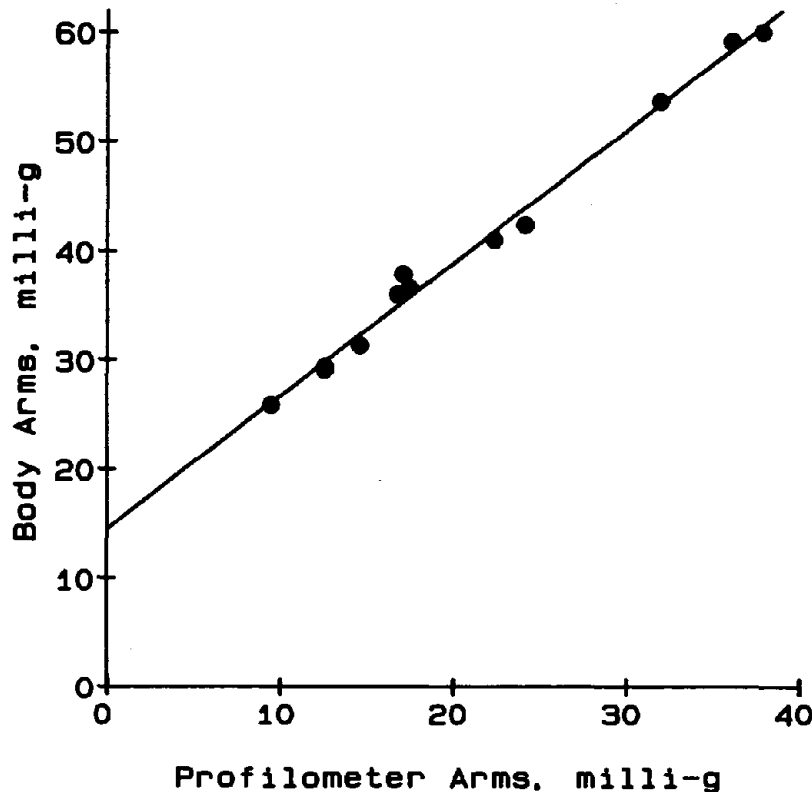


Figure 52. Root-mean-square acceleration, A_{rms} , computed by applying human-response weighting to data from body accelerometer, versus A_{rms} computed from road profilometer profiles.

that a body accelerometer with appropriate frequency weighting can be used as a RTRRM, to be calibrated using an absolute road profiling system. This type of calibration accounts for body acceleration that is induced by engine and drive train vibration, so that the concerns, expressed earlier in this report, about the use of accelerometers to obtain "absolute" roughness ratings do not apply here.

Figure 53 shows these same values of A_{rms} from the body accelerometer plotted against the Mays index obtained from the road profilometer profile and software. The correlation is also good ($r^2 = 0.986$), indicating that there is promise for frequency-weighted body acceleration to be used as a surrogate for a Mays Ride Meter.

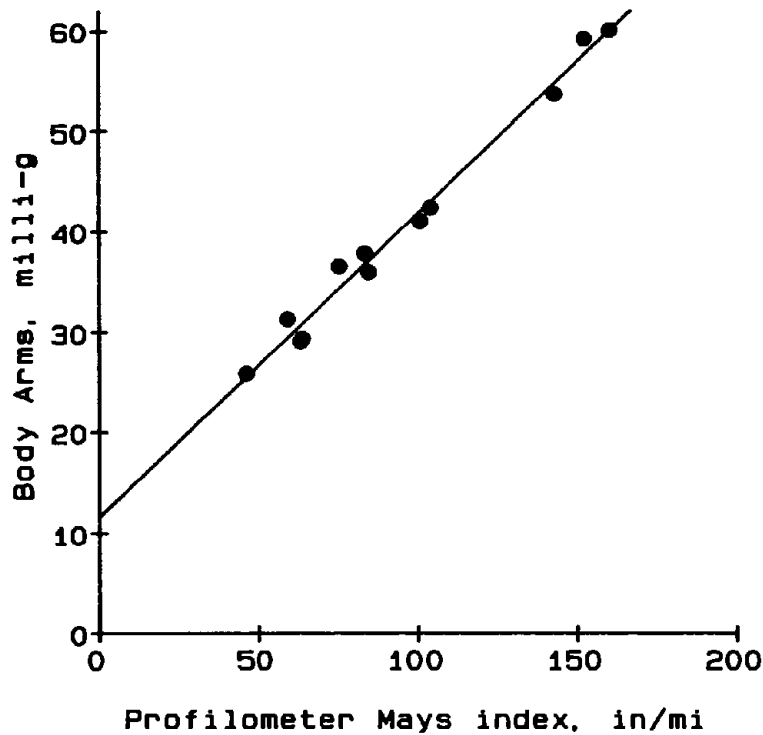


Figure 53. Root-mean-square acceleration, A_{rms} , computed by applying human-response weighting to data from body accelerometer, versus Mays index computed from road profilometer profiles.

4. CONCLUSIONS

An extensive series of measurements was made of the performance of a particular model of an inertial road profiling system (a Model 690DNC Road Profilometer, manufactured by K. J. Law Engineers, Inc.) in order to examine its accuracy and repeatability. The vehicle in which the inertial road profiling system (IRPS) was installed was equipped with accelerometers to measure the vertical vibration of both the axle and the body of the vehicle, with a linear potentiometer to measure the relative displacement between the axle and the body of the vehicle, and a commercial response-type road roughness measurement (RTRRM) system (a Mays Ride Meter, manufactured by the Rainhart Co.). Data collected with the RTRRM and with the auxiliary accelerometers and the linear potentiometer were compared with single-number ratings of road roughness as computed from the profiles measured using the IRPS. Some of the conclusions reached during this study are summarized below.

Road Profilometer Test Results

- The accuracy of the IRPS for profiling was conservatively estimated to be approximately ± 0.03 in (1σ), based on analysis of the component sources of error. [see pp. 15-17]
- The overall profiling accuracy of the IRPS was tested by comparison with filtered rod-and-level data taken from four road profiles. The agreement between the two (see Fig. 14) was at about the 0.01 in level, slightly better than the value estimated above from the individual component sources of error. This test is sensitive to the longest wavelengths (low spatial frequencies) in the profile, not to the high spatial frequencies. [see pp. 24-31]
- A test of the accuracy of the IRPS at high spatial frequencies is its response to a pulse input, formed by profiling a flat plate. In this case the agreement between the measured and simulated profilometer response was quite good. [see pp. 33-37]
- The accuracy for determining the weighted (to simulate human response) root-mean-square acceleration of the vehicle body, as computed from the profile measured by the IRPS, was estimated to be ± 1.2 percent (1σ), based on analysis of the component sources of error. The accuracy for determining the Mays index was expected to be about the same. [see pp. 16-17]
- There is a practical limit to the repeatability in measuring road profiles because there is imprecision involved in locating the wheeltrack and in initiating the beginning of a surface to be profiled. The variability in the Mays indices computed for profiles measured on three road surfaces was of the order of 3.5 to 5 percent of the average Mays index for the road surface, based on data recorded using the same vehicle operator, who attempted to drive in the same wheeltracks during successive measurements. [see p. 48]

- Comparison of the Mays index and weighted root-mean-square acceleration, computed from IRPS profiles, with the same descriptors computed from rod-and-level measurements were encouraging but limited because of the difference in the high-spatial-frequency content of the two sets of profiles. [see pp. 38-51]

Response-type Road Roughness Measurement System Test Results

- The linearity of the optical encoder in the Mays Ride Meter was found to be good provided the lamp was carefully aligned. [see pp. 52-56]
- Good correlation was found between Mays indices measured using the Mays Ride Meter and those computed from the profile obtained by the IRPS. [see pp. 57-61]
- Analysis of signals from the linear-displacement transducer confirmed literature findings with regard to the effects of quantization and hysteresis on the Mays index. [see p. 59]
- Analysis of signals from the body and axle accelerometers revealed substantial contributions from engine and drive-train induced acceleration, essentially independent of road roughness. [see pp. 61-74]
- Good correlation was found between weighted (to simulate human response) vertical root-mean-square acceleration of the vehicle body, as measured by an accelerometer, and that computed from the profile measured by the IRPS. [see pp. 74-75]

APPENDIX A: ROD-AND-LEVEL ANALYSIS PROGRAM

In order to compare the rod-and-level data to the profilometer data, several software features of the Law road profilometer and one from the UMTRI system were duplicated in a BASIC program. This program had the capabilities to read the profile data stored on the disk in ASCII format, to apply either one of two digital, high-pass filter algorithms, and to calculate two road roughness parameters from the filtered profiles.

The main menu of the program, shown in figure 54, has seven options. Under the first option, the raw rod-and-level data are read from the disk. With the second option, the raw road profile is graphed on the CRT and on an HP 7550A plotter. Options three and four are the high-pass filters. The first simulates the three-pole, Butterworth filter used by the FHWA/Law road profilometer. The second simulates the moving average filter in the UMTRI profiling system. With option five, either one of the filtered profiles may be graphed on the CRT and the plotter. Option six produces a calculation of Mays index (MI) and rms acceleration (A_{rms}) and option seven allows the user to quit the program.

The three key subroutines are the Butterworth and moving average filters and the subroutines to do the statistical calculations. Flow charts of these routines are shown in figures 55 to 57. Several points should be noted concerning them.

Figure 55 shows the main elements of the three-pole, Butterworth filter. The summations contributing to $W_f(i)$ in the main loop are the digital forms of integrations associated with the high-pass filter. Several summation parameters are used in the code to carry out the calculations represented by the single equation in the flow chart.⁽²⁾

The UMTRI moving average filter is shown in figure 56. This is a phase-corrected filter that takes a moving average of data points centered on the point under examination and then subtracts the average from the data point. The averaging routine has a moving average window width that determines the nominal filter cutoff length. Points within a distance $L/2$ of the ends of the profile present a problem because points that should contribute to the moving average are missing from the data set. This is handled in a simple way by extrapolating the rod-and-level data at each end of the data set. The slopes of the $L/2$ lengths of profile at each end are calculated, and new points are generated beyond the ends of the profile that lie on the sloped lines.

The subroutine for performing the calculations of single-number roughness ratings, shown in figure 57, is discussed on pp. 43-44.

- 1 — Load the unfiltered road data from disk.
- 2 — Draw the unfiltered road profile.
- 3 — Filter the road data by a three pole, Butterworth technique and store the filtered profile.
- 4 — Filter the road data with a moving average technique and store the filtered profile.
- 5 — Graph the filtered data on the plotter.
- 6 — Calculate the Mays index and rms acceleration.
- 7 — Quit the program.

Figure 54. Main menu of NBSROAD.BAS program.

The input data are:

the unfiltered profile - ROAD(N),
 number of profile points - N
 sampling interval - S,
 the cutoff length - L.

The output result is:

the filtered profile $W_f(N)$

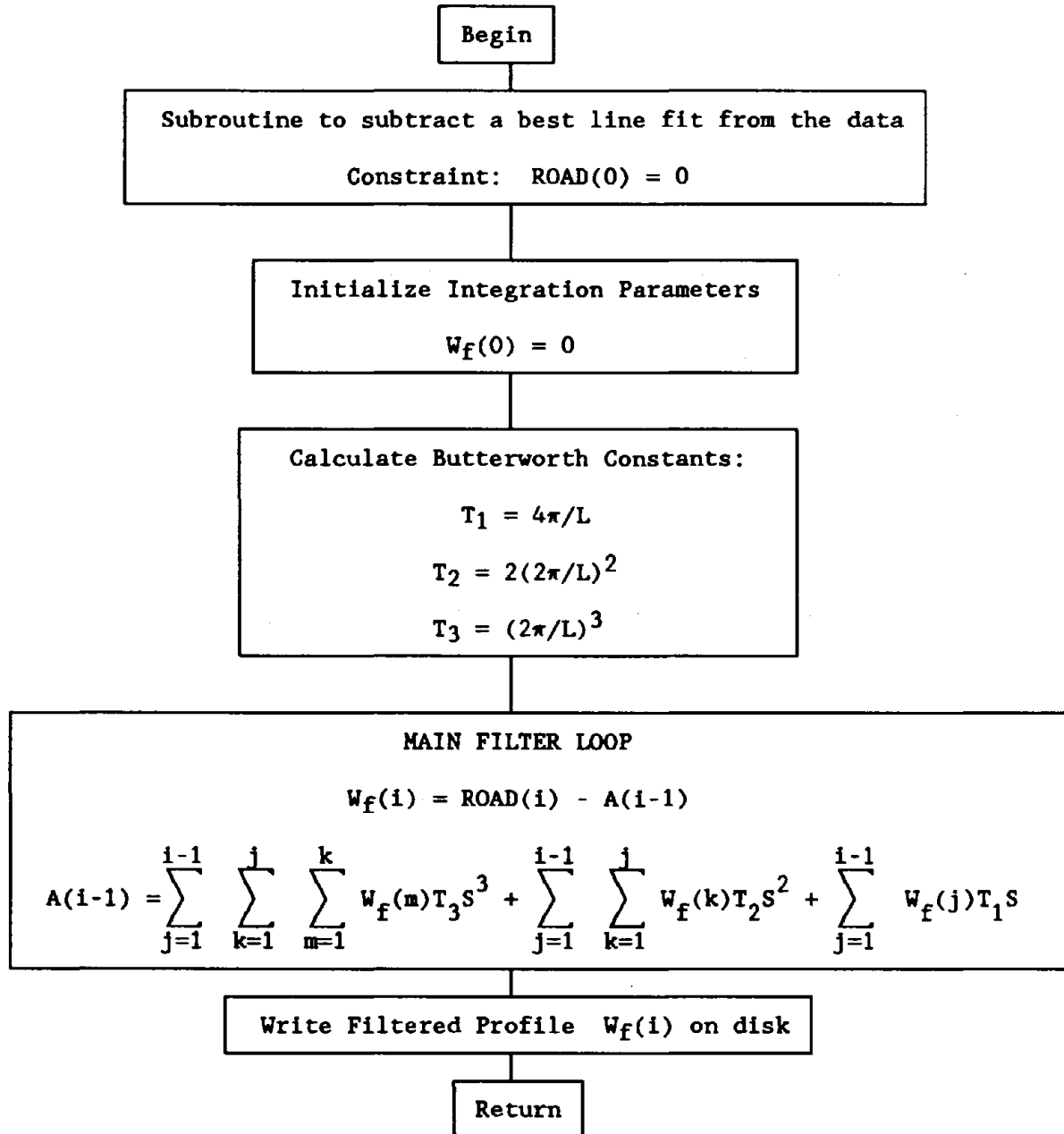


Figure 55. Flow chart of main elements in the 3-pole Butterworth filter subroutine used in the K. J. Law Model 690DNC road profilometer.

The input data are:

the unfiltered profile - ROAD(N),
number of profile points - N
sampling interval - S,
the cutoff length - L.

The output results:

the filtered profile $W_f(N)$

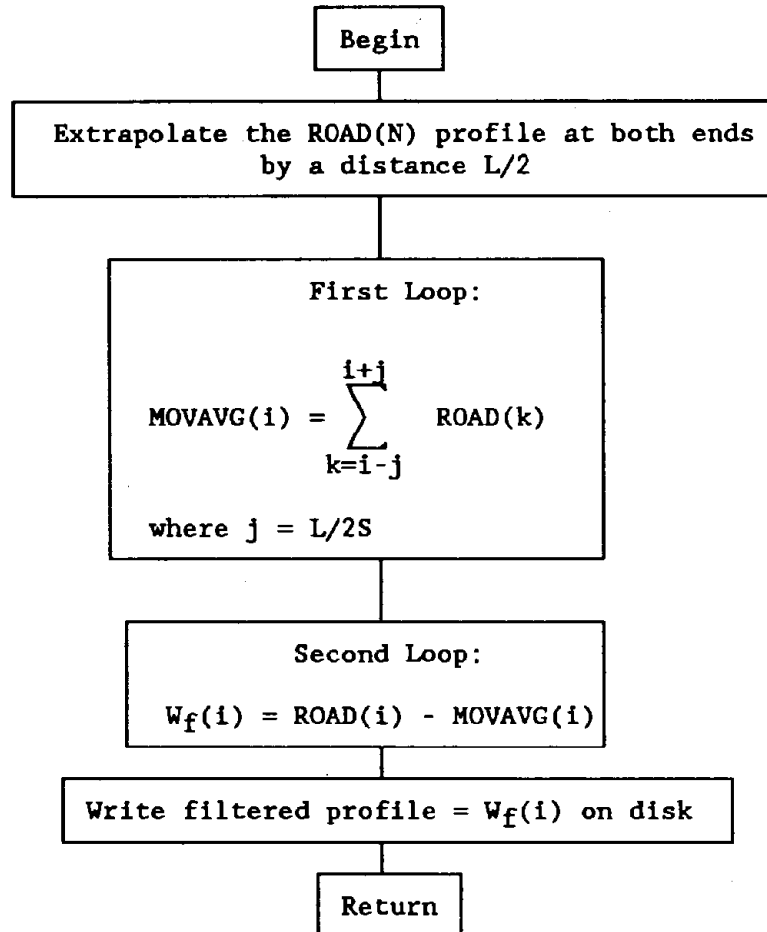
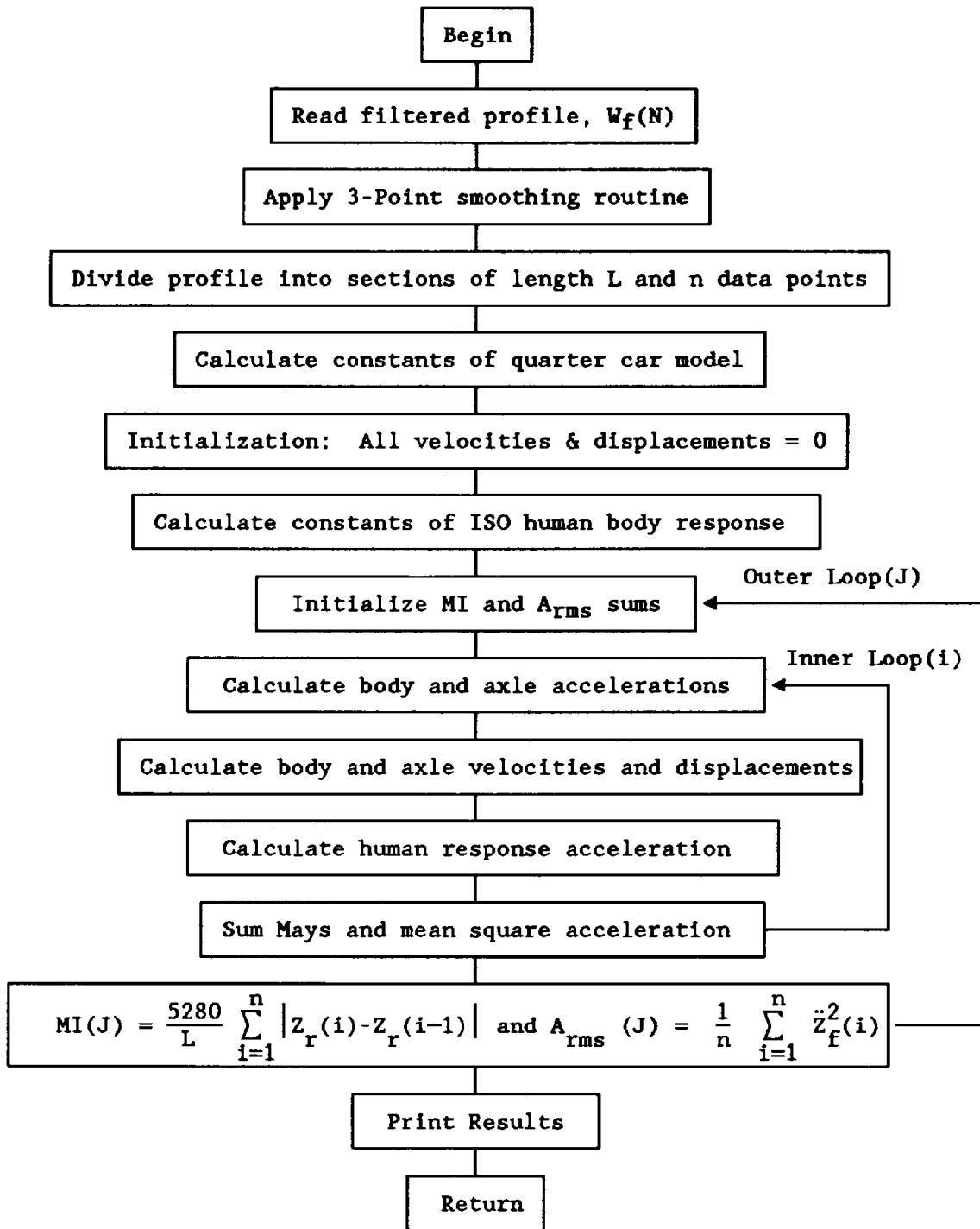


Figure 56. Flow chart of main elements in the UMTRI moving-average filter subroutine.



$z_r(i) = s_i - u_i$ (see equation 13)

\ddot{z}_f = sprung-mass acceleration filtered by human response function

Figure 57. Flow chart of subroutine to calculate Mays index and rms acceleration from profile data.

REFERENCES

- (1) E. B. Spangler and W. J. Kelley, "GMR Road Profilometer: A Method for Measuring Road Profile," General Motors Research Publication GMR-453 (1964).
- (2) E. B. Spangler, "Method and System for Measurement of Road Profile," U.S. Patent 4,422,322 (1983) and 4,741,207 (1988).
- (3) G. K. Watugala, "Determination of Road Roughness from Inertial Road Profilometer Data," Ph.D. Thesis, The University of Pennsylvania (University Microfilms Intl., Ann Arbor, MI, 1984).
- (4) "Road Profilometer Model 690DNC User's Manual," (K. J. Law Engineers, Inc., Farmington Hills, MI, 1986).
- (5) M. R. Hagan and M. W. Sayers, "Methodology for Road Roughness Profiling and Rut Depth Measurement - Reference Manual," UMTRI Report No. 87-6 (University of Michigan Transportation Research Institute, Ann Arbor, MI, 1987).
- (6) M. W. Sayers, T. D. Gillespie, and M. R. Hagan, "Methodology for Road Roughness Profiling and Rut Depth Measurement - User's Manual," UMTRI Report No. 87-5 (University of Michigan Transportation Research Institute, Ann Arbor, MI, 1987).
- (7) T. D. Gillespie, M. W. Sayers, and L. Segel, "Calibration of Response-Type Road Roughness Measuring Systems," National Cooperative Highway Research Program Report 228 (National Research Council, Washington, DC, 1980).
- (8) M. Sayers, Development, Implementation, and Application of the Reference Quarter-Car Simulation, pp. 25-47 in "Measuring Road Roughness and Its Effect on User Cost and Comfort," ASTM Special Technical Publication 884, T. D. Gillespie and M. Sayers, eds. (American Society for Testing and Materials, Philadelphia, PA, 1985).
- (9) E. B. Spangler and W. J. Kelly, "Use of the Inertial Road Profilometer in the Ohio DoT Pavement Management System," (Surface Dynamics, Inc., Bloomfield Hills, MI, 1987), p. 86.
- (10) International Standard 2631, "Guide for the Evaluation of Human Exposure to Whole-Body Vibration," (International Organization for Standardization, Geneva, Switzerland, 1987).
- (11) Draft International Standard ISO/DIS 8041, "Human Response to Vibration - Measuring Instrumentation" (International Organization for Standardization, Geneva, Switzerland, 1987).

- (12) J. C. Wambold, Road Roughness Effects on Vehicle Dynamics, pp. 179-196 in "Measuring Road Roughness and Its Effect on User Cost and Comfort," ASTM Special Technical Publication 884, T. D. Gillespie and M. Sayers, eds. (American Society for Testing and Materials, Philadelphia, PA, 1985).
- (13) M. W. Sayers, T. D. Gillespie, and C. A. V. Queiroz, "The International Road Roughness Experiment," World Bank Technical Paper No. 45, (The World Bank, Washington, DC, 1986).
- (14) ASTM Standard E 1082, "Standard Test Method for Measurement of Vehicular Response to Traveled Surface Roughness," (American Society for Testing and Materials, Philadelphia, PA, 1985).
- (15) Mays Ride Meter Booklet, 3rd Ed. (Rainhart Co., Austin, TX, 1973).
- (16) ISA S37.12, Standard for Potentiometric Displacement Transducers (Instrument Society of America, Pittsburgh, PA, 1982).
- (17) W. Gulden, "Calibration Procedures for Roadmeters," Report No. FHWA-TS-86-201 (Federal Highway Administration, McLean, VA, 1986).
- (18) J. C. Wambold, et al., "Implementation of an Automated Rating Procedure for Pavement Surface Roughness," Final Report FHWA/PA-82/004 (Pennsylvania Department of Transportation, Harrisburg, PA, 1982).
- (19) J. C. Wambold and J. J. Henry, "The Pavement Roughness Research Facility and the Skid Resistance Research Facility," PTI Report 8418 (Pennsylvania Transportation Institute, Pennsylvania State University, University Park, PA, 1984).
- (20) ASTM Standard Practice for Calibration of Systems Used for Measuring Vehicular Response to Pavement Roughness, January 1989 draft.
- (21) M. W. Sayers and T. D. Gillespie, "The Ann Arbor Profilometer Meeting," Final Report FHWA/RD-86/100 (Federal Highway Administration, Washington, DC, 1986).
- (22) Spangler, E. G., et al., "Use of the Inertial Profilometer to Calibrate the Commonwealth of Kentucky Department of Highways Mays Ride Meter Systems," Draft Report submitted to the American Society of Testing and Materials, Philadelphia, PA, 1987.